DISCRETE ALGORITHMS FOR MORPHOLOGICAL FILTERS IN GEOMETRICAL METROLOGY

SHAN LOU

A thesis submitted to the University of Huddersfield in partial fulfilment of the requirements for the degree of Doctor of Philosophy

The University of Huddersfield

May 2013

COPYRIGHT STATEMENT

ABSTRACT

In geometrical metrology, morphological filters are useful tools for the surface texture analysis and functional prediction. Although they are generally accepted and regarded as the complement to mean-line based filters, they are not universally adopted in practice due to a number of fatal limitations in their implementations — they are restricted to planar surfaces, uniform sampled surfaces, time-consuming and suffered from end distortions and limited sizes of structuring elements.

A novel morphological method is proposed based on the alpha shape with the advantages over traditional methods that it enables arbitrary large ball radii, and applies to freeform surfaces and non-uniform sampled surfaces. A practical algorithm is developed based on the theoretical link between the alpha hull and morphological envelopes. The performance bottleneck due to the costly 3D Delaunay triangulation is solved by the divide-and-conquer optimization.

Aiming to overcome the deficits of the alpha shape method that the structuring element has to be circular and the computation relies on the Delaunay triangulation, a set of definitions, propositions and comments for searching contact points is proposed and mathematically proved based on alpha shape theory, followed by the construction of a recursive algorithm. The algorithm could precisely capture contact points without performing the Delaunay triangulation. By correlating the convex hull and morphological envelopes, the Graham scan algorithm, originally developed for the convex hull, is modified to compute morphological profile envelopes with an excellent performance achieved.

The three novel methods along with the two traditional methods are compared and analyzed to evaluate their advantages and disadvantages. The end effects of morphological filtration on open surfaces are discussed and four end effect correction methods are explored. Case studies are presented to demonstrate the feasibility and capabilities of using the proposed discrete algorithms.

ACKNOWLEDGEMENTS

I would like to express my appreciation to all the people who explicitly and implicitly supported me during my doctoral research.

First and foremost, I would present my deepest gratitude to my main supervisor Professor Xiangqian (Jane) Jiang, who has given me the precious opportunity to engage in the study of surface filtration techniques with sufficient supports on research and finance. Her proficiency and knowledge on surface metrology, coupled with the practical view on instrument and manufacture, are of tremendous help for this work.

Special thanks go to my second supervisor, Professor Paul J. Scott, for providing me with a continuous stream of evaluable guidance and suggestion for my work. His extensive knowledge in mathematics and experiences in practical algorithm development are of paramount contribution to the completion of this thesis.

I would also like to express my gratitude to Dr Wenhan Zeng, Dr Xiangchao Zhang, Dr Phillip Cooper, Dr Hussein Abdul-Rahman for guidance on mathematics and surface metrology, Dr Paul J. Bills for instruction on practical applications, and all other colleagues in the EPSRC Centre for advanced metrology.

My thanks also go to my former employer, Wilcox Associates, Inc. Hexagon Metrology, especially the development manager of the portable group, Troy Johnson, and the team member, Andy Roberts, who led me into the world of geometrical metrology and raised my interests in algorithm development.

Finally, I own my sincere thanks and appreciation to my parents Guangda Lou and Zhihua Wang, and my beloved wife Wenjuan Wu for their loving considerations and great confidence in me all through these years, with whom I can share my joy of success and from whom I can gain motivation, encouragement and comfort.

TABLE OF CONTENT

LIST OF FIGURES

LIST OF TABLES

PUBLICATION LIST

1. Lou, S., Jiang X. and Scott, P. J. 2011 Fast algorithm to morphological filters, *Journal of Physics: Conference Series* 311(1): 012001.
2. Lou, S., Jiang X. and Scott, P. J. 2011 Morphological Filters Based on Motif Combination for Surface Functional Evaluation, *Proceedings of the 17th International Conference on Automation & Computing,* 133-137.
3. Jiang X., Lou, S. and Scott, P. J. 2012 Morphological Method for Surface Metrology and Dimensional Metrology Based on the Alpha Shape, *Measurement science and technology*, 23(1): 015003.
4. S. Lou, X. Jiang, P. J. Scott 2012 Algorithms for Morphological Profile Filters and Their Comparison, *Precision Engineering*, 36(3): 414-423.
5. Lou, S., Jiang X. and Scott, P. J. 2012 An Efficient Divide-and-Conquer Algorithm for Morphological Filters, *12th CIRP Conference on Computer Aided Tolerancing*.
6. Bills, P. J., Lou, S. and X. Jiang 2012 Development of morphological filtering method for specification and characterisation of hip replacement taper junctions, *Proceedings of the 12th EUSPEN International Conference*, 125-128.
7. Lou, S., Jiang X. and Scott, P. J. 2013 Correlating motif analysis and morphological filters for surface texture analysis, *Measurement*, 42(2): 993-1001.
8. Lou, S., Jiang X. and Scott, P. J. 2013 Application of the morphological alpha shape method to the extraction of topographical features from engineering surfaces, *Measurement*, 42(2): 1002-1008.
9. Lou, S., Zeng, W., Jiang, X. and Scott, P. J. 2013 Robust filtration techniques in geometrical metrology and their comparison, *International Journal of Automation and Computing*, 10(1): 1-8.
10. Lou, S., Jiang X., Bills, P. J. and Scott, P. J. 2013 Defining true tribological contact through application of the morphological method to surface topography, *Tribology Letters*, 50(2): 185-193.

1. INTRODUCTION

1.1 Background

The surface of a component is an interface limiting the body of the component and separating it from the surrounding medium, which governs the functional behaviours of the product, whether that be a mechanical, tribological, hydrodynamic, optical, thermal, chemical or biological property, all of which are of tremendous importance to product performance (Jiang 2009; Bruzzone *et al.* 2008). Surfaces have always been fundamentally important in traditional industries. A good surface allows automobile engines to have reduced running-in times and to be more fuel efficient with reduced emission. It also enables optical components to have smoother surfaces such that they scatter less light and have better optical qualities (Jiang *et al.* 2007a). They are even more significant to modern cutting-edge technologies, such as nanotechnology, biotechnology and energy-technology. Following the trend of miniaturization of these products nowadays, either the reduction of object geometry or the refinement of micro and nano-details on macro objects, surfaces and their properties become the dominant factor in the functionality of products (Whitehouse 2012).

Many emerging products and devices are based on achieving surfaces with special functionalities. Manufactured items such as micro- and nanometre scale transistors, micro electro mechanical systems (MEMS) and nano electro mechanical systems (NEMS), microfluidic devices, optics components with freeform geometry and structured surface products are clear evidence of products where the surface plays the functional role (Jiang *et al.* 2007b). Hydrophobic products, such as roof tiles and fabrics, can be obtained by texturing the surfaces to achieve the lotus effect (Bruzzone *et al.* 2008). For optics in ground- and space-based telescopes, in defence- and satellite-based image based imaging systems and in large laser facilities, smooth surfaces with complex optical shapes are required with precision reaching the level of atomic magnitude. Similar accuracy is also demanded in implantable medical devices, e.g. artificial hip and knee joints, where micrometre form and nanometre roughness requirements are specified in order to reduce the generation of wear debris (Jiang &

Whitehouse, 2012). Figure 1.1 shows a BioMEMS with selective surface textures for the generation of droplets having a 20 pl volume (De Chiffre *et al.* 2003). Figure 1.2 presents an F-theta lens with the shape error less than 0.3 μm peak-to-valley and the surface roughness S_a less than 4 nm (Brinksmeier & Preuss 2012).

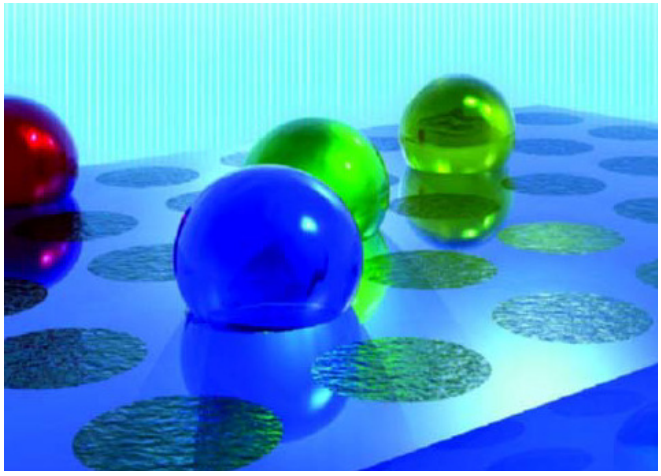

Figure 1.1 BioMEMS

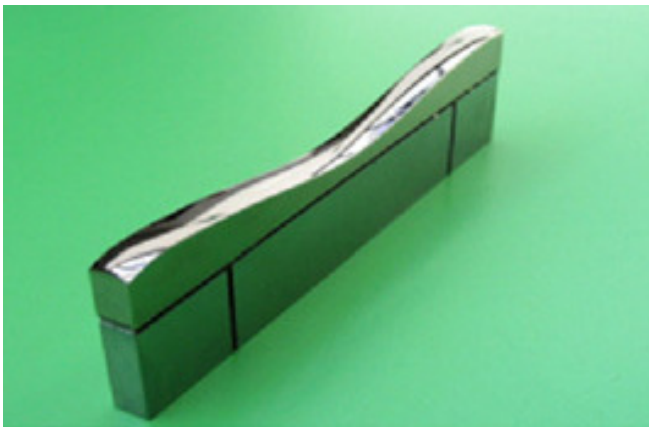

Figure 1.2 F-theta lens

Surfaces and their measurement, provide a link between the manufacture of these engineering components and their use (Whitehouse 1978). Surface metrology is the study of surface topography – measurement of small scale geometrical features on surfaces. It has profound influences on manufacture quality as it plays two important roles. See Figure 1.3. On one hand, it helps to control the manufacture process: monitor changes in the surface texture and indicate changes in the manufacturing process such as machine tool vibration and tool wear (Peters *et al.* 1979; Trumpold

2001). On the other hand, it helps functional prediction: characterize geometrical features that will directly impact on tribology and physical properties of the whole system (Unsworth 1995; Sayles 2001; Whitehouse 2001), for instance, the friction of two contact surfaces and the optical fatigue of one reflecting surface. Controlling the manufacture helps repeatability and hence quality of conformance. Functional prediction helps performance and assists in its optimization (Whitehouse 2002).

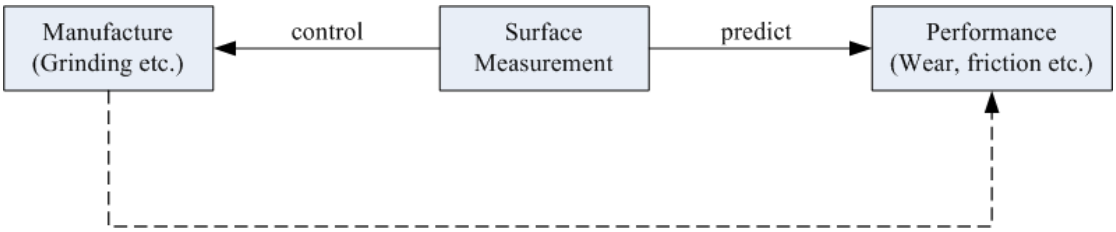

Figure 1.3 Surface measurement helps manufacture and function

1.2 Filtration techniques for geometrical metrology

1.2.1 Motivation

The early use of surface measurement was mainly to control the manufacturing process. In practice what happened was that a component was made and tried out. If it functioned satisfactorily, the same manufacturing conditions were used to make the next part and so on for all subsequent parts (Whitehouse 1978). It soon became apparent that the control of surface texture was being used as an effective go-gauge for the process. The surface texture is a fingerprint of all process stages of the manufacturing process. The effects of process and machine tool are always present in surface textures. The former is called the roughness and the latter the waviness. The roughness is inevitable – it is the mark of the process, but the waviness – usually of longer wavelength – is a result of a problem of the machine tool and in principle could be avoided. Also, in addition to roughness and waviness, even longer wavelengths can be introduced into the surface geometry by weight deflection or long-term thermal effects. These cause errors in the general shape of the part, that is, deviation from the shape required and specified by the designer (Whitehouse 2002).

Filtration is the means by which various components of the surface texture, namely roughness, waviness and form, are extracted from the measured data for

further characterization, see Figure 1.4. By separating surface profile into various bands, it is possible to map the frequency spectrum of each band to the manufacturing process that generated it (Raja *et al.* 2002).

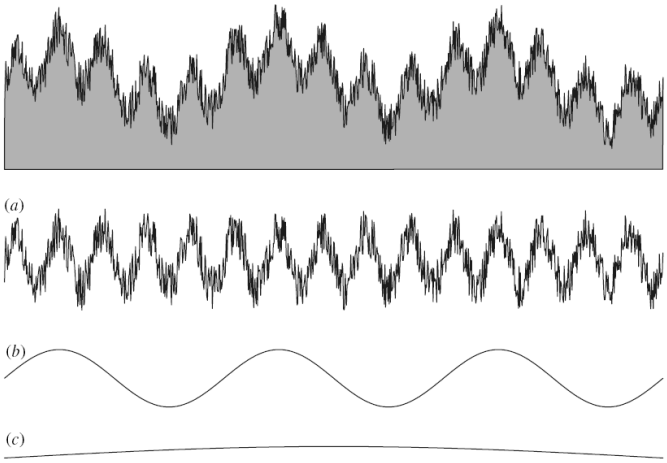

Figure 1.4 Geometrical components of a surface profile. (a) roughness; (b) waviness; (c) form

On the other hand, surface analysis techniques, including the filtration techniques, were also motivated by predicting and optimizing the functional performance. One of the initiatives of surface metrology was the need for studying tribological properties and optical properties of components. Surfaces of components were considered important in terms of friction and optical reflection. Much emphasis was placed on friction because it is fundamental in the performance of moving systems. Wear is often the result of too much friction, and lubrication is mainly devoted to reducing friction. Contact mechanisms are fundamental and the geometry of contact depends strongly on the surface topography (Jiang *et al.* 2007a). Some surface parameters have been attempted to link the function. For example, extreme statistics may be related with the corrosion and fatigue of components and average statistics may contribute to conductivity and reflectivity (Whitehouse 2001).

Although filtration techniques are primarily used for the analysis of surface textures, with increased data densities in dimension metrology, they are being applied as a means of data smoothing. For example, dimensional measurements performed by the Coordinate Measurement Machine (CMM) equipped with optical scanning probes typically include all measured data in an "as collected" manner. As data densities

have increased, there has been an increased awareness that there is a great deal of noise in these high density datasets. This noise can be the result of such things as the surface roughness of the component being measured, or caused by the dirt or machining chips on the component, or due to the errors in the measurement system, e.g. vibration or electronic noise etc. In many cases it is desirable to filter out this noise to achieve a more stable dataset that is perhaps more indicative of the attributes that are to be assessed (Malburg 2002).

1.2.2 Historical development

The 1950s saw two attempts to separate the waviness from the profile so that the roughness could be characterized. One was graphical, simulating electrical filters in the meter circuit (Muralikrishnan & Raja 2009). The raw profile was divided into segments of equal length, and in each segment a mean line was drawn that captures the slope of the profile in that segment. The roughness profile was obtained by considering the deviation from the mean line. Thus it was designated the mean line system (M-system). The other was mechanically simulating the contact of a converse surface, e.g. a shaft, with the face of the anvil of a micrometer gauge (Whitehouse 2002). It appeared as a large circle rolling across over the profile from above and was entitled the envelope system (E-system).

The first practical mean-line filter used in surface texture measurement is the analogue filter proposed by Reason et al (1944). Reason issued a comprehensive description and analysis of the M-system. He was the first to make the distinction between form deviation, waviness and roughness, when specifying the quality of shafts and holes. The analogue filter was constructed by a two-resistor-capacity (2RC) network. Reason reported the phase error and profile deformation due to filtering, but he considered its effect is negligible in computing R_a and R_q.

Von Weingraber (1956) concentrated his effort on developing the Envelope system. The E-system bases the reference lines upon the loci of centres of circles of different radii rolled along the profile. As Figure 1.5 demonstrates, the locus of the centre of the larger circle gives the *curve of form*, while that of the smaller circle gives the *contacting profile*. The area between the ideal geometrical profile and the curve of form represents the errors of form; the area between the curve of form and the

contacting profile represents the waviness; and the area between the contacting profile and the measured profile represents the roughness (Thomas 1999).

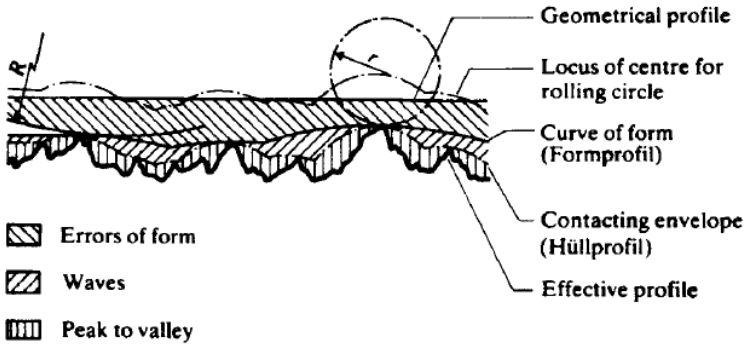

Figure 1.5 Terminology of the E-system of reference lines in which the filters are two circles of radius r and R rolling along the profile (Olsen 1963)

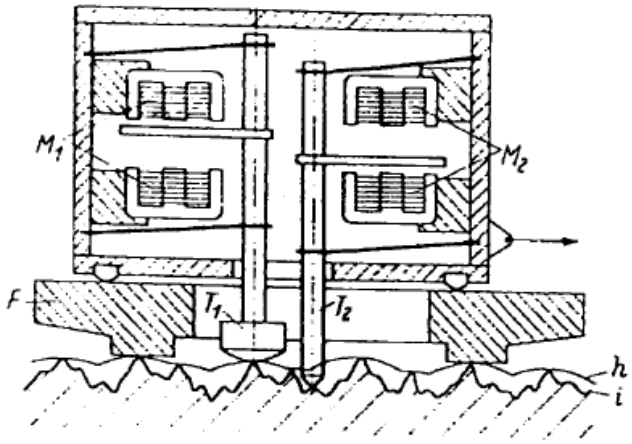

Figure 1.6 Probe for E-system: T1 Skid, T2 stylus

The difficulty appeared in building practical instruments as two elements are needed: a spherical skid to approximate the 'enveloping circle' and a needle-shaped stylus moving in a diametral hole of the skid to measure the roughness as deviation with respect to the "generated envelope", see Figure 1.6. The advantages of the E-system were claimed to be that it is more physically significant in that many engineering properties of a surface are determined by its peaks. Standard radii were 25 mm for roughness and 250 mm for waviness, though other radii have been proposed (Radhakrishnan 1972). The standing objection opposed by Reason was that the choice of the rolling circle radius is as arbitrary as the choice of cut-off in the M-

system and no practical instrument using mechanical filters could be made at that time.

The discussion about the reference systems lasted for at least one decade between 1955 and 1966 (Peters 2001). Around 1960, with the advent of digital processing techniques, the M-system became pre-eminent. In 1963, Whitehouse and Reason (1963) simulated the 2RC filter digitally. They described the filter using a weighting function that depended on the cut-off wavelength. A cut-off wavelength serves a similar purpose as the size of a segment in graphical analysis. In 1967, Whitehouse (1967/68) formally introduced the phase-corrected filter and digital filters were also made. It was adopted by the international standard and formally referred as the "standard wave filter". This phase-corrected digital filter was a significant step forward in the development of mean-line filters because it had a major impact upon the interpretation of surface roughness.

The phase-corrected digital filter still has problems, one being that it distorted the profile at the ends. In 1986, the three main surface texture instrument manufactures (Hommelwerk, Mahr and Taylor Hobson) had reached a consensus, with the Gaussian filter being chosen as the new filter for separating differing wavelengths. This recommendation was adopted by ISO, resulting in ISO 11562 (1996) in which the Gaussian filter is given as the standardized phase-corrected profile filter for surface texture.

The Gaussian filter, although a good general filter, is not applicable for all functional aspects of a surface, for example in contact phenomena, where the E-system method is more relevant. The advent of fast practical computers, which can be used in association with measurement instruments, had virtually eliminated the need for any hardware implementation for the E-system (Tholath & Radhakrishnan 1999). Furthermore, there were growing evidences showing that the E-system method can give better results in functional prediction of surface finish in the analysis of mating surfaces, such as contact, friction, wear, lubrication and failure mechanism (Westberg 1997). The M-system techniques are usually used to separate form, waviness and roughness, nevertheless there was little correlation between roughness parameters and functional requirements in that functional behaviour of components are more related with geometrical properties of their surfaces. In this aspect the logic of the E-system was sounder in comparison to the M-system. This concept also gained great ground in

form measurement. CMMs using spherical probe tips are essentially performing this procedure of filtering in measurements.

The French industry adopted an alternative approach to filtration to the M-system and the E-system, called roughness and waviness (R&W), also known as the motif method, which sets out to extract functionally significant features from surface profiles for a particular application. The conceptual foundation of the method is described by Fahl (1982). The method began as a purely graphical approach, where an experienced operator would draw on a profile graph an upper envelope that subjectively joined the highest peaks of the profile. Base on this procedure, "insignificant" peaks are combined to form "significant" ones, from which surface texture parameters could be calculated. From the standpoint of classification, the motif method does not belong to the M-system, but a simulation of the E-system (Jiang *et al.* 2007a).

Both the M-system and the E-system approaches have their advantages and limitations. Arguing that one is better than the other without any concrete proof from the application area is not convincing (Radhakrishnan & Weckenmann 1998). Actually rather than competing with each other, the M-system and the E-system are complementary to each other, contributing to a better solution to surface measurement.

1.2.3 Recent development

In the last two decades, more advanced filtration techniques emerged as a result of urgent needs for the analysis of surfaces with complex geometry and high precision produced by modern manufacturing technologies.

The M-system was greatly enriched by incorporating advanced mathematical theories. The Gaussian regression filter overcame the problem of end distortion and poor performance of the Gaussian filter in the presence of significant form component (Seewig 2006), while the robust Gaussian filter solved the problem of outlier distortion in addition (Brinkmann *et al.* 2001; Zeng *et al.* 2010). The Spline filter is a pure digital filter, more suitable for form measurement (Krystek 1996a). Based on L_p approximation, the robust Spline filter is insensitive with respect to the outliers (Krystek 2005; Goto *et al.* 2005; Zeng *et al.* 2011a). By applying wavelet theory, the Spline-wavelet filters provide a multi-resolution access to partitioning a surface into multiple wavelength bands (Jiang *et al.* 2000). More recently, a method of Gaussian

filtering for freeform surface was developed by solving the diffusion equation which overcomes geometrical distortion in the presence of non-zero Gaussian curvature (Jiang *et al.* 2011a).

Meanwhile the E-system also experienced significant improvements. By introducing mathematical morphology, morphological filters emerged the superset of the early envelope filter, but offering more tools and capabilities (Srinivasan 1998). The basic variation of morphological filters includes the closing filter and the opening filter. They could be combined to achieve superimposed effects, referred to as alternating symmetrical filters. Scale-space techniques further developed morphological filters. Similar to wavelet based techniques in the M-system, scale-space techniques provide a multi-resolution analysis to surface textures whereby various scales of geometrical features can be extracted from a surface and assessed separately (Scott 2000).

In 1996, ISO set up a group, under the convenorship of Scott (ISO/TC 213 1996). This work has resulted in the establishment of a standardized framework for filters, giving a mathematical foundation for filtration, together with a toolbox of different filters (Srinivasan 2000 *et al.*; Krystek *et al.* 2000). Information concerning these filters has been or is about to be published as a series of technique specifications (ISO 16610 series 2010), to allow metrologists to access the usefulness of the recommended filters. So far, only profile filters have been published, including the following classes of filters.

(1) *Linear filters*. The M-system filters belong to this category, such as the Gaussian filter, the Spline filter and the Spline-wavelet filter.

(2) *Robust filters*. Filters that are robust against specific profile phenomena such as spikes, scratches and steps, including the robust Gaussian filter and the robust Spline filter.

(3) *Morphological filters*. The E-system filters belong to this category and include closing and opening filters using either a disk or a horizontal line segment.

(4) *Segmentation filters.* Filters that partition a profile into portions according to specific rules. The motif approach belongs to this class.

1.3 Aims and objectives

During the last two decades, in contrast to fabulous progress achieved in the Gaussian filter, the Spline filter and their robust versions, there was not such an echo in respect to morphological filters. Even though morphological filters are generally accepted and regarded as the complement to mean-line based filters, they are not universally adopted due to a number of limitations caused by their current implementation and lack of capabilities requested by modern product technologies, which as a consequence restrict the prevalence of morphological filters.

This thesis aims to develop efficient discrete algorithms for morphological filters with capabilities of evaluating modern surfaces including freeform surfaces, non-uniform sampled surfaces and closed surfaces and explore their applications in the field of geometrical metrology. The major objectives that this thesis attempts to address are outlined below:

(1) Review the development of filtration techniques in geometrical metrology, especially morphological filters. Investigate conventional implementations of morphological filters and survey their applications in the field of geometrical metrology.

(2) Develop discrete algorithms for morphological filters. The algorithms are expected to overcome the deficits of traditional methods. It should be efficient in performance, robust against possible singularities, available for arbitrary large size of structuring element, applicable for complex surfaces, including freeform surfaces, non-uniform sampled surfaces (e.g. surfaces sampled by a CMM) and closed surfaces.

(3) Evaluate and verify the designed algorithms. Compare the designed algorithms with conventional methods in terms of their capabilities, computations, performances and limitations.

(4) Investigate the end effects of morphological filtering on open surfaces and create correction methods for end effects.

(5) Explore the applications of the designed methods in the field of geometrical metrology, including surface metrology and dimensional metrology.

1.4 Structure of thesis

The thesis is structured in the following fashion.

In Chapter 2, we review the four basic morphological operations, namely dilation, erosion, closing and opening as well as the granulometry transform. They are the foundation of mathematical morphology. Morphological image processing techniques are also stated in a brief manner. Afterwards the basic principles and practical applications of morphological operations are recalled, including the dilation and erosion operation, the closing and opening filter, the alternating symmetrical filter and scale-space techniques. Following that, the conventional supporting algorithms for morphological filters are reviewed.

Aiming at the limitations of traditional methods, Chapter 3 proposes a novel method, which utilizes the theoretical link between the alpha hull and morphological operations. This chapter first gives a brief introduction to alpha shape theory and then presents the link between the alpha hull and morphological envelopes. Based on their relationship, a practical algorithm is developed that corrects possible singularities caused by data spikes and reduces the amount of calculation for open profiles/surfaces. Aiming to improve the performance of the proposed alpha shape method, an optimization is constructed using the divide-and-conquer approach.

In Chapter 4, another two novel algorithms are proposed based on searching contact points on the surface, namely those points on the surface being in contact with the structuring element in the traversing process. This chapter first analyzes the limitations of the alpha shape method. Then a series of definitions, propositions and comments related with the search of contact points are proposed and mathematically proved based on alpha shape theory. A recursive algorithm is developed on the basis of these comments.

The other method is proposed by linking morphological envelopes with the convex hull. Viewing the convex hull as a special morphological envelope, the Graham scan algorithm, originally developed for the convex hull, is modified to calculate morphological profile envelopes.

Chapter 5 makes a detailed comparison of the proposed algorithms with the existing algorithms in four aspects: algorithm verification, algorithm analysis,

performance evaluation and areal extension. By examining these aspects, a thorough insight into the merits and shortcomings of these algorithms is obtained.

Chapter 6 studies the end effects of morphological filtration on open surfaces. Four methods for end effects correction are developed comprising infinity padding, point symmetrical reflection, line symmetrical reflection, polynomial extrapolation and linear prediction. These methods are coupled with an optimization technique of using contact points aiming to improve computation efficiency. A discussion is made to derive their pros and cons.

Chapter 7 illustrates four case studies of the application of the proposed methods. First the proposed areal methods are used to extract topographical features from engineering surfaces, including surfaces measured from a tooth implant, a femoral component of artificial knee joint and a bullet. Then they are applied to the filtration of freeform and non-uniform sampled surfaces. Following that, morphological filters are employed in roundness measurement using the alpha shape method. Finally the methods searching for contact points in association with high accuracy instruments are utilized to evaluate the underlying form of the textured surface of hip replacement taper junction.

The thesis concludes in Chapter 8 by summarising the accomplished work in this research and discussing the future work.

2. LITERATURE REVIEW

Morphological filters are defined on the basis of four basic morphological operations, namely dilation, erosion, opening and closing. These operations are the foundation of mathematical morphology. Mathematical Morphology was firstly used for image processing and gradually extended to other disciplines, including surface metrology and dimensional metrology. This chapter will review several basic concepts of mathematical morphology. Afterwards definitions, specifications and applications of morphological filters will be discussed. Finally, existing algorithms for morphological filters will be presented and analyzed in details.

2.1 Mathematical morphology

Mathematical morphology is a mathematical discipline established by two French researchers Jorge Matheron and Jean Serra in the 1960s. An overview of their work is given in Serra (1982). The central idea of mathematical morphology is to examine the geometrical structure of an image by matching it with small patterns at various locations in the image. By varying the size and the shape of the matching patterns, called the structuring elements, one can extract useful information about the shape of the different parts of the image and their interrelation (Heijmans 1995). Four basic morphological operations, namely dilation, erosion, opening and closing, form the foundation of mathematical morphology.

2.1.1 Morphological operations

Dilation combines two sets using the vector addition of set elements. The dilation of A by B is

$$D(A,B) = A \oplus \check{B}, \tag{2.1}$$

where $\check{B}$ is the reflection of B through the origin of B.

It is defined on the basis of vector addition, also known as the Minkowski addition, which was first introduced by Minkowski (1903). The Minkowski addition of two input sets A and B is the set:

$$A \oplus B = \{c \mid c = a + b, a \subseteq A \ \& \ b \subseteq B\}. \tag{2.2}$$

Figure 2.1 presents an example of dilating a square by a disk. The dilation of the light colour square by a disk results in the dark colour square with round corners.

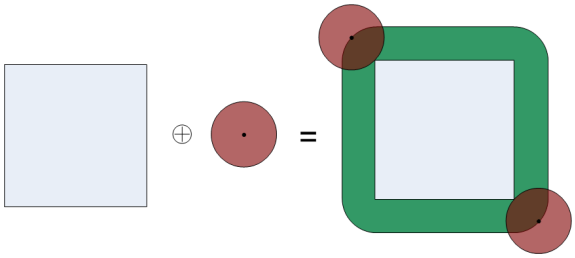

Figure 2.1 Dilation of a square by a disk

Erosion is the morphological dual to dilation. It combines two sets using the vector subtraction of set elements. The erosion of A by B is

$$E(A,B) = A \ominus \check{B}, \tag{2.3}$$

where

$$A \ominus B = \overline{\overline{A} + B}. \tag{2.4}$$

and $\overline{A}$ is the complementation of A.

An example of erosion is illustrated in Figure 2.2. The erosion of the light colour square by a disk generates the dark colour square.

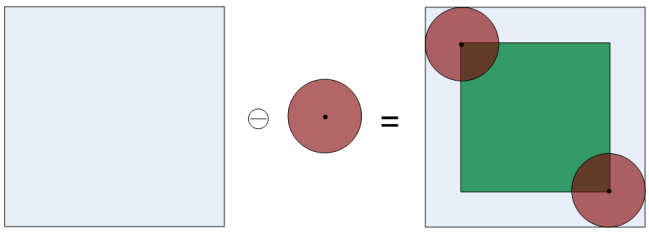

Figure 2.2 Erosion of a square by a disk

Opening and closing are dilation and erosion combined pairs in sequence. The opening of A by B is obtained by applying the erosion followed by the dilation,

$$O(A,B) = D(E(A,B), \check{B}). \tag{2.5}$$

In Figure 2.3, the opening of the light colour square by a disk generates the dark colour square with round corners.

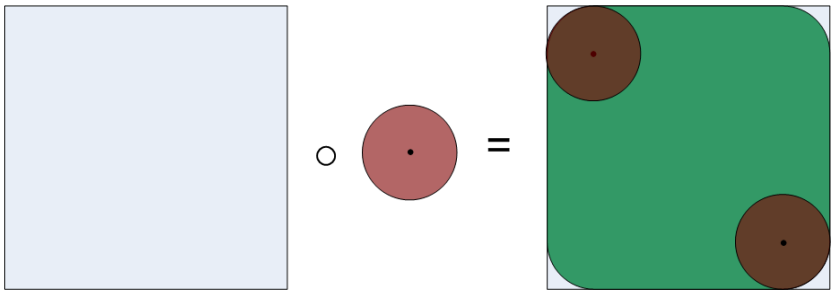

Figure 2.3 Opening of a square by a disk

Closing is the morphological dual to opening. The closing of A by B is given by applying the dilation followed by the erosion,

$$C(A,B) = E(D(A,B),\check{B}). \tag{2.6}$$

In Figure 2.4, the closing of the light colour shape (union of two squares) by a disk results in the union of the light colour shape and the dark colour areas.

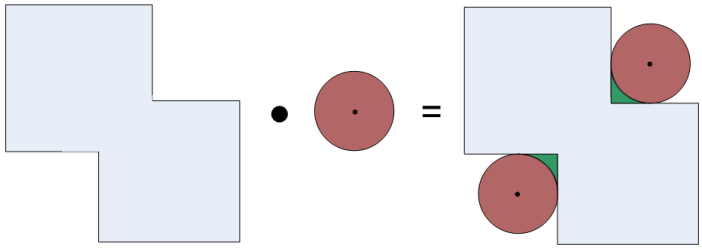

Figure 2.4 Closing of an union of two squares by a disk

2.1.2 Granulometry

The granulometry was first introduced by Matheron (1975) to compute the size distribution of grains in the input set. The concept of the granulometry may be likened to the sifting of rocks in a gravel heap. The rocks are sifted through screens of increasing size, leaving only the rocks that are too big to pass through the sieve. The process of sifting the rocks at a particular size is analogous to the opening of an image using a particular size of structuring element. The residual after each opening is often

collated into a granulometrical curve, revealing useful information about the distribution of object size in the image (Soille 1999).

Figure 2.5 illustrates an example of using the granulometry to extract shapes (Asano 1999). The original image consisting of different scales of shapes is filtered by a sequence of opening with increasing size. Since the opening removes the portion of the image smaller than the structuring element, the difference of the image opened by the structuring elements of size n and $n+1$ contains the portion whose size is exactly n. Thus various sizes of shapes can be extracted from the differences.

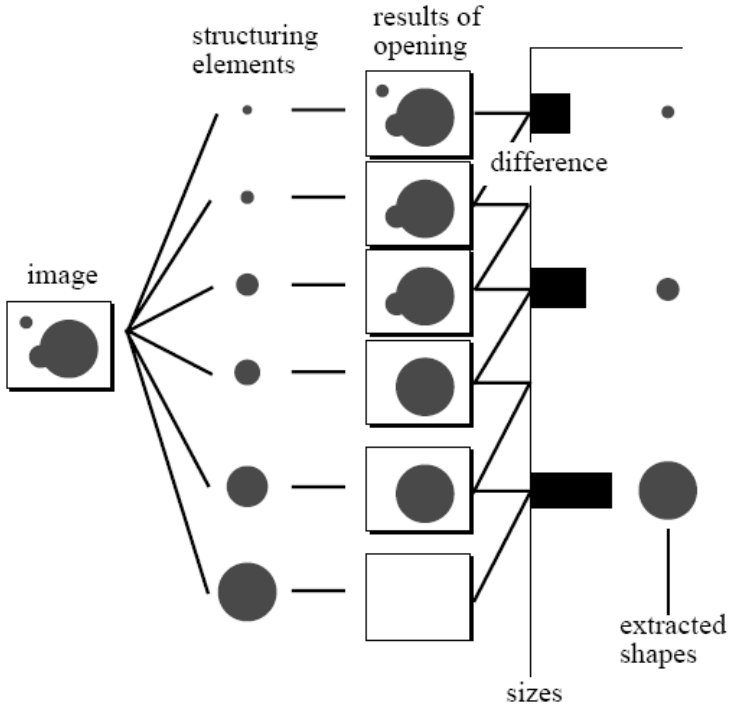

Figure 2.5 Granulometry and size distribution

2.1.3 Morphological image processing techniques

Mathematical morphology had a wide application in image processing from its birth. In image processing and analysis, it is important to extract features of objects, describe shapes and recognize patterns. Such tasks often refer to geometric concepts, such as size, shape and orientation. Mathematical morphology takes these concepts from set theory, geometry, and topography and analyzes geometrical structures in an image. The following lists several commonly used morphological image processing techniques (Shih 2009).

- *Boundary extraction*. It extracts the boundary of an image and empty object inside. For a binary image A, it requires first the eroding of A by a structuring element B and then taking the set difference between A and its erosion. The size of structuring elements determines the thickness of the object contour.
- *Region filling*. It is to fill value 1 into the entire object region of a binary image. Region filling starts by assigning 1 to pixel p inside the object boundary, and then grows by performing iterative dilations until the iteration converges.
- *Thinning and Thickening*. Thinning reduces objects to the thickness of one pixel, but does not change the object's connectivity. Thickening is the morphological dual to thinning. It is used to grow some concavities in an object, but it does not cause merging of disconnected objects.
- *Skeletonization*. It is similar to thinning, but explores in greater details the structure of an object. The skeleton emphasizes certain properties of images, for instance, curvatures of the contour correspond to topological properties of the skeleton.
- *Pruning*. The skeleton of a pattern after thinning usually appears as extra short noisy branches. Pruning is used to clean up these noises as a post processing technique.

2.1.4 Morphological operations on sets and functions

In the literature of morphological image processing, both the input set and the structuring element of morphological operations are treated as the sets. In binary morphology, the sets are defined in $\mathbb{R}^2$. In grey-scale morphology the morphological operations are invoked on the functions defined over a domain in $\mathbb{R}^2$ (Srinivasan 1998). Morphological operations on functions can be mathematically linked to morphological operations on sets through "fill" transforms (Dougherty 1992). Fill transforms convert the curve defined by the function to a two-dimensional set and the surface defined by the function to a three-dimensional set (ISO 16610-40 2010). If the function curve or surface is closed, then the fill transform produce the interior region of the closed curve or surface. Figure 2.6 shows such an example. If the function curve or surface is not closed, then a special fill transform called the "umbra transform" may be applicable. Figure 2.7 demonstrates an example of the umbra

transform. In this example, a curve $f(x)$ is defined over a finite interval of x. Its umbra is the entire two-dimensional region under the curve of the function $f(x)$. Similarly, the umbra of a surface $f(x, y)$ is the entire three-dimensional region under the surface of the function $f(x, y)$. In general, morphological operations of functions of n variables can be shown to be equivalent to the corresponding operations on sets in $\mathbb{R}^{n+1}$. Thus, morphological operations of functions can be derived and justified from the set definitions.

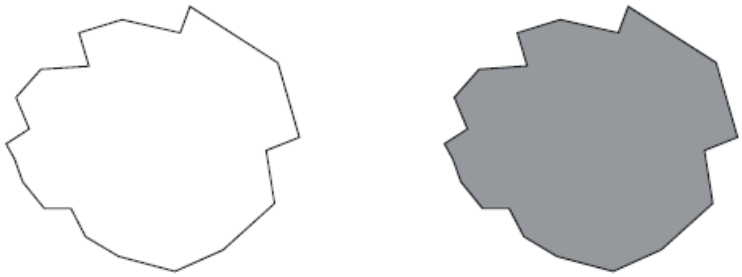

Figure 2.6 Fill transform of a closed curve on the left to a two-dimensional set on the right

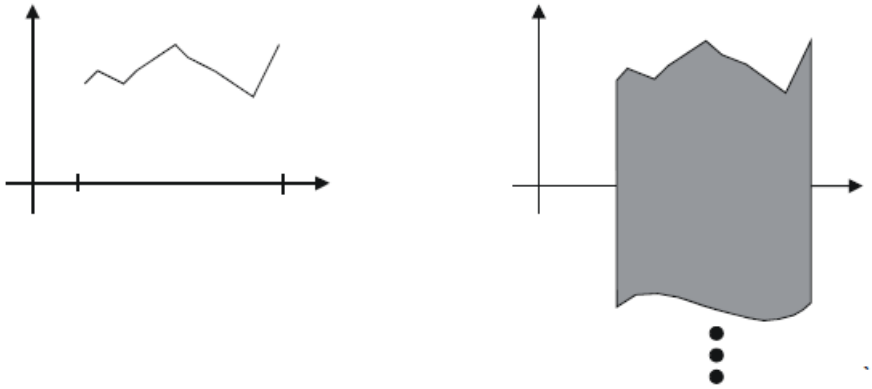

Figure 2.7 Umbra transform of an open curve on the left to a two-dimensional set on the right

2.2 Morphological filters

Morphological filters are evolved from the early envelope filter proposed by Von Weingraber (1956), which is performed by rolling a ball over the surface. The locus of the centre of the rolling ball followed by an offset of the ball radius gives the envelope and it was then considered as the reference line. See Figure 2.8. The

deviation from the envelope was fine texture or roughness. The envelope filter is quite different from mean-line based filters in that the envelope is mainly determined by geometrically prominent peaks on the surface while mean line based filters generate the reference line by an averaging process. In contrast to mean-line based filters, the envelope filter could give better results in function-oriented specification of surface finish due to the two following reasons (Dietzsch *et al.* 2008):

(1) The envelope system depends on geometrical characteristics of the workpiece, which are closely related to functional requirements of workpieces: sliding, adhering, sealing, assembly etc.

(2) With the M-system, there is only little correlation between the standardized surface roughness parameters and functional requirements, while the E-system offers a common reference system to associate all the geometrical elements, including dimension, orientation, form, waviness and roughness.

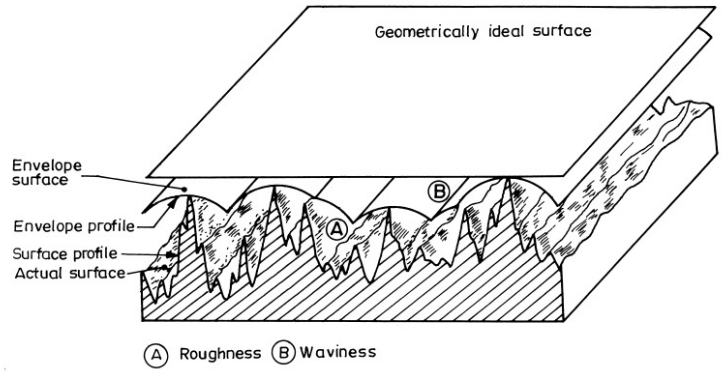

Figure 2.8 Profile and surface envelope (Haesing 1964)

2.2.1 Closing and opening filters

In ISO 16610-41 (2010), morphological filters are defined on the basis of morphological operations and related properties: "*Morphological filters are morphological operations that are monotonically increase and idempotent*".

Morphological operations have some basic properties as they are listed below:

Let $F(A,B)$ denote a morphological operation where A is the input set and B the structuring element.

(1) Rigid motion invariant: an operation does not change under rigid body transformation. If $tF(A,B) = F(tA,B)$ where t is any rigid body transformation, then $F(A,B)$ is rigid motion invariant.

(2) Monotonically increasing: an operation preserves the set containment condition on its operands. If $A_1 \supset A_2 \Rightarrow F(A_1,B) \supset F(A_2,B)$, then $F(A,B)$ is monotonically increasing.

(3) Idempotent: applying the operation one more times does not change the outcome. If $F(F(A,B),B) = F(A,B)$, then $F(A,B)$ is idempotent.

(4) Extensive: the outcome of the operation contains the input. If $F(A,B) \supset A$, then $F(A,B)$ is extensive.

(5) Anti-extensive: the outcome of the operation is contained in the input. If $F(A,B) \subset A$, then $F(A,B)$ is anti-extensive.

The properties of the four morphological operations are listed in Table 2.1 (ISO 16610-1 2010). From the table, it can be seen that closing and opening are both monotonically increasing and idempotent, and dilation and erosion are monotonically increasing but not idempotent. Hence according to the definition of morphological filters, opening and closing are two types of morphological filters whereas dilation and erosion are not.

Table 2.1 Summary of properties of morphological operation

	Dilation	Erosion	Closing	Opening
Rigid motion invariant	Yes	Yes	Yes	Yes
Monotonically increasing	Yes	Yes	Yes	Yes
Idempotent	No	No	Yes	Yes
Extensive	Yes	No	Yes	No
Anti-extensive	No	Yes	No	Yes

ISO 16610 also defines envelope filters that they are rigid motion invariant, monotonically increasing, idempotent and extensive/anti-extensive (extensive for upper enveloper and anti-extensive for lower enveloper). Closing is the upper envelope filter since its output envelops the input profile or surface. Similarly, opening is the lower envelope filter. They differ from the traditional envelope which

in essence is the dilation offset by disk radius towards profiles. As is clearly shown in Figure 2.9, the resulting closing envelope (the solid curve) is a concave structure, whereas the offset dilation envelope (the dotted curve) is a convex structure.

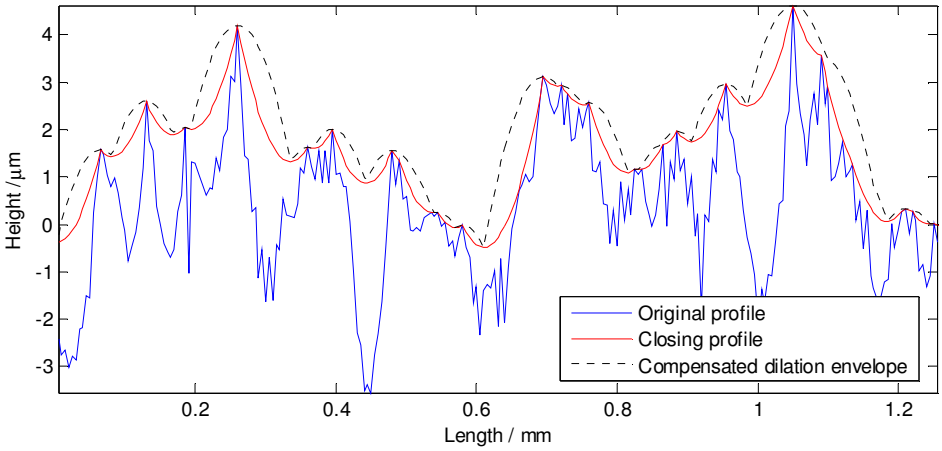

Figure 2.9 The morphological closing profile and the obsolete envelope profile

Figure 2.10 and Figure 2.11 illustrate two examples of applying the closing and opening operation on an open profile with the disk structuring element respectively. The closing filter is obtained by placing an infinite number of identical disks in contact with the profile from above along all the profile and taking the lower boundary of the disks (Scott 2000). On the contrary the opening filter is achieved by placing an infinite number of identical disks in contact with the profile from below along all the profile and taking the upper boundary of the disks.

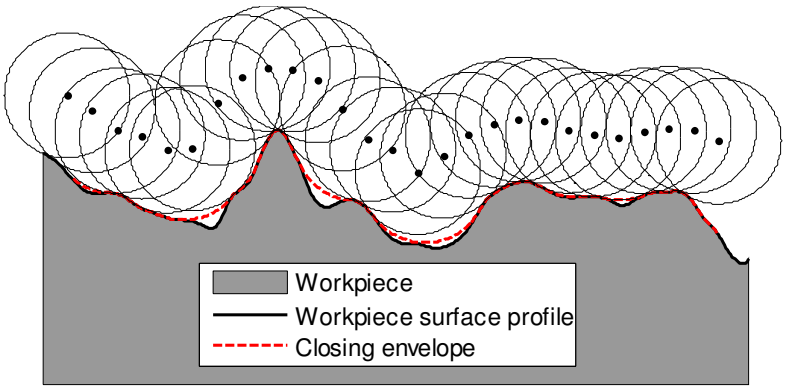

Figure 2.10 The closing envelope of an open profile by a disk

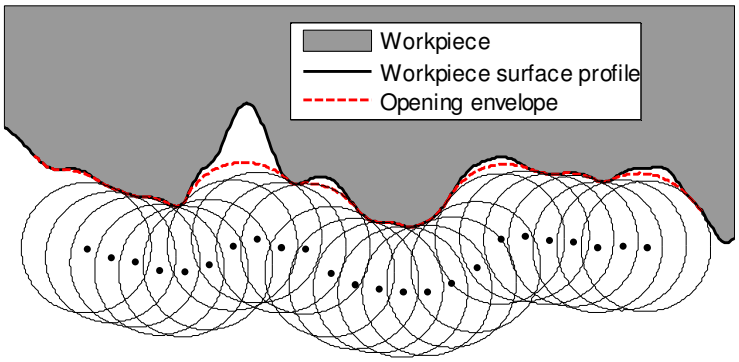

Figure 2.11 The opening envelope of an open profile by a disk

It is obviously revealed that the closing filter suppresses the valleys on the profile which are smaller than the disk radius in size, meanwhile the peaks remain unchanged. Conversely the opening filter suppresses the peaks on the profile which are smaller than the disk radius in size, while it retains the valleys. The selection of the disk radius depends on the size of physical features on the surface of workpiece. Except circular structuring elements, the other most commonly used structuring element presented in ISO 16610 is flat structuring elements, for instance, the horizontal line segment for profile data. If not particularly stated, the circular structuring element shall be the default option (ISO 16610-41 2010).

Table 2.2 lists the "For-Against-Interesting" arguments of morphological filters (ISO 16610-1 2010).

Table 2.2 "For-Against-Interesting" Arguments of morphological filters

For	Against	Interesting
Definition of mechanical surface	Range of application not fully established	Different to Fourier Wavelenghs
Simulates contact phenomena	Outlier sensitive	Non-linear filter
Does not distort Chebyshev Fits		Default filter for establishment of datums
Closed Profiles: no end effects		
Nested set of mathematical Models		
No need to remove form		
Compact support		
Random data spacing possible		
Faster than Gaussian		

2.2.2 Alternating symmetrical filters

ISO 16610-49 (2010) gives the definition of the alternating symmetrical filter that it satisfies the sieve criterion and can eliminate the peaks and valleys below a given scale. The scale is a nesting index. The sieve criterion is a criterion where two mappings applied one after another to a profile/surface is entirely equivalent to applying one mapping with the highest scale. It is like the process of sifting solid particles by two sieves with different mesh openings. The remains left by two sieves are the same as those left with bigger mesh openings.

The alternating symmetrical filter combines the opening and closing of a particular scale in certain sequences. The opening and closing filter will remove peaks and valleys whose widths are less than the given scale respectively. Serra (1982) showed that there are only four possibilities for composing the opening $O_j()$ and closing $C_j()$ with a given scale j and they are morphological filters satisfying the sieve criterion. The four possible combinations are listed below:

$$m_j = O_j(C_j); \qquad n_j = C_j(O_j); \quad r_j = C_j(O_j(C_j())); \qquad s_j = O_j(C_j(O_j()))$$

Thus it is possible to use four different types of combinations for alternating symmetrical filters: the closing-opening filter (M-sieve), the opening-closing filter (N-sieve), the closing-opening-closing filter (R-sieve) and the opening-closing-opening filter (S-sieve). If not particular stated, the M-sieve is the default option.

Table 2.3 lists the "For-Against-Interesting" arguments of alternating symmetrical filters (ISO 16610-1).

Table 2.3 "For-Against-Interesting" arguments of alternating symmetrical filters

For	Against	Interesting
Well defined	Range of application not fully established	Different to Fourier Wavelengths
Nested set of mathematical models	Published algorithms slower than Gaussian	Non-linear filter
Naturally robust		Ball defined by curvature not wavelength
Easy to compute		Sampling theorems (Not Nyquist)
Multi-resolution type analysis possible		Reconstruction possible
End effects easy to handle		
Form removal not necessary		
Defined similar to cut-off wavelengths		

2.2.3 Scale-space techniques

Scale-space techniques are a type of sieving techniques, which could date back to the morphological granulometry (Matheron 1989). It is similar to the process of sieving small solid particles with a series of sieves with increasing mesh openings. The sieve with the smallest opening is used firstly. The grains that are bigger than the mesh opening are kept and counted. The remnant grains are then sifted by the bigger sieve and this process continues until all the sieves are used. In this way grains are classified according to the size of mesh openings.

Scale-space techniques could decompose a signal (profile/surface) into objects of different scale. It uses alternating symmetrical filters of increasing scales to construct a ladder structure as shown in Figure 2.12. The first rung S_0 is the original signal. At each rung in the ladder the signal is filtered by an alternating symmetrical filter at the scale order $i+1$ (M_{i+1}) to obtain the next space scale representation of the signal S_{i+1} which becomes the next rung and a component d_{i+1} that is the difference between the two rungs. In this manner signals at different scales are separated from each other.

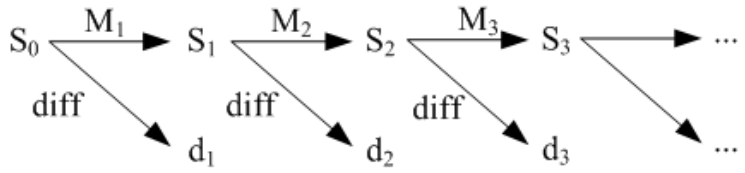

Figure 2.12 The ladder structure of scale space

Scale-space techniques provide a multi-resolution method to decompose signals with wavelet-based filters being another type of multi-scale approach in surface metrology (Jiang *et al.* 2001; Xiao *et al.* 2001). The scale of the alternating symmetrical filter at each rung works like a cut-off value λs . Therefore a "transmission bandwidth" can be defined by calculating the height difference between two rungs: $S_i - S_j$. The scale i is equivalent to the cut-off value λs and the scale j is equivalent to the cut-off value λc .

In comparison to the famous Nyquist theorem used to sample and reconstruct a signal in the frequency domain (Nyquist 1928), for morphological operations and filters, no universal equidistant sampling can be found without loss of information.

However, there are a number of morphological sample theorems which limit the amount of information that is lost. Scale-space techniques are one of these theorems. The original signal could be sampled with various scales and can be reconstructed by reversing the ladder structure mentioned above:

$$S_0 = S_n + \sum_{i=1}^{n} d_i \tag{2.7}$$

The cut-off wavelengths of the multi-scale analysis are always in a constant ratio of 2 to each other. This value is yielded by the experiences in dealing with multi-scale analysis. This ratio is nearly optimal since this value is, on one hand, large enough to clearly differentiate the details of different levels; on the other hand, it is not so large that significant details are lost (Krystek 2004). Based on this recognition, morphological scale-space techniques also choose a ratio of the scales of approximately 2: 1 μm, 2 μm, 5 μm, 10 μm, 20 μm, 50 μm, 100 μm, 200 μm, 500 μm, 1mm, 2mm, 5mm, 10mm, ⋯. This series has an additional advantage that it is consistent with the recommended stylus tip radii of surface texture (ISO 3274 1996). The smallest value of this series is limited by the morphological sampling theorem and therefore can not be smaller than the value of the sampling interval in length. It is sensible to let the series start with the value of stylus tip radius used for the measurement. In principle, there is no upper limit to values for the scale series.

2.3 Applications of morphological operations

Although morphological operations are not as commonly used as the mean-line based filtration techniques, they are of great value if not consciously recognized in practice.

2.3.1 Applications of the dilation and erosion operation

- Surface scanning

The scanning of the workpiece surface using a tactile probe, e.g. the analog probe or the touch trigger probe, is a very common practice in geometrical measurement and a hardware implementation of morphological dilation operation (Krystek 2004). The workpiece surface as the input set is dilated by the structuring element, the probe tip to generate the morphological output, the measured surface, which is also called the

traced surface. Figure 2.13 illustrates the scanning process of a tactile probe. The scanning measurement is conducted by traversing the tip over the surface. The tip centre data are recorded at each sampling position and these sampled data form a discrete presentation of the measured surface. In ISO 3274 (1996), the traced surface profile is defined as "*locus of the centre of a stylus tip which features an ideal geometrical form (conical with spherical tip) and nominal dimensions with nominal tracing force, as it traverses the surface within the intersection plane*".

In common practice, the probe tip employed for scanning used to be small in size. However, the tip size still influences the precision measurement of workpiece surfaces. Figure 2.14 demonstrates the effect of the probe tip traversing over the workpiece surface. By comparing the traced profile with the real workpiece profile in the figure, it is evident that the probe tip tends to round off peaks on the profile making it broader, nevertheless the peak height remains constant. The valleys on the profile are smoothed by the tip becoming narrow, meanwhile the valley height is reduced as well (Dagnall 1998). This effect introduces distortion into measurement of workpiece surfaces and is called as the mechanical filtration effect of tips. For the measurement of workpiece surfaces, especially for the freeform shaped workpieces, the distortions caused by the tip mechanical filtration effect appreciably influences the precision of measurement. Thus the correction to the traced surface is desired in order to restore to the real workpiece surface. However the traced surface is unable to be perfectly reconstructed to the real surface, but only to an approximate one, i.e. the real mechanical surface.

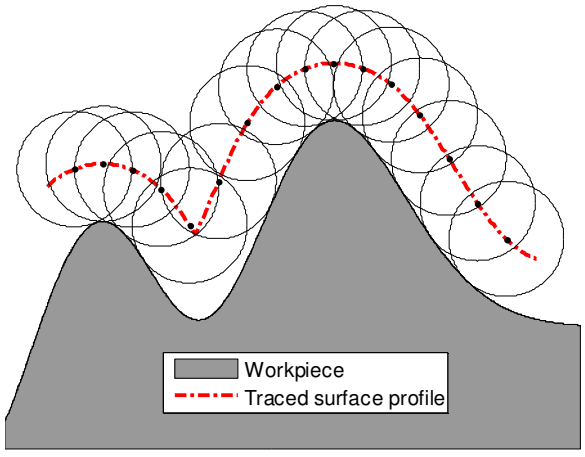

Figure 2.13 A probe tip scanning over the workpiece surface

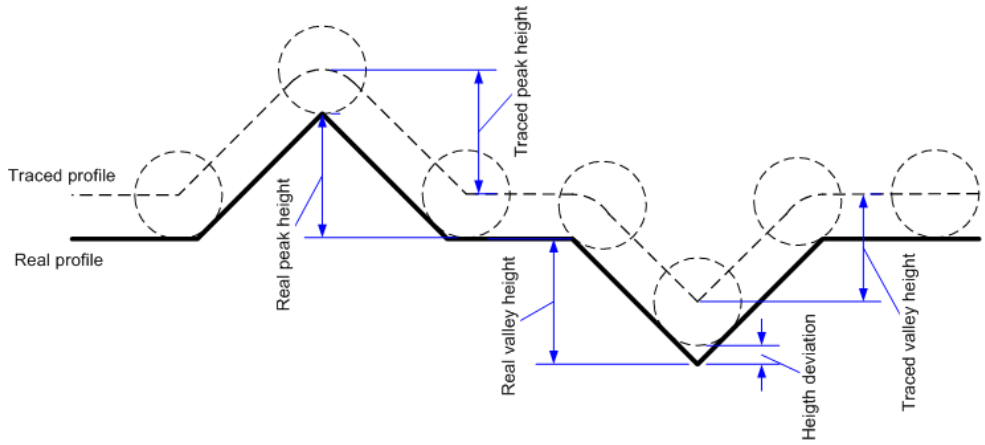

Figure 2.14 Mechanical filtration effects of the probe tip

- Real mechanical surface reconstruction

ISO 14406 (2003) presents the definition of mechanical surface: "boundary of the erosion, by a sphere of radius r, of the locus of the centre of an ideal tactile sphere, also with radius r, rolled over the real surface of a workpiece." Figure 2.15 demonstrates the reconstruction process. Use an ideal sphere with the same size to the probe tip to roll over the traced profile, i.e. the dilated profile by the probe tip (which is already presented in Figure 2.13), the locus of the sphere centre is treated as the mechanical surface. Rolling the ball from the below of the traced surface is in essence an erosion operation.

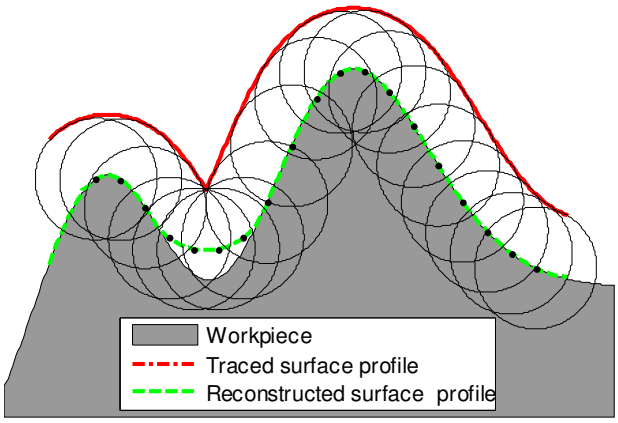

Figure 2.15 Reconstruction of the mechanical surface

It is obvious that the morphological erosion operation is unable to perfectly reconstruct the original real surface of the workpiece. It was reported that morphological operations can only reconstruct those portions of the surface where

their local curvatures are larger than that of the probe tip (Roger *et al.* 2005; Dietzsch *et al.* 2007). This indicates that the real mechanical surface differs from the real surface at the locations where the local surface curvature is small than the tip. Thus the reconstructed real mechanical surface varies with the probe tip size. Figure 2.16 presents such an example. Large probe tips tend to reduce and smooth the surface irregularities, while small tips enable the reconstructed surface to be more approximate to the real surface. The smaller the tip is, the closer the real mechanical surface approximates to the real surface.

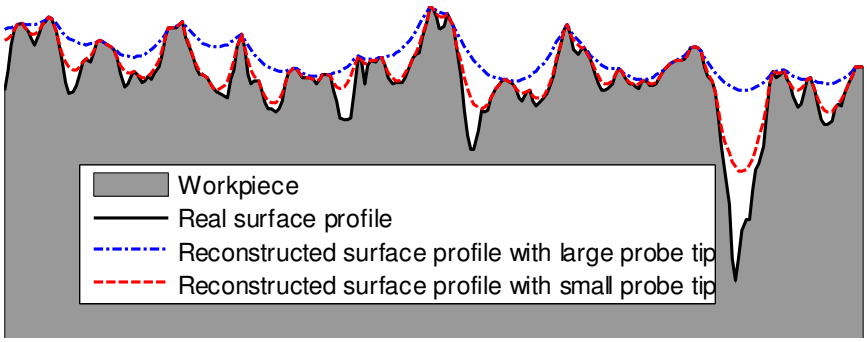

Figure 2.16 Reconstructed real mechanical surfaces vary with the tip size

In industry, the practical implementation of the reconstruction of the real mechanical surface varies from the application requirements. For surface texture instruments, for instance, the profilometer and the atomic force microscope, the reconstruction is usually performed by morphological image processing techniques (David & Fransiska 1993; Villarrubia 1996), whereas in dimensional metrology, for example, coordinate measurement, the reconstruction is usually implemented by the probe radius compensation. Compared to surface texture instruments, sampling of coordinate measurement machine (CMM) is usually less dense and the probe tip much bigger. As Figure 2.17 illustrates a couple of sampling positions, the contact points of the probe tip to the workpiece surface are obtained by compensating the tip radius in the direction of the surface normal at the contact point. The normal vectors for compensation are achieved either by estimating from the measured tip centre data in the case that the surface is densely scanned and nominal data is unavailable (Mayer *et al.* 1997; Wozniak *et al.* 2009), or by using the nominal vector at the matching point on the nominal surface model of the workpiece, e.g. the CAD model (Liang & Lin

2002; Yin *et al.* 2003). Although dimensional metrology and surface metrology employ different routes, both of them are essentially morphological reconstruction to the real surface.

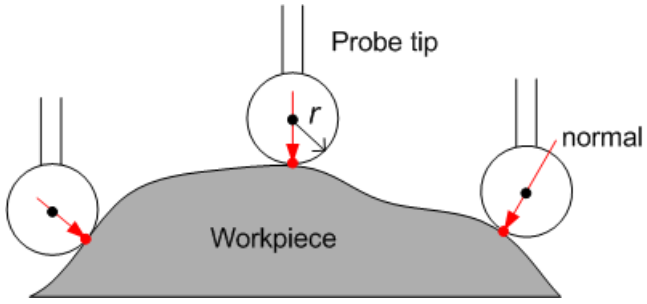

Figure 2.17 The radius compensation of CMM measurement

2.3.2 Applications of the closing and opening filter

- Form approximation

It has been illustrated that morphological envelopes could be utilized to approximate the form of functional surfaces for conformable interfaces (Malburg 2003), for instance a soft gasket in contact with a solid block in order to provide sealing function. The long wavelength component of the block surface could be tolerated by the compatibility of the gasket material while the middle wavelength components result in highly localized contacts. See Figure 2.18. The morphological closing envelope with the circular disk structuring element is used to approximate the conformable gasket surface such that the void areas between the conformable surface and the rigid surface can be obtained to characterize the sealing or load distribution. The radius of the circular structuring element should be chosen based on the compression and bending properties of the conformable component.

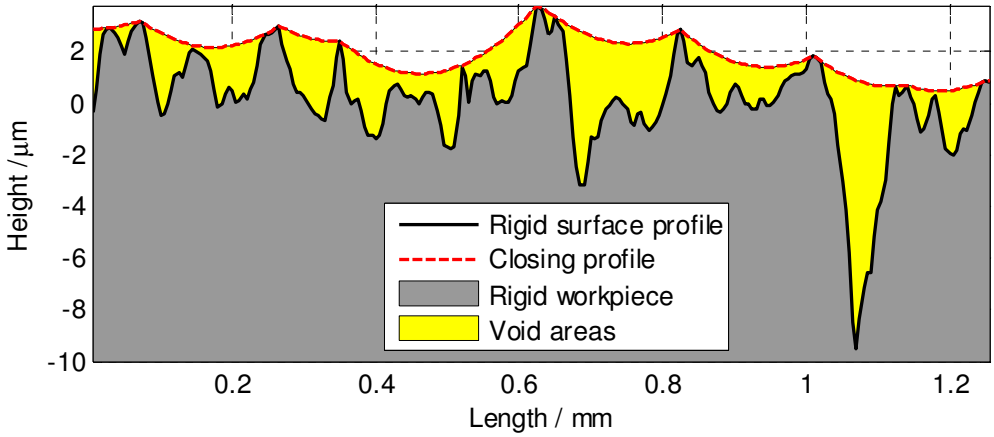

Figure 2.18 Conformable surface form approximation

- Uncertainty zone for possible reconstruction

The workpiece surface is the set of features that physically exist and separate the entire workpiece from the surrounding medium. The inspection of geometrical information of the workpiece surface is conducted by measuring the surface at certain sampling interval, using either the contact measurement instruments (e.g. CMM) or non-contact ones (e.g. interferometer). Either of them generates a series of sampled points, which form a discrete representation of the original surface. It should be noticed that the sampled points in this scenario differ from those presented in the preceding cases in that they are supposed to be the contact points on the real workpiece surface, instead of the tip centre points for tactile measurement. For non-contact measurement, the sample data are all "contact points". It may be desired to reconstruct the original continuous workpiece surface from the discrete sample points. In the theory of signal processing, the Nyquist theorem indicates that an infinitely long band-limited signal could be perfectly reconstructed without loss of information from the discrete data sampled at regularly spaced intervals if that interval is smaller than half of the minimal wavelength comprised by the original signal. In mathematical morphology, there is no theorem equivalent to the Nyquist theorem in that a universal equidistant sampling scheme can be found without loss of information, however there are a number of morphological sampling theorems to limit the amount of information lost (Haralick *et al.* 1989).

Figure 2.19 illustrates an example of determining the uncertainty zone for the reconstruction of the original surface from a sequence of sampled points taken by a

circular disk structuring element. The morphological sampling theorem takes the prerequisite that the surface profile Z under the examination remains unchanged after applying the opening and closing operation by a particular structuring element SE (e.g. a disk) of a given size (e.g. the disk radius), i.e. $C(Z,SE) = Z = O(Z,SE)$. If the original surface Z is sampled with a sampling interval strictly less than the size of SE, yielding a sampled surface Z_s, the original profile is supposed to lie in the region constructed by the opening envelope $O(Z_s)$ and the closing envelope $C(Z_s)$. This region defines the uncertainty zone in which the original profile lies, i.e. $C(Z_s,SE) \le Z \le O(Z_s,SE)$ (ISO 14406 2003).

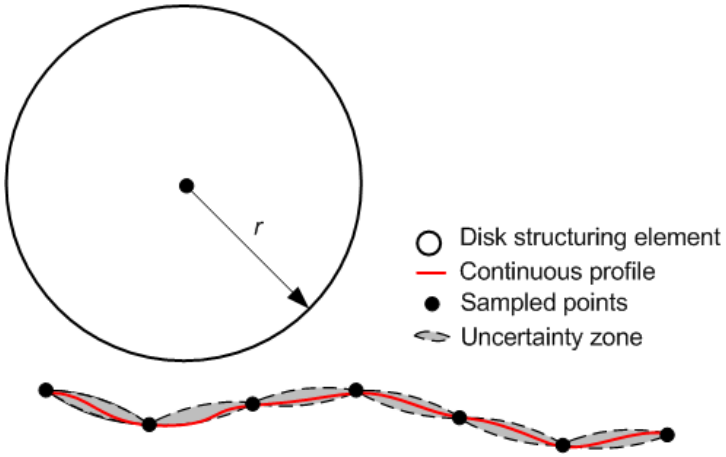

Figure 2.19 The uncertainty zone for possible reconstruction

- Volume-scale analysis

Volume-scale analysis, also known as the variation method, is an areal fractal method (Dubuc *et al.* 1989). It estimates the volume between morphological opening and closing envelopes about a surface using square horizontal flat structuring elements. The size of the structuring elements is varied and the change of volume is recorded. The logarithm of the volume is plotted against the scale of the elements, i.e. the length of the sides of the square structuring elements. See Figure 2.20. As the scale increases so does the volume. The fractal dimension is the slope of the plot, d, plus two, which can be used to indicate the geometric complexity of or intricacy components of a fractal or partially fractal surface (ISO 25178-2 2007).

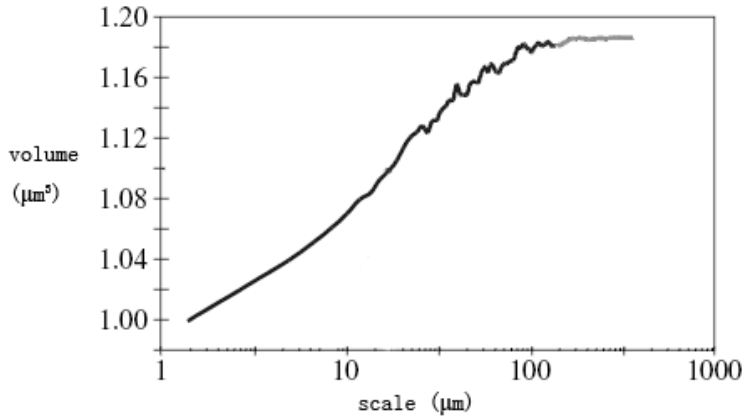

Figure 2.20 Volume-scale plot of a surface

2.3.3 Applications of the alternating symmetrical filter

In engineering, surfaces with stratified functional properties are very common, for instance, the inner surface of cylinder liners for automotive engines. These kinds of surfaces are composed of deep valleys superimposed by plateaux. The plateaux support force, bearing and friction while the valleys serve as lubricant reservoirs and distribution circuits. The traditional method for the analysis of these surfaces is performed by applying the two-stage Gaussian filter, the so-called R_k filter. However there are several drawbacks of this method (Jiang 2010). Firstly, it was derived from the empirical foundation with a significant assumption: the surface contains a relatively small amount of waviness. It is ambiguous and confusing. Secondly, running-in and running-out sections are generated from the Gaussian filter. These sections truncate the profile and only the remained of the measurement data after the truncation are used in evaluation. Thirdly, the form component needs to be removed from the profile before the Gaussian filter could be applied to the data.

In contrast, morphological filters are suited for this kind of surfaces (Lou *et al.* 2011). Using morphological filters, the profile does not need to be pre-processed to remove the form. The roughness profile can be obtained over the complete measurement length if the end effects are cared for, therefore the roughness profile does not have running-in and running-out sections being "removed". Figure 2.21 presents such an example. The experimental profile was extracted from a plateau honed surface. The morphological alternating symmetrical filter, combination of first the closing filter and then the opening filter, with disk radius 5 mm, is employed to generate the reference line. As illustrated in Figure 2.21, the special alternating

symmetrical filter reference line basically follows the form of the closing envelope, which is suitable for surfaces where valley features play a dominant role. The closing filter suppresses all the valleys on the original profile that are smaller than the disk radius and the opening filter removes all the peaks on the resulting closing envelope accordingly. The roughness profile is obtained by subtracting the reference line from the original profile.

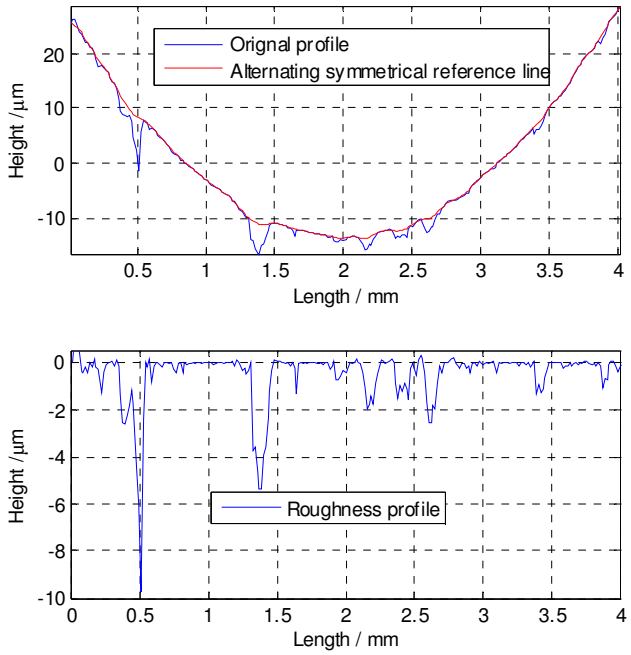

Figure 2.21 Roughness profile resulting from the alternating sequential filter with disk radius 5 mm

Other similar examples include the decomposition of the surface topography of an internal combustion engine cylinder to characterize wear, whereby the plateau roughness and valley was separated and analyzed respectively (Decenciere & Jeulin 2001).

The alternating symmetrical filter uses the structuring element with same size for both opening and closing. The size of the structuring element can even vary according to the requirement of real practices (Kumar & Shunmugam 2005; 2006). Such a kind of filter is referred to as the alternating sequential filter in mathematical morphology.

2.3.4 Applications of scale-space techniques

Examples of using scale-space technique were illustrated in ISO 16610-49 (2010). Figure 2.22 shows a profile which is from a milled surface and was measured with a 5 μm tip stylus. The series of scale values (0.01 mm, 0.02 mm, 0.05 mm, 0.1 mm, 0.2 mm, 0.5 mm, 1 mm, 2 mm, 5 mm) was used starting with the first value (0.01 mm) larger than the stylus tip radius (5 μm).

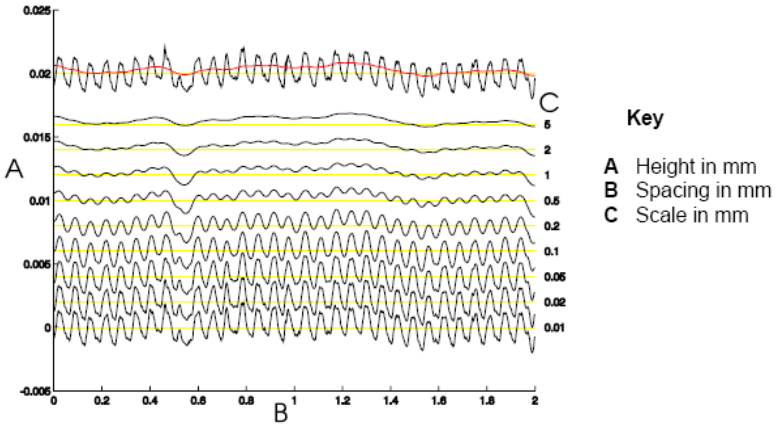

Figure 2.22 Successively smoothed profiles from a milled surface using a circular disk

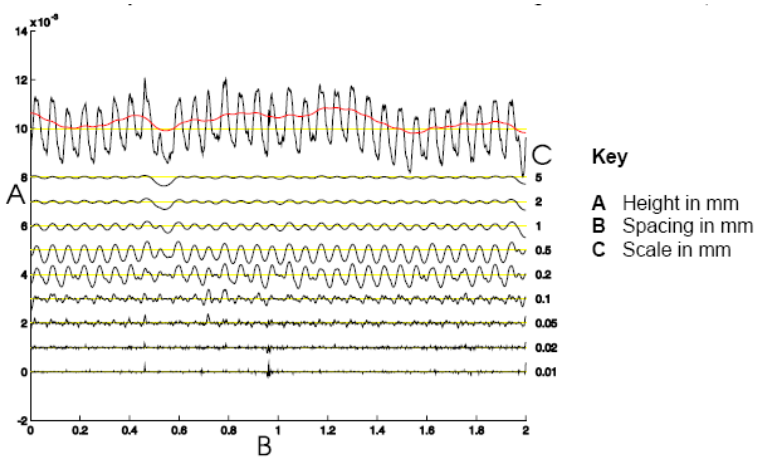

Figure 2.23 Differences on a profile from a milled surface using a circular disk

Figure 2.23 shows the differences between successively smoothing. The deflective milling mark can easily be identified at scales 2 mm and 5 mm and milling marks at scales 0.5 mm and 0.2 mm.

Muralikrishnan & Raja (2005) employed scale-space techniques to analyze the cylinder liner whose inner is a plateau honed surface. It is similar to the case presented by Decenciere & Jeulin (2001). But the notable difference between the two cases is the size of features on the surface was not known in advance while in the former case the size of features was estimated by physical comments.

2.4 Existing algorithms for morphological filters

2.4.1 Naive algorithm

Morphological operations were initially employed in image processing as nonlinear methods. The data processed by morphological operations are the sets composed by image pixels in form of regular grids. For metrological applications, the profile and areal data is usually viewed as the function of one and two variables defined on the sets. Shunmugam & Radhakrishnan (1974) presented an algorithm in a similar manner to image processing. This method is a direct implementation to morphological operations, thus we call it the "naive" algorithm for convenience.

The naive algorithm was originally developed to compute the covering envelope of the disk as it rolls over the profile. The envelope is the locus of the centre of the rolling disk, usually compensated by the disk radius. The uncompensated envelope is in essence the morphological dilation of the profile data. If the disk rolls over the profile from below, the envelope of the rolling disk is the erosion of the profile. Thus according to the definition of morphological operations (Serra 1982), morphological closing and opening could be obtained by combining the dilation and erosion pairs in sequence, either dilation followed by erosion or vice versa.

The naive algorithm takes discrete representation of the input profile and the structuring element as illustrated in Figure 2.24 (The structuring element is a disk in this example). The disk ordinates e_i are computed from the disk centre to the two ends. These ordinates are placed over the profile ordinates with the disk ordinate e_1 over the profile point p_j with height ordinate z_j. The ordinate where the mapping pair $\{(e_i, z_j) | (i = j)\}$ gives the maximum value $\max(e_i + z_j)$ determines the height of the disk centre. The envelope ordinate is given by $\left(\max(e_i + z_j) - e_1\right)$. This procedure

is repeated for all the profile ordinates to obtain the whole envelope. In this sense, the naive algorithm conforms to the definition of the morphological dilation and erosion which are defined as the Minkowski addition and subtraction of the input set and the structuring element respectively.

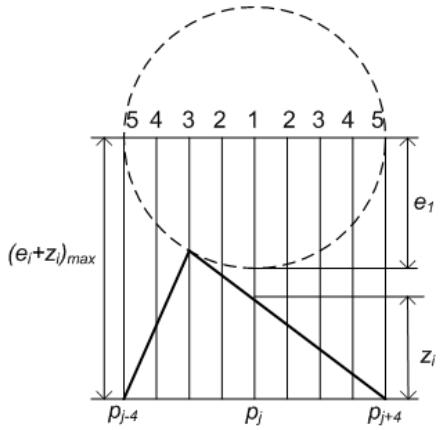

Figure 2.24 Computation of the profile upper envelope

ISO 16610-41 (2010) also presents a basic method to compute discrete morphological filters. The Matlab implementation of this method was presented by Srinivasan (1998). It puts the origin of the structuring element at every point of the input profile, as illustrated for a few positions of a circular structuring element for dilation in Figure 2.25. The extreme value at each position is collected and they form the output envelope. The extreme heights for input points are the results of adding the ordinates of input profile points with the ordinates of sample points on the disk, as marked by the top-most stars at vertical lines in the figure.

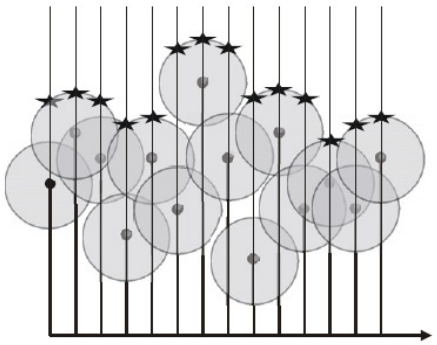

Figure 2.25 Dilation of the profile with a circular structuring element

Essentially the basic approach presented by ISO 16610 is equivalent to the one proposed by Shunmugam & Radhakrishnan (1974). They both take discrete forms of the input profile and the structuring element and compute the envelope ordinate at each sampling position. Figure 2.26 presents the pseudocode of the naive algorithm for morphological dilation. Due to the duality of morphological dilation and erosion, the erosion of opening profiles could be easily computed by first flipping the structuring element and later flipping the dilation result, i.e.,

$$Erosion(X, B) = -Dilation(X, -B). \tag{2.8}$$

Combining morphological dilation and erosion in two opposite sequences results in morphological closing and opening. Figure 2.27 illustrates an example of applying the closing filter to a profile using the naive algorithm. The experimental profile consists of 250 sample data with sampling interval 5 μm. The profile is filtered by a 0.5 mm disk.

```
Algorithm Dilation(X, B)
{Given a profile dataset X with n points and the structuring}
{element B, compute the dilation D of  X  by B.}

j = 1;
m = B.length/2;
while j <= n do
      D(j) = max(z(j-m) : z(j+m) + B);
end while;
return D;
```

Figure 2.26 The Naive algorithm for morphological dilation operation

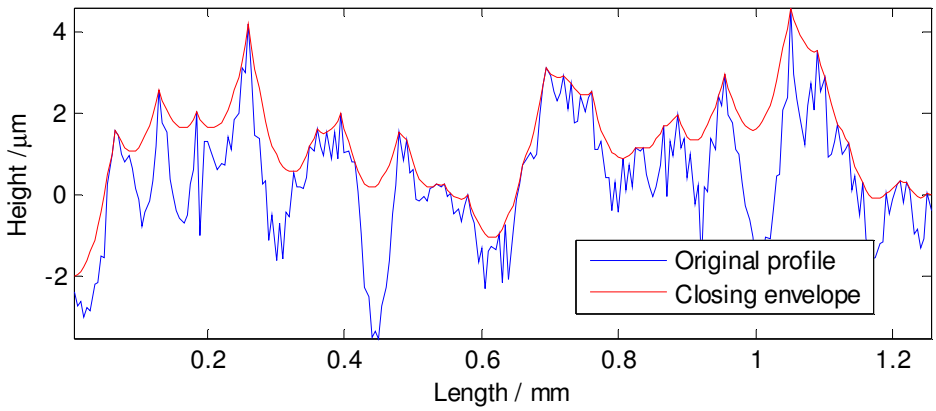

Figure 2.27 The closing envelope computed by the naive algorithm

Several optimization techniques were proposed to improve the efficiency of the naive algorithm (Radhakrishnan & Von Weingraber 1969; Tholath & Radhakrishnan 1999). These methods identify the "prominent" peaks on the surface and only consider the peak points instead of all the points on the surface while calculating the envelope, thus the computation efficiency was improved. However these methods took several prerequisites, for example the radius of the rolling ball is assumed to be larger than the maximum height of surface irregularities, and there was no evidence showing that they could give the correct results.

Another possible solution for morphological filters is also indicated by ISO 16610-41 (2010):"*any technique that can compute Minkowski addition and subtraction can be used to compute closing and opening morphological filters and the respective envelope filters*". However existing algorithms for Minkowski operations run in time complexity $O(n^2 \log n)$ (O'Rourke 1994), therefore they are not suitable for the computation of morphological filters.

2.4.2 Motif combination algorithm

Scott (1992) proposed an alternative way to calculate the profile envelope using the motif combination. A couple of definitions were given as the data type used in the algorithm.

Events: an event splits the profile into a number of discrete sections. The events might be the highest points on all the local peaks or all the upcrossing of the profile through a reference line or even every sample point of the profile. They are numbered in order along the profile. The initial set of events is all the sample points on the profile.

Motif: a motif (i, j), where $i < j$, consists of that section of the profile between the i th and j th events.

Motif Combination Test: it is performed on two adjacent motifs (say, two motifs (i, j) and (j, k)) with the common event (say, j) to determine if the common event is significant or not. If the event is not significant, two adjacent motifs to that event are combined (say, motifs (i, j) and (j, k) are combined to form a new motif (i, k)) and thus the event is eliminated. For rolling a disk on the profile, the functional motif

combination test is to check if the disk is possible to contact the common event by placing the disk on two adjacent motifs.

The motif combination algorithm starts with the set of all events, namely all the sample data on the profile, and then it eliminates the insignificant events by repeatedly applying the motif combination test until all adjacent motifs pass the test. Scott found a set of criteria that the motif combination had to satisfy so that the order of the motif combinations did not matter, they all resulted in the same final motifs. Both the rolling disk and the sliding line segment satisfy these criteria. The pseudocode of the motif combination algorithm is presented in Figure 2.28.

```
Algorithm MotifCombination(X, B)
{Given a dataset X with n points and the structuring}
{element B, compute the final motifs motifs }

Chain list motifs= {(p1, p2), (p2, p3), …, (pn-1, pn)};
while 1
      if CombineMotifs(motifs, B)
            break;
      end if;
end while;
return motifs;

Procedure CombineMotifs(motifs, B)
flag = false;
motif1 = motifs(1);
for i = 2 to motifs.length
      motif2 = motifs(i);
      if CombineTest(motif1, motif2, B)
            motif1 = {motif1.Start, motif2.End};
            motifs.Remove(motif2);
            flag = true;
      end if;
end for;
return flag;
```

Figure 2.28 The motif combination algorithm for morphological filters

The profile motif combination method results in a sequence of final motifs which are significant. The set of events specifying these motifs are the points which may contact the disk while it is traversing the profile. With the significant motifs, the envelope ordinates of the circular structuring element are computed by interpolating points on the arcs determined by the motifs at each sampling position. For the line segment structuring element, the profile envelope ordinates are given by the smaller one of the two events of each final motif. Using this method, the same experimental

profile data used previously is filtered by the morphological closing filter with the disk of the same radius. Figure 2.29 illustrates the closing envelope along with the upper envelope covering the final significant motifs.

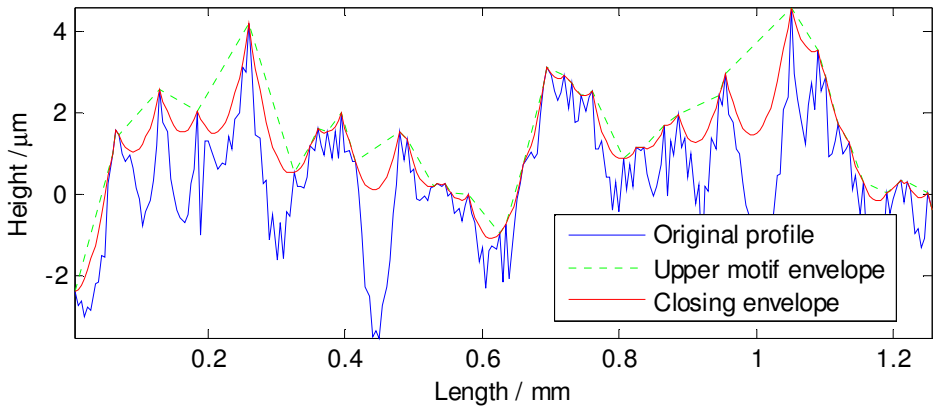

Figure 2.29 The closing envelope and the upper envelope covering the final significant motifs computed by the motif combination algorithm

2.4.3 Limitations

The naive method of morphological filters, although easy to implement, has a couple of limitations. It is restricted to "planar" surfaces in that it models the surface as the height variation with respect to sampling positions, which is similar to the grey tone image. These surfaces are actually two-dimension manifolds embedded in the Euclidean spaces $\mathbb{R}^3$ (Jiang *et al.* 2011a). With the advancement of modern manufacturing techniques, freeform surfaces with complex geometry emerge, for example, the surface of the F-theta lens, where no rotational or translational symmetry can be observed. For freeform surfaces, the data might be specified by coordinate pairs/triplets rather than regular surface heights. The naive method does not work for freeform surfaces. Even for planar surfaces, they are not robust against rotation in space. Another shortcoming lies in the destructive end effects for surfaces in the presence of a significant form component. With the advancement of measurement capability of current instruments, there is a trend that the measured data consist of both the dimensional information (size, form etc.) and that of the surface texture. As a result, the filtration will be badly distorted in boundary regions when using structuring elements of a large size.

A further issue regarding the naive method is its inaccuracy in capturing the contact points of the measured surface with the structuring element, which are physically important because these points could provide a general indication of surface portions which are most likely to be active in the initial stages of wear. The detection of the contact points by the naive method is impractical due to the fact that this method is dependent on the numerical comparison between the original data and the closing or opening envelope, namely the measured points on the original profile that do not change with the closing or opening operation. This comparison is limited to the accuracy of the algorithm and sensitivity to round off errors in calculation. This situation is further worse when sampling the structuring element discretely.

Besides the limitations mentioned above, morphological filters also suffer from two practical issues raised in the employment of the naive method. For one thing, for areal surface dataset with a large quantity of measured points, the method is extremely time-consuming. Even using the current available commercial surface analysis software, e.g. Mountain Map (Digital Surf), the performance is far from satisfactory. Not to mention the size of structuring elements is also restricted from growing too big due to the fact that the computational time is in logarithmical proportion to the size of structuring elements. For example, Mountain Map costs a couple of seconds for computing the morphological closing envelope of a $20\ \mu m \times 20\ \mu m$ surface with 512×512 points using a ball with radius 2 μm, but around ten minutes when the ball radius goes up to 40 μm, and the ball radius available is limited in that it cannot go beyond 40 μm. For another, the existing methods are acting in a similar manner to image processing where the data are treated as uniformly distributed pixels, and are unsuited to non-uniform sampled data. This further limits their usage in the field of dimensional metrology where adaptive sampling is allowed.

The motif combination method achieved much better performance. However it is limited to profile data. For areal data, no literature can be found for calculating morphological envelopes. Even though there exist areal extensions to profile motifs (Scott 1998; Scott 2004; Barre & Lopez 2000), areal motifs can not be employed to compute morphological filters due to the fact that the combination of areal motifs is totally different from the functionality of morphological areal filters, e.g. rolling a ball over the surface.

2.5 Summary

The basis of morphological filters is in mathematical morphology. The morphological closing filter and open filter are derived from morphological operations; scale-space techniques originate from the granulometry transform. Initially mathematical morphology was mainly developed in image processing, it was then introduced into other disciplines, including geometrical metrology. Compared to the mean-line filtration techniques, morphological filters are more relevant to geometrical properties of surfaces and are thus suitable for the functional prediction of surfaces.

Morphological filters are generally accepted and regarded as the complement to mean-line filters. They have found many applications in real practice. The scanning process of a tactile probe and the reconstruction of real mechanical surface are dilation and erosion operations respectively. The closing and opening filter could suppress valleys and peaks on surfaces respectively. They are able to approximate the form of functional surfaces. The region constructed by the closing and opening envelopes provides an uncertainty zone for possible reconstruction of original surfaces from discrete sampled data, with limited loss of information. The volume-scale fractal analysis is conducted on the basis of computing morphological opening and closing envelopes. The alternating symmetrical filter is an optimal alternative to the two-stage Gaussian filter for the evaluation of stratified functional surfaces. Scale-space techniques can decompose the surface into different scales in a similar manner to wavelet based techniques.

The existing implementations of morphological filters have a number of shortcomings. They are either limited to planar surfaces, unsuitable for uniform sampled surfaces or hard to extend to areal data. The poor performance in case of huge areal data (e.g. surfaces larger than 1024×1024) and large structuring element is another deficit. Some of them badly suffer from the end distortion in the presence of data consisting of significant form component. Due to these limitations, morphological filters are not universally adopted in practice.

Motivated by modern manufacturing and measuring technologies, there is a big demand for morphological filters with capabilities in dealing with surfaces with complex geometry and adaptive sampling, accuracy in capturing the contact points on surfaces, and efficiency in computing large datasets.

3. MORPHOLOGICAL METHOD BASED ON THE ALPHA SHAPE

In this chapter, a novel morphological method is proposed with the aim of overcoming the deficits of traditional methods. The closing and opening envelopes with the circular structuring element are generated by rolling a ball over the surface from above and below respectively. These envelopes are closely related to the hull obtained by rolling the ball over the discrete point set sampled on the surface, which is a special geometrical structure called the "alpha hull". This chapter will first give an introduction to the alpha hull and its related geometrical structure, the "alpha shape". Afterward the link between the alpha hull and morphological operations will be presented. Following that, a practical algorithm for morphological filters will be developed on the basis of alpha shape theory. The nomenclature for this chapter is given by Table 3.1.

Table 3.1 Nomenclature

$X \subset R^d$	Point set X in R^d
∂b	The boundary of b
$S_\alpha(X)$	The alpha shape of the point set X with the alpha ball radius α
σ_T	k-simplex where $\lvert T \rvert = k+1$
$DT(X)$	Delaunay triangulation of the point set X
$C_\alpha(X)$	The alpha complex of the point set X with the alpha ball radius α
X^c	The complement of X
$H_\alpha(X)$	The alpha hull of X

3.1 Alpha shape for shape description

The alpha shape was introduced by Edelsbrunner in the 1980's aiming to describe the specific "shape" of a finite point set with a real parameter controlling the desired level of details (Edelsbrunner & Muche 1994). Conceptually the alpha shape is a generalization of the convex hull of a point set. Imagine a huge block of styrofoam

making up the space containing some solid particles. To use a spherical eraser of radius α to carve out all the styrofoam blocks from inside and outside without bumping into the solid particles (see Figure 3.1), it will eventually end up with an object with arcs, caps and points. The boundary of the resulting object is called the alpha hull. If the round faces of the object are straightened by line segments for arcs and triangles for caps, another geometrical structure, the alpha shape, forms (Fischer 2000).

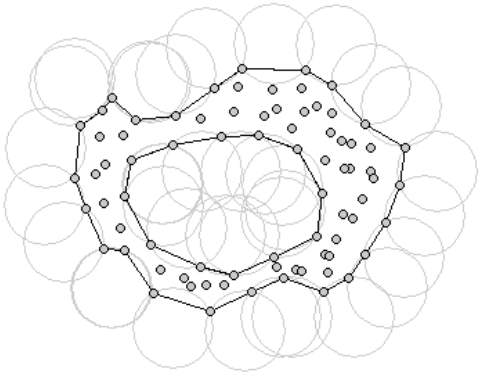

Figure 3.1 Alpha hull and alpha shape of planar points

3.1.1 Alpha shape

In the context of the alpha shape, the sphere eraser in the above example is called the alpha ball. It is formally defined as an open ball of radius α. Given a point set $X \subset R^d$, a certain alpha ball b is empty if $b \bigcap X = \varnothing$. With this, a *k*-simplex σ_T is said to be α-exposed if there exists an empty alpha ball b with $T = \partial b \bigcap X$ ($|T| = k+1$) where ∂b is the surface of the sphere (for *d*=3) or the circle (for *d*=2) bounding b, respectively. For $0 \le \alpha \le \infty$, the alpha hull of X, denoted by $H_\alpha(X)$, is defined as the complement of the union of all empty α-balls.

Definition 3.1 $\partial S_\alpha(X)$, the boundary of the alpha shape of the point set X, consists of all *k*-simplices of X for $0 \le k < d$ which are α-exposed,

$$\partial S_\alpha(X) = \{\sigma_T \mid T \subset X, |T| = k+1, \sigma_T \ \alpha - exposed\} \tag{3.1}$$

3.1.2 Delaunay triangulation

The computation of the alpha shape is based on the Delaunay triangulation which is one of the most exhaustively examined problems in computational geometry (O'Rourke 1994). Given a point set $X \subset R^d$, the Delaunay triangulation is a triangulation $DT(X)$ such that no point in X is inside the circumsphere of any d-simplices σ_T with $T \subset X$. The relationship between the Delaunay triangulation and the alpha shape is that the boundary of the alpha shape ∂S_α is a subset of the Delaunay triangulation of X , namely

$$\partial S_\alpha(X) \subset DT(X). \tag{3.2}$$

3.1.3 Alpha complex

The relationship (3.2) means all the simplices in $DT(X)$ are candidates for the alpha shape. In order to further find which simplex in $DT(X)$ belongs to $\partial S_\alpha(X)$, another concept, the alpha complex $C_\alpha(X)$, was introduced by Edelsbrunner & Muche (1994).

Set ρ_T the radius of the smallest circumsphere b_T of σ_T . For $k=3$, b_T is the circumsphere; For $k=2$, b_T is the great circle; And for $k=1$, the two points in T are antipodal on b_T .

For a given point set $X \subset R^d$, the alpha complex $C_\alpha(X)$ is the following simplicial subcomplex of $DT(X)$. A simplex $\sigma_T \in DT(X)$ ($|T| = k+1$, $0 \le k \le d$) is in $C_\alpha(X)$ if:

- $\rho_T < \alpha$ and ρ_T -ball is empty, or
- σ_T is a face of other simplex in $C_\alpha(X)$.

The link between the alpha complex and the alpha shape is: the boundary of the alpha complex makes up the boundary of the alpha shape, i.e.

$$\partial C_\alpha(X) = \partial S_\alpha(X) \in DT(X). \tag{3.3}$$

3.2 Link between the alpha hull and morphological operations

The boundary of the alpha hull is obtained by rolling the alpha ball over the point set. By intuition the alpha hull seems very similar to the secondary morphological operations, opening and closing, as the alpha ball acts as a spherical structuring element and the input set as the points set. In fact a theoretical link exists between the alpha hull and morphological opening and closing, as proved by Worring and Smedulers (1994). They extended Edelsbrunner's work, proposed the alpha graph and utilized it to describe the boundary of the point set. They also found the relationship between the alpha graph and the opening scale space from mathematical morphology. Based on that, it was proved that the alpha hull is equivalent to the closing of X with a generalized ball of radius $-1/\alpha$. Hence from the duality of the closing and the opening, the alpha hull is the complement of the opening of X^c with the same ball as the structuring element.

3.3 Proposed algorithm based on alpha shape

In surface metrology and dimensional metrology, surfaces are measured by measurement instruments. The measured points are a discrete representation of the surface. Viewing this sampled data as a finite point set in the context of the alpha shape and according to the link between the alpha hull and morphological operations, we employ the alpha shape to compute morphological filters for surfaces.

3.3.1 Spike detection and points interpolation

In practical measurement of surfaces, it may happen that sharp spikes exist in sample data. Sometimes the space between the peak point and the pit point is quite large so that the ball will run into the interior of the profile/surface. This is not allowed in reality because the real surface is physically continuous and won't allow the ball to enter. The difference between the physical continuity of the surface and the discrete representation of the sample data is the quintessence of this problem.

To correct these singularities, sharp spikes should be detected and enough points linearly interpolated on the ridge of the spike to prevent the ball from passing through. The whole process is elaborately depicted in Figure 3.2 for the case of profile data. p_1, p_2, …, p_{10} are the sample points on the original profile. $p_3p_4p_5$ forms a local peak. p_3 and p_4 are spacing so far from each other that the ball could roll into the

profile interior. In this case the additional points i_1, i_2 (and more if needed) are linearly interpolated to reduce the gap between p_3 and p_4. For areal data, surfaces can degenerate to profiles if considering them as the composition of parallel profile sections. There is a trivial difference between the closing envelope and the opening envelope in their spike detection. For the closing envelope, it suffices to detect peak spikes in that the closing envelope is only determined by peaks, and valleys could be ignored. As opposed it is enough to search valleys for the opening envelope because the opening envelope is only affected by valleys.

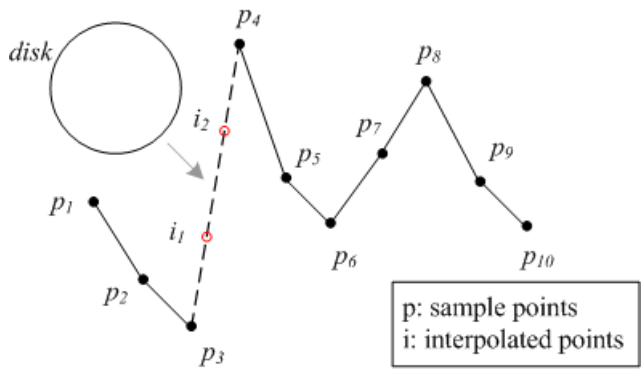

Figure 3.2 Spikes detection in measured data

3.3.2 Alpha shape computation

With the justified data, the next step of the computation is to triangulate the dataset by the Delaunay triangulation and subsequently obtain the facets of the boundary of the alpha shape, which are also contained in the boundary of the alpha complex ∂C_α according to Section 3.1.

Delaunay triangulation results in a series of k-simplices σ ($k=2$ for profiles, which are triangles, and $k=3$ for surfaces, which are tetrahedrons). These k-simplices can be categorized into two groups: k-simplices σ_p whose circumsphere radius is larger than the radius of the rolling ball α, and k-simplices σ_{np} whose circumsphere radius is no larger than the radius of the rolling ball α.

σ_p consists of two parts: the $(k-1)$-simplices σ_{int} interior to σ_p, and the $(k-1)$-simplices σ_{reg} that bounds its super k-simplices σ_p. See Figure 3.3. We

called σ_{reg} the regular facets. σ_{np} is comprised of three components: the $(k-1)$-simplices σ_{ext} out to C_α, part of the regular facets σ'_{reg} shared by both σ_p and σ_{np}, and the $(k-1)$-simplices σ_{sing} that are the other part of ∂C_α. We call σ_{sing} the singular facets. σ_{sing} differs from σ_{reg} in that it does not bound any super k-simplices. σ_{sing} satisfies two conditions as follows:

- The radius of its smallest circumsphere is smaller than α.
- The smallest circumsphere is empty.

The regular facets σ_{reg} and the singular facets σ_{sing} form the whole boundary of the alpha complex, i.e. the boundary of the alpha shape, as the equation (3.5) presents.

$$\partial S_\alpha = \partial C_\alpha = \sigma_{reg} + \sigma_{sing} \tag{3.5}$$

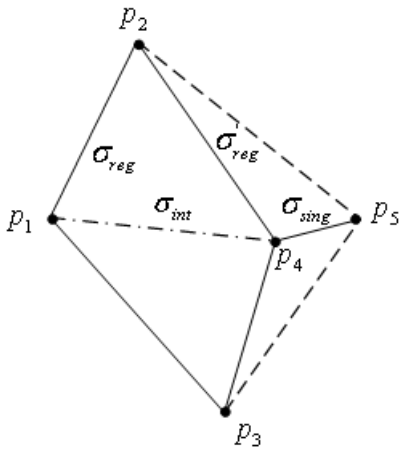

Figure 3.3 Regular and singular faces

The skeleton of the algorithm for computing the regular facets and the singular facets of ∂S_α is given by Figure 3.4. The *DelaunayTri* operation generates a list of *k*-simplex σ_{k+1} (*k=2* for profile data and *k=3* for areal data). The algorithm loops to check if each (*k-1*)-simplex σ_k is the regular facet σ_{reg} or the singular facet σ_{sing}. The regular facets and the singular facets are computed separately so that they could be handled respectively by later manipulations. The *CircumSphere* operation computes the radius of the circumsphere of σ_{k+1}. *SmallCircumSphere* operation calculates the radius of the smallest circumsphere of σ_k. The *Unique* operation checks if σ_k's super

simplices σ_{k+1} with their circumsphere radius larger than α are unique. The *IsSphereEmpty* operation detects if the circumsphere of σ_k is empty.

Aiming to improve the algorithm efficiency, a useful property of the alpha shape is applied to speed up the *IsSphereEmpty* operation, i.e. empty ball testing. This property is that to test whether the circumsphere of a facet is empty it suffices to check whether the opposite vertices of its super simplices are out to the circumsphere boundary. It is much more efficient than checking all other points, which could be huge in the case of areal data. Figure 3.5 illustrates an example of the sample points of a surface along with the facets of ∂S_α. In fact, the vertices of these boundary facets are the points on the surface that contact the ball (disk) as it is rolling over the surface all around.

```
Procedure AlphaShape (X, α)
{Given a justified dataset X and the chosen ball radius α, computes}
{two lists σ_reg, σ_sing  of the regular facets and the singular facets }
{of the boundary of the alpha shape of X.}
Begin
    σ_{k+1} =DelaunayTri(X);
    i=1; j=1;
    for each σ_k do
        r=CircumSphere(σ_{k+1});
        if r<α
            if Unique(σ_k)
                σ_reg(i)= σ_k;
                i=i+1;
            end if;
            continue;
        end if;
        r=SmallCircumSphere(σ_k);
        if r<α
            if IsSphereEmpty(σ_k)
                σ_sing(j)= σ_k;
                j=j+1;
            continue;
            end if;
        end if;
    end for;
    return (σ_reg, σ_sing);
end AlphaShapes;
```

Figure 3.4 Skeleton of the algorithm to compute the facets of the boundary of the alpha shape

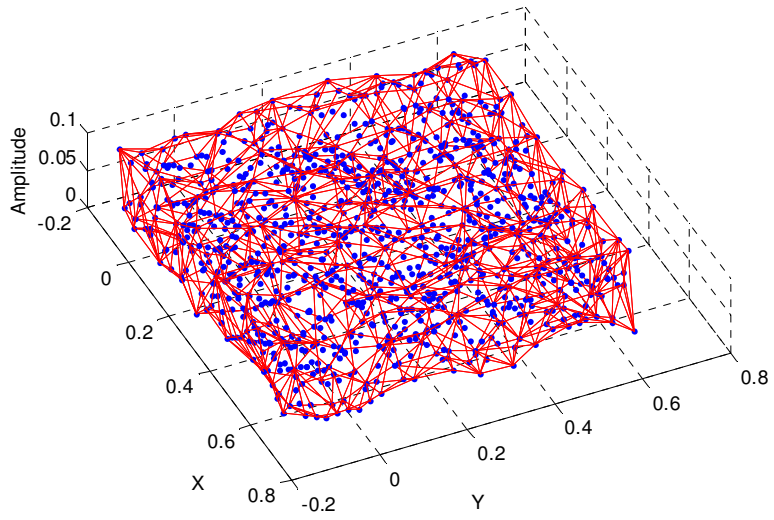

Figure 3.5 Areal sample points of a surface and the facets of the boundary of the alpha shape

3.3.3 Facets reduction

Having the facets of ∂S_α, opening and closing envelopes could be calculated. For open profiles/surfaces, not all but parts of the facets of ∂S_α are needed for the computation of an envelope. For closing envelopes, only the upper part of the regular facets is of interest, and vice versa for opening envelopes. Therefore the number of the regular facets used for the envelope computation could be reduced by extracting those facets which are possible candidates for the computation.

Supposing there are no re-entrant features on the surface, regular facets can be separated according to their normals. We define the normal of a facet as the vector that is perpendicular to the facet and pointing from the interior of boundary shape to its outside. The regular facet has a unique super simplex. The opposite vertex in its super simplex could help to justify the normal vector from two possible candidate perpendicular vectors. Figure 3.6 illustrates how a facet normal is achieved for profile data. p_1p_2 is one of the regular facets. p_o is the opposite vertex of its super simplex $p_1p_2p_o$. The facet p_1p_2 has two possible normal vectors, n_1 pointing outward, and n_2 pointing inward. The vector e which is from p_o to one of the facet vertices (p_1 or p_2) determines the outward direction. Being consistent with the orientation of e, n_1 is chosen as the normal of the facet p_1p_2. This method could be also reasonably extended to areal data.

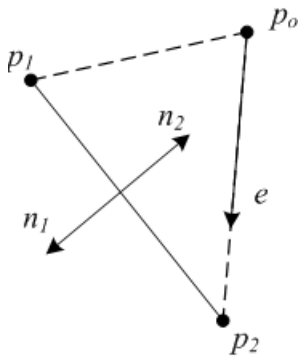

Figure 3.6 Determination of the normal of a regular facet

Once the normals of the regular facets are settled, the separation of the upper part and lower of regular facets is available. The regular facets are connected and their normals are oriented consistently. As to the upper part of the regular facets, their facet normals are oriented upward, and vice versa. Thus this property could be used to separate the upper part and lower part of the regular facets. Figure 3.7 demonstrates the separation of the upper regular facets and the lower regular facets. f_1, f_2, $\cdots$, f_5 are part of the regular facets of the boundary of the alpha shape, with n_1, n_2, $\cdots$, n_5 being their normals respectively. Suppose the ball is rolling from f_1 to f_5. The normal of first three facets n_1, n_2, n_3 are oriented consistently (all of them are pointing upward). Then the ball continues to roll to the facet f_4, the facet normal n_4 turns to orient downward, and n_5 keeps consistent with n_4, orienting downward also. Hence the facets can be separated into two parts: f_1, f_2, f_3 are the upper facets, and f_4, f_5 are the lower facets. For the computation of the closing envelope, the lower facets f_4, f_5 are neglected because they have no impact on the computation of the closing envelope.

For the singular facets, this idea does not make sense for two reasons. On one hand, the singular facet may have more than one super simplex, therefore unable to determine its normal. On the other hand, even though a singular facet only has one super simplex, it is still hard to determine the normal because the singular facets could be disconnected and the vector e used in figure 3.6 cannot indicate the outward or inward orientation.

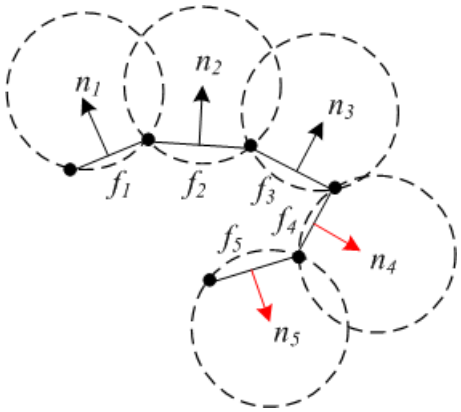

Figure 3.7 Separation of the upper regular facets and the lower regular facets

3.3.4 Envelope coordinate calculation

The final step is the calculation of the envelope coordinates. For each sample point, there is a one-to-one corresponding point on the envelope. These points form a discrete representation of the envelope. Each facet of the boundary of the alpha shape determines its counterpart on the alpha hull. Due to the fact that the target envelope is contained in the alpha hull, we project the sample points onto the alpha hull in the direction of the local gradient vector and record the extreme project coordinates, namely the envelope point for this sample point.

For "planar" open surfaces, all of the local gradient vectors are supposed to be perpendicular to the reference plane, i.e. the amplitude direction. Figure 3.8 illustrates the acquisition of the closing envelope points by projecting them onto the alpha hull for the planar open profile data (a) and areal data (b) respectively. In Figure 3.8(a), the facet f determines an arc $\overset{\frown}{p_1p_2}$ from the point p_1 to p_2, which is a part of the alpha hull. The sample point p has its sampling position s between the sampling position s_1 and s_2 for p_1 and p_2 respectively. p is projected to the arc $\overset{\frown}{p_1p_2}$ in the amplitude direction to obtain the envelope point v. In Figure 3.8(b), the facet f determines a cap $\overset{\frown}{p_1p_2p_3}$ as a part of the alpha hull. The sample point p has its sampling position s inside the triangle area $\Delta s_1s_2s_3$. s_1, s_2 and s_3 are the sampling position for p_1, p_2 and p_3 respectively. p is projected to the cap $\overset{\frown}{p_1p_2p_3}$ in the direction of amplitude to obtain the envelope point v. The extreme projection heights for all the sample positions are recorded (Highest heights for the closing envelope and lowest heights

for the opening envelope). These extreme projection coordinates are the final results for the target envelope.

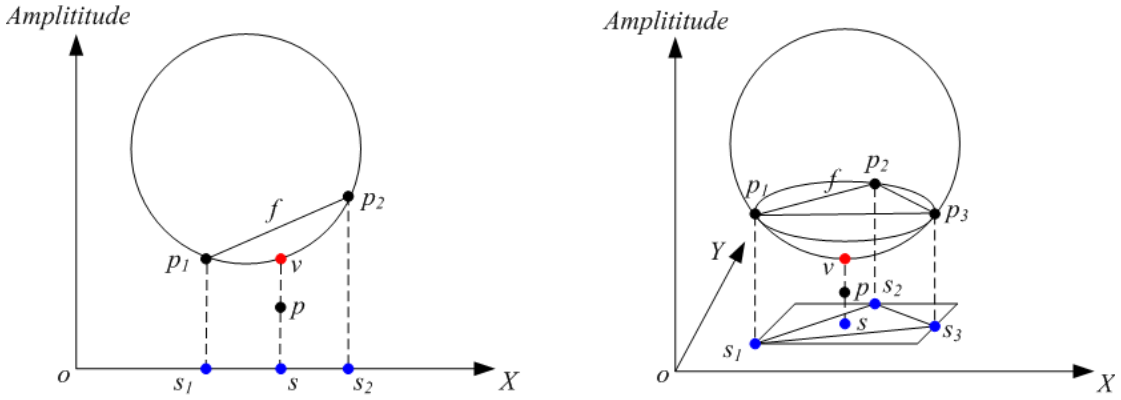

Figure 3.8 The acquisition of the closing envelope points by projecting onto the alpha hull for the planar open profile (a) and open surface (b).

Similar to the naive algorithm and the motif combination algorithm presented in Chapter 2, the alpha shape algorithm was performed on the same experimental profile data with a 0.5 mm disk. Figure 3.9 shows the resultant closing envelope as well as the alpha shape boundary facets marked by the line segments.

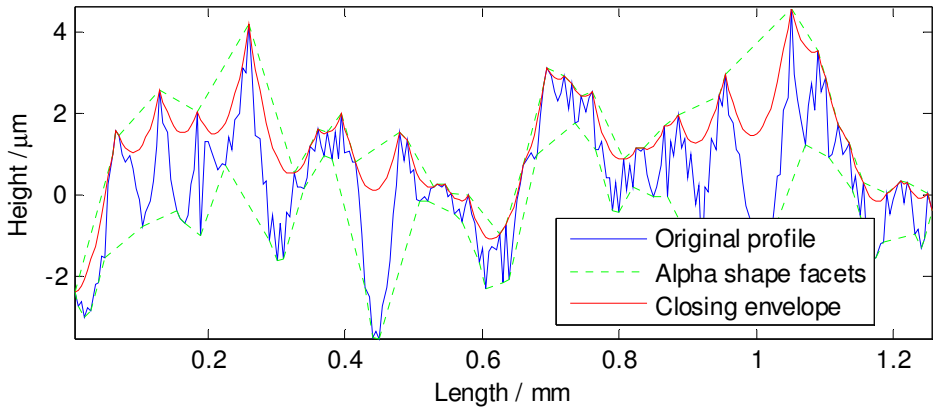

Figure 3.9 The closing envelope and the alpha shape facets computed by the alpha shape algorithm

3.4 Divide and conquer optimization

The alpha shape method could overcome the deficits of the naive algorithm, there is, however, a performance bottleneck. The Delaunay triangulation on which the alpha shape method depends is costly in both computation time and memory for large areal datasets. Practical experiments show the surface that the alpha shape method can calculate is limited to 1024×1024 points in size and the computation of surfaces which exceeds this size is easy to get the "out of memory" error. Thus a more efficient method is required to overcome this constraint.

Aiming to break the computation constraint of the 3D Delaunay triangulation, the divide and conquer optimization is introduced into the computation of morphological filters. The basic scheme of the divide and conquer approach is to break a problem into several sub-problems that are similar to the original problem but smaller in size, solve the sub-problems recursively and then combine these solutions to create a solution to the original problem (Cormen *et al.* 1989).

In the context of the alpha shape method, the vertices of the alpha facets are physically important because they are those points on the surface which are in contact with the rolling ball. We call them the contact points. In mathematical morphology, these points are the ones on the surface which remain unchanged before and after morphological closing and opening operations. The morphological envelope of a surface is determined by these contact points. Thus in order to reduce the computation of morphological envelopes, the surface could be represented by its contact points instead of all of the sampled points.

By applying the divide and conquer method, the surface could be divided into a series of small sub-surfaces. Each sub-surface is rolled by the ball to generate a set of contact points. Afterward the resulting contact points from each sub-surface are merged to reconstruct a super set of contact points. Roll the ball over this combined set and an updated set of contact points is yielded with the fake contact points removed on joint sections. In such a manner, the contact points of the original surface are found.

As aforementioned, the alpha shape method depends upon the 3D Delaunay triangulation of the sampled points of the surface. Engineering surfaces usually contain a large amount of data, especially using high speed optical instruments. The

3D Delaunay triangulation for such kind of super large datasets is both time and memory consuming. It was reported that the data structure of the 3D Delaunay triangulation is not suitable for dataset of millions of points (Bernardini *et al.* 1999). Using the divide and conquer method, the surface with a huge number of data points is partitioned into small sub-surfaces recursively, until the computation of 3D Delaunay triangulation is fast enough for each sub-surface.

Following the three typical steps of the divide and conquer paradigm, i.e. divide, conquer, combine, at each level of the recursion, the details of each step are illustrated below. Figure 3.10 presents an example surface (100 x 100 points) as well as its boundary alpha shape facets generated by the alpha shape method. The example surface is then divided into four smaller sub-surfaces with 50 x 50 points for each individual one, see Figure 3.11. The search of contact points on these sub-surfaces is conquered by applying the alpha shape method. Figure 3.12 graphs the contact points and the boundary alpha shape facets of four sub-surfaces respectively. Finally the contact points of four sub-surfaces are merged together and the alpha shape method is applied to the combined set to generate the final boundary alpha shape facets, see Figure 3.13. It is notable in the figures that the contact points on joint section before merging are no longer in the set after the merge. The comparison of the indices of vertices of boundary facets demonstrated in Figure 3.13 and those presented in Figure 3.10(b), which are generated by applying the alpha shape method directly, indicates the boundary facets computed by the two methods coincide with each other. For convenience of demonstration, this example only illustrates one recursion. For large areal surfaces, more recursions might be demanded.

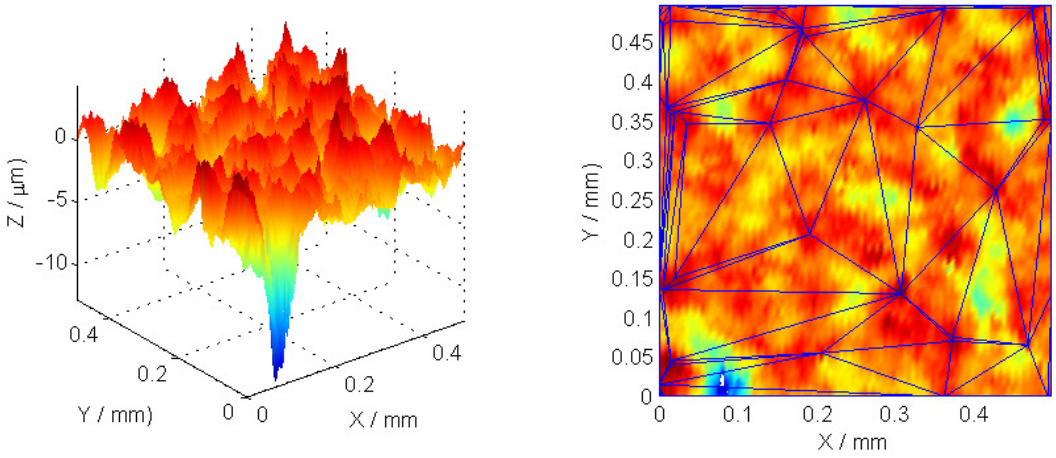

(a) (b)

Figure 3.10 An example surface and it boundary alpha shape facets. (a) Raw surface. (b) Boundary facets superimposed on the surface.

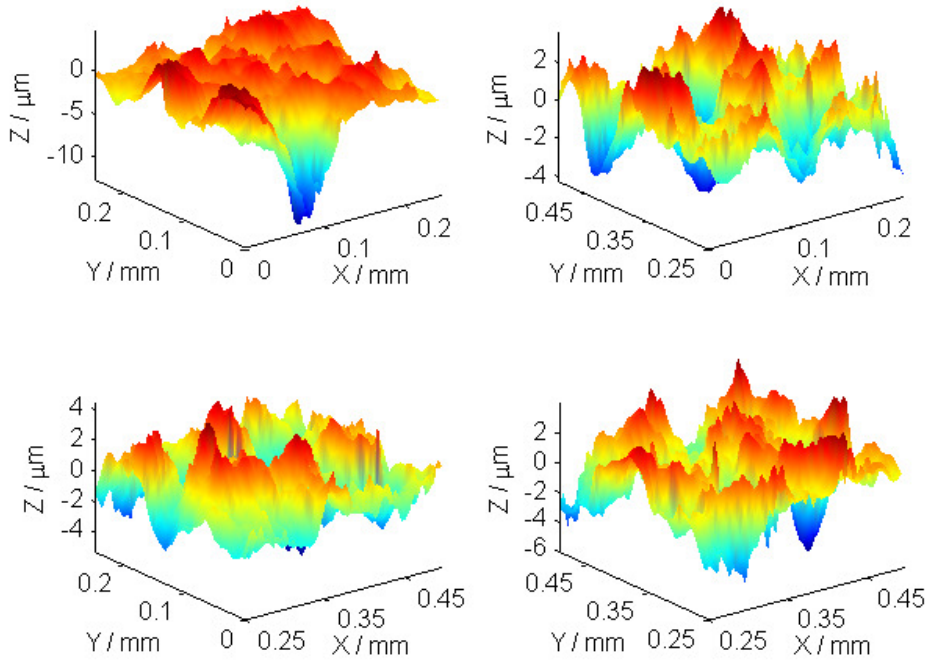

Figure 3.11 Four divided sub-surfaces

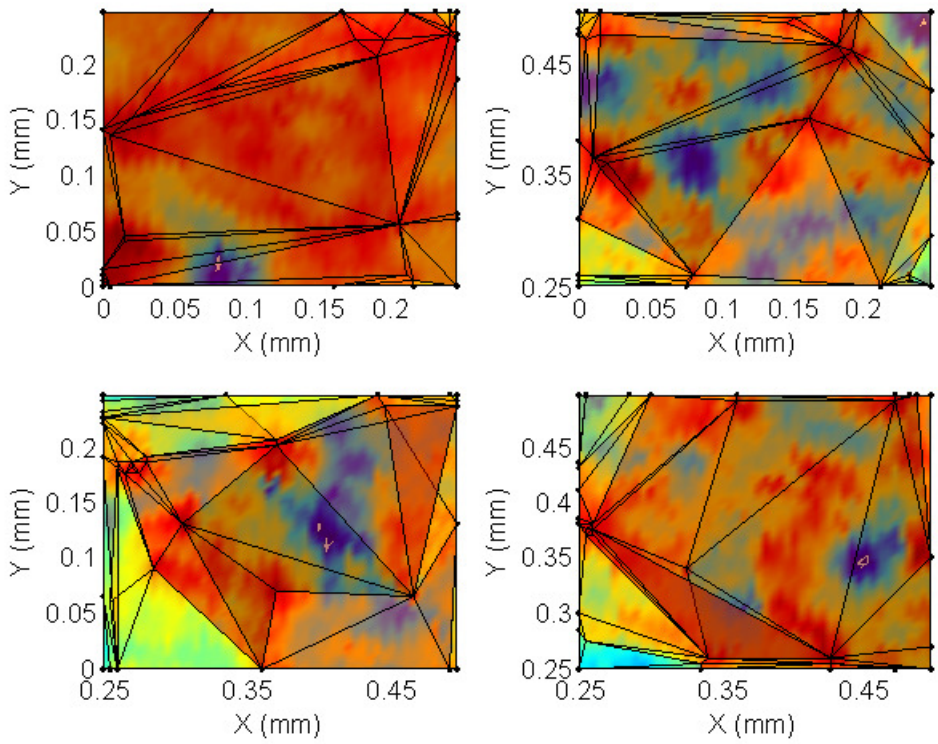

Figure 3.12 Contact points and boundary alpha shape facets of four sub-surfaces

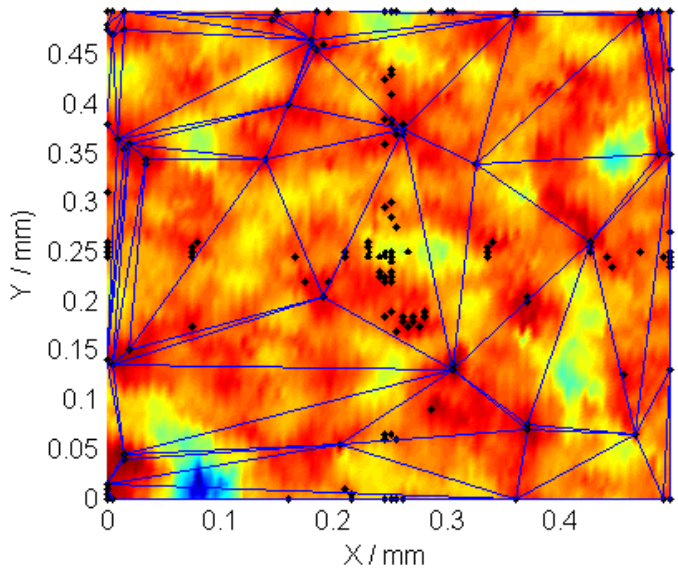

Figure 3.13 The merged contact point set and final boundary alpha shape facets

3.5 Summary

Aiming to solve the limitations of existing algorithms for morphological filters, a novel approach is proposed based on the alpha shape, providing the merits that

arbitrary large ball radii are available, freeform surfaces and non-uniform sampled surface applicable. The proposed approach utilizes the theoretical link between the alpha hull and the morphological closing and opening envelopes. A practical algorithm was developed that corrects possible singularities caused by data spikes and reduces the amount of computation for open surfaces. The alpha shape method depends on the Delaunay triangulation, with an additional merit that the triangulation data can be reused for multiple attempts of the ball radius. It could save a great deal of computing time considering in practice a multitude of trials may be made for choosing an appropriate ball radius.

The alpha shape method has the bottleneck in computation in the case of large areal datasets in that the 3D Delaunay triangulation is costly. An optimization method is developed based on the divide-and-conquer procedure to improve the performance of the alpha shape algorithm, which will be validated in Chapter 6.

4. ALGORITHMS SEARCHING CONTACT POINTS ON THE SURFACE

The alpha shape algorithm is much superior to the naive algorithm in that it provides more capabilities in dealing with modern surfaces. The divide and conquer optimization helps to improve its performance in the case of computing large areal datasets. However they still depend on the Delaunay triangulation, which might be redundant for the computation of a single morphological envelope. This chapter explores novel algorithms searching contact points on the surface without performing the Delaunay triangulation.

4.1 Redundant information of the Delaunay triangulation

In Edelsbrunner's theory the alpha shape is extracted from the Delaunay triangulation. The whole family of alpha shapes can be generated from Delaunay triangulation, from the point set itself ($\alpha \to 0$) to the convex hull of the point set ($\alpha \to \infty$). Therefore the Delaunay triangulation data could be reused for multiple attempts of ball radii for the same dataset. It is an advantage for the computation of morphological envelopes in that there is no need to perform the Delaunay triangulation every time for various radii attempts on the same dataset. Thus the reuse of triangulation saves a great deal of computing time. It meanwhile could be a drawback because the Delaunay triangulation is costly for large areal datasets. Given a single radius, the Delaunay triangulation contains much more information than is necessary to generate the corresponding alpha shape with the given radius. For large areal data, the 3D Delaunay triangulation consumes a great deal of computational time and memory. Thus in this sense it is a waste of time to achieve the desired alpha shape with redundant computation.

The divide-and-conquer optimization method provides a practical solution to overcome this problem. However it is not a fundamental change to the alpha shape method because the Delaunay triangulation is still required. An alternative solution is to find the alpha shape facets without performing the Delaunay triangulation. In fact the vertices of the alpha shape facets are those points on the surface that contact the

ball as it rolls over the surface, namely the contact points. By investigating these special points, it is possible to find the alpha shape facets.

4.2 Definition, propositions and comments of contact points

4.2.1 Mathematical definition of contact points

In physics, the contact points are those points on the surface which are in contact with the moving structuring element. Thus these points give an indication which surface portions in the neighbourhood of these contact points are most likely to be active in the contact phenomenon. By identifying the contact points, those areas of a surface that may be especially susceptible to wear at process start-up can be readily identified and remedial action taken if necessary.

As mentioned in Chapter 3.4, from a point of view of mathematical morphology, the contact points are those points on the surface which remain constant before and after morphological closing/opening operations. Based on the mapping between the alpha hull and morphological opening and closing envelopes, the formal mathematical definition of the contact point is given by Definition 4.1 as follows:

Definition 4.1 Given the sampled point set $X \subseteq \mathbb{R}^d (d = 2,3)$ and $\delta \le \alpha \le \infty$ (δ : sampling interval), the contact points $P(\alpha)$ are those sampled points $\{p_i \mid p_i \in X\}$ that are on the boundary of the alpha shape $\partial H_\alpha(X)$:

$$P(\alpha) = \{p_i \mid p_i \in X, p_i \in \partial H_\alpha(X)\}.$$

4.2.2 Propositions of contact points

Proposition 4.1 Given the point set $X \subseteq \mathbb{R}^d (d = 2,3)$ and $\delta \le \alpha_1 \le \infty$, $\delta \le \alpha_2 \le \infty$, if $\alpha_1 \le \alpha_2$, then $P(\alpha_2) \subseteq P(\alpha_1)$.

Proof. $\alpha_1 \le \alpha_2 \Rightarrow H_{\alpha_1}(X) \subseteq H_{\alpha_2}(X)$ (Fischer 2000). By Definition 4.1, $P(\alpha_1) = \{p_i \mid p_i \in X, p_i \in \partial H_{\alpha_1}(X)\}$, $P(\alpha_2) = \{p_i \mid p_i \in X, p_i \in \partial H_{\alpha_2}(X)\}$. Hence $H_{\alpha_1}(X) \subseteq H_{\alpha_2}(X)$ implies $P(\alpha_2) \subseteq P(\alpha_1)$.

Proposition 4.2 Given the point set $X \subseteq \mathbb{R}^d (d = 2,3)$ and $\delta \le \alpha \le \infty$. The convex hull points must all be contact points.

Proof. Let $\alpha' \to \infty$, hence $\lim_{\alpha' \to \infty} H_{\alpha'}(X) = Conv(X)$. By Definition 4.1 $P(\alpha') = \{p_i \mid p_i \in X, p_i \in \partial H_{\alpha'}(X)\}$, then $P(\alpha') = \{p_i \mid p_i \in X, p_i \in \partial Conv(X)\}$, namely $P(\alpha')$ is the convex point set. By Proposition 4.1, $\alpha \le \alpha' \Rightarrow P(\alpha') \subseteq P(\alpha)$. Thus the convex hull points must be contained in $P(\alpha)$.

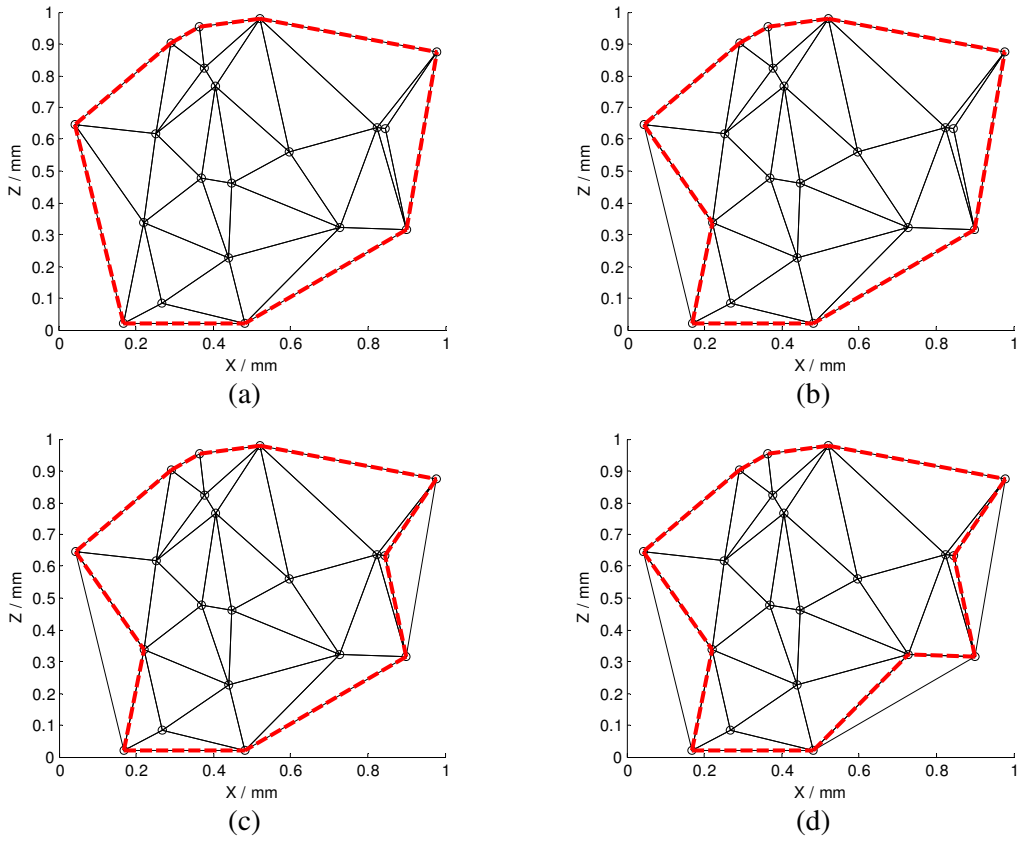

Figure 4.1 The Delaunay triangulation of the planar point set and the boundary facets of the alpha shapes of various disk radii: (a) $\alpha = 1$ mm; (b) $\alpha = 0.5$ mm; (c) $\alpha = 0.4$ mm; (d) $\alpha = 0.3$ mm

Figure 4.1 presents an example illustrating the boundary facets of the alpha shapes with different disk radii for planar point set. The scattered points marked by spots are connected by the Delaunay triangulation simplices as presented by joint triangles. The boundary facets of the alpha shapes are extracted from the Delaunay triangulation, graphed as the bold dotted lines. Four sub-figures present the corresponding alpha shape boundary facets with radius 1 mm, 0.5 mm, 0.4 mm and 0.3 mm respectively. In Figure 4.1(a), the boundary facets are the outmost faces of the Delaunay triangulation, which are actually the convex hull faces. If the vertices of the

boundary alpha shape facets are examined, i.e. the contact points of the alpha ball (disk), it can be found that the contact points of Figure 4.1(a) with radius 1 mm are contained in Figure 4.1(b) with radius 0.5 mm. In sequence, this relationship is also true for Figure 4.1(b) and Figure 4.1(c), Figure 4.1(c) and Figure 4.1(d). This fact is consistent with Proposition 1 and 2.

4.2.3 Comments for searching contact points

Following the definition of the contact point and two associated propositions, a set of comments are proposed with proofs attached for the search of contact points. For convenience of explanation, we take the morphological closing profile filter and the circular structuring element (disk) as the objective for illustration. These comments can easily be extended to the opening filter, planar structuring elements and areal data. In the context of the statement below, *a* and *b* are two known contact points, r is the given radius of the ball (disk).

Comment 4.1 If there are points lying above σ_{ab} (left/positive side of $\overrightarrow{ab}$), then the contact point is the furthest point orthogonal to $\overrightarrow{ab}$.

Proof. Suppose there exist some points above σ_{ab}. See Figure 4.2. The furthest point p_2 is the convex point for the point set $\{a, b, p_i\}$ (Barber *et al.* 1996). By Proposition 4.2, the convex point must be the contact point. Thus p_2 must be the contact point.

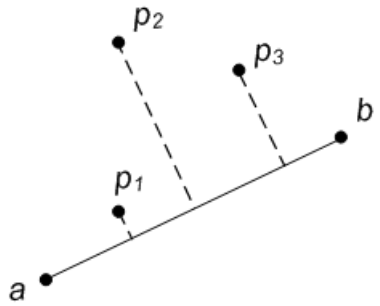

Figure 4.2 Search the furthest point orthogonal to $\overrightarrow{ab}$

Comment 4.2 If there are no points lying above σ_{ab} and there exist points $\{p_i\}$ in the circular section $\overset{\frown}{ab}$ of the alpha ball with radius $\alpha = \max\{r, \frac{1}{2}|ab|\}$, then the contact point *c* is the one among the points $\{p_i\}$ in $\overset{\frown}{ab}$, which satisfies the condition: the

circumscribed circle of σ_{abc} have the largest radius among the circumscribed circles of $\{\sigma_{abp_i}\}$.

Proof. First consider the case $|ab| \le 2r$. See Figure 4.3. a, b could determine an unique alpha ball B with radius r. Since there exist points in the circular section $\overset{\frown}{ab}$ (the shadowed part in the figure), $B \cap X = \{p_i\} \neq \varnothing$, thus σ_{ab} is not α-expose. By Definition 3.1, $\sigma_{ab} \notin \partial H_r(X)$. Let $\{\rho_i\}$ be the radius of the circumscribed circle of $\{\sigma_{abp_i}\}$ and c the point with $\max(\rho_i)$. The circumcircle of σ_{abc} must be empty, thus $c \in \partial H_{\max(\rho_i)}(X)$. By Proposition 1, $\max(\rho_i) > r \Rightarrow P(\max(\rho_i)) \subseteq P(r)$. By Definition 3.1, $c \in P(\max(\rho_i))$. Thus $c \in P(r)$, c is the contact point.

Then consider the other case $|ab| > 2r$. See Figure 4.4. Since $|ab| > 2r$, fit an alpha ball with radius $\frac{1}{2}|ab|$ passing through the points a, b with the centre at the middle of σ_{ab}. Similar to the previous case, we could prove $c \in P(\frac{1}{2}|ab|)$. Then by Proposition 4.1, $\frac{1}{2}|ab| > r \Rightarrow P(\frac{1}{2}|ab|) \subseteq P(r)$, thus $c \in P(r)$, c is the contact point.

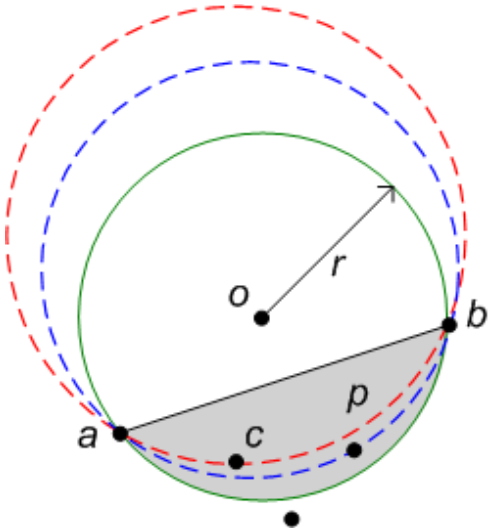

Figure 4.3 Search the contact point with $|ab| \le 2r$

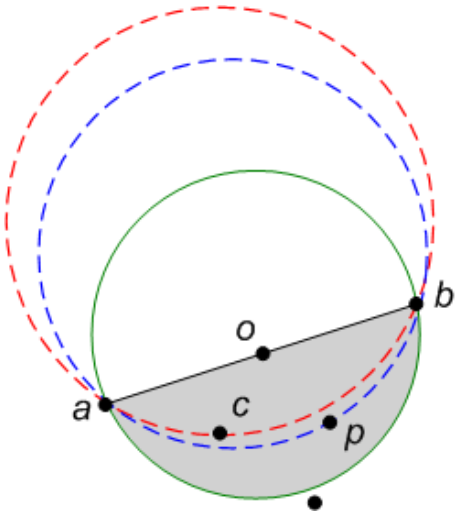

Figure 4.4 Search the contact point with $|ab| > 2r$

Comment 4.2 If there are points $\{p_i\}$ lying below σ_{ab} (right/negative side of $\overrightarrow{ab}$) and no point above, σ_{abp_i} has an unique circumscribed circle with radius α. If the centre of the circumscribed circle is on the positive side of σ_{ab}, the circle has the positive radius $+\alpha$, otherwise the negative radius $-\alpha$.

See Figure 4.5. σ_{abp_i} has its circumcircle centre o_1 above σ_{ab}, thus it has a positive radius. Conversely, the centre of the circumcircle of σ_{abc_2} lies below σ_{ab}, therefore the radius is negative. The critical case is that of σ_{abp} which has its circumcircle centre o at the centrepoint of σ_{ab}. In this case it is taken that the radius is positive.

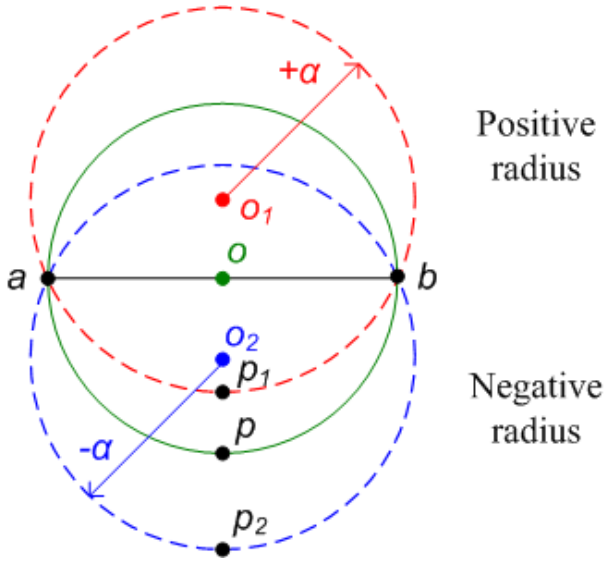

Figure 4.5 The signed circumscribed circle radius

Comment 4.3 If $|ab| > 2r$ and there are no points lying above σ_{ab} and also no points in the circular section $\overset{\frown}{ab}$ of the alpha ball with radius $\alpha = \frac{1}{2}|ab|$, then the contact point is the one c that satisfies the condition: the circumscribe circle of σ_{abc} has the largest radius among the circumscribed circles of $\{\sigma_{abp_i}\}$.

Proof. See Figure 4.6. There is no point in the circular section $\overset{\frown}{ab}$, thus the centre of circumscribed circles of $\{\sigma_{abp_i}\}$ locates at the negative side of the chord $\overline{ab}$. Thus their radii are negative. The circumscribe circle with the largest radius (smallest in absolute value) must be empty, thus $c \in \partial H_{|\alpha|}(S)$. $|\alpha| > r \Rightarrow c \in \partial H_r(S)$. By Proposition 4.1, we have $c \in P(r)$.

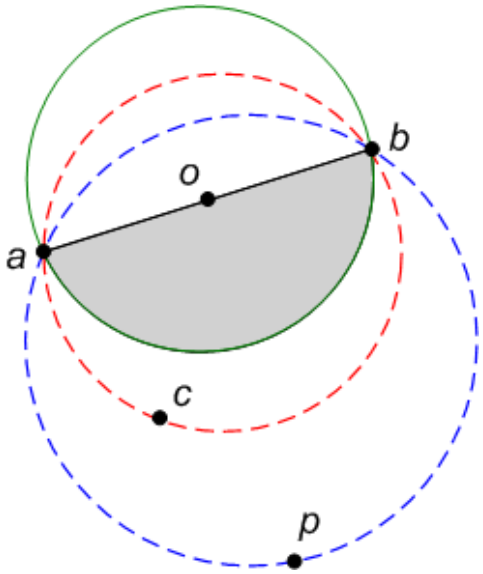

Figure 4.6 Search the contact point with $|ab| > 2r$

Comment 4.4 If $|ab| \leq 2r$ and there are no points lying above σ_{ab} and also no points in the circular section $\overset{\frown}{ab}$ of the alpha ball with radius r, then $\sigma_{ab} \in \partial H_r(X)$.

Proof. a, b could determine an alpha ball B with radius r. If there is no point lying above σ_{ab} and no point in the circular section $\overset{\frown}{ab}$, then $B \bigcap X = \varnothing$. Thus σ_{ab} is α-expose. By Definition 1, $\sigma_{ab} \in \partial H_r(X)$.

By introducing the signed circumcircle radius, Comment 4.2 and Comment 4.3 could be merged into one operation: calculate the signed circumcircles and find the point with the biggest radius. That point is the contact point. To determine the termination of the searching procedure, Comment 4 suggests three conditions. These conditions, however, can be easily examined by the point distribution below σ_{ab}. See Figure 4.7. First of all, $|ab|$ has to be smaller than $2r$, which means the alpha ball (disk) is larger than the smallest circumcircle of σ_{ab}. In Figure 4.7, there are 7 sample points between a and b. They fall into three categories:

(1) Points lying in the circular segment $\overset{\frown}{ab}$ of the alpha ball, such as p_3 and p_7 in the figure. These points may be contact points. They are featured by the positive radii $\{\rho_i\}$ of the circumcircle of $\{\sigma_{abp_i}\}$ and $\rho_i >= r$.

(2) Points lying in the circular section $\overset{\frown}{ab}$ of the smallest circumcircle of σ_{ab}, but not in category (1), such as p_1, p_4 and p_6. These points cannot be contact points, as they have positive radii $\{\rho_i\}$ of the circumcircle of $\{\sigma_{abp_i}\}$, but $\rho_i < r$. Thus in this case $0 \le \rho_i < r$.

(3) Points not contained in categories (1) and (2), such as p_2 and p_5 in the figure. These points cannot be contact points, as they have negative radii $\{\rho_i\}$ of the circumcircle of $\{\sigma_{abp_i}\}$, i.e., $\rho_i < 0$.

To sum up, the searching procedure exits and $\sigma_{ab} \in \partial H_r(X)$ when no points lie above σ_{ab}, $|ab| \le 2r$ and $\rho_i < r$.

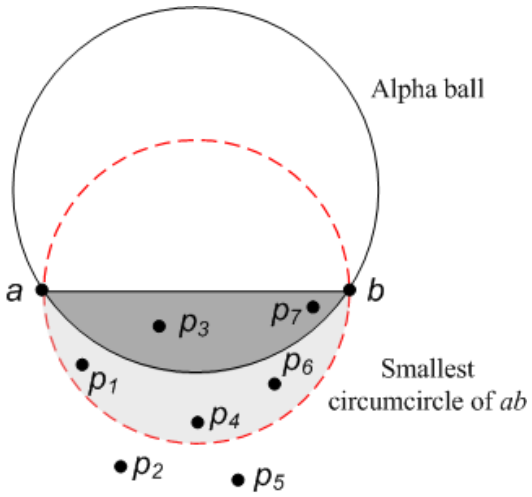

Figure 4.7 The distribution of sample points below *ab*

Proposition 4.1, 4.2 and Comment 4.1-4.4 establish the searching order for the contact points. It first targets the convex hull points, which corresponds to rolling a disk with infinitely large radius over the profile. If no convex hull point is found above the evaluating facet, the contact point is sought by computing the signed circumcircles radii. The contact point is the one that has the largest circumcircle radius. This is equivalent to rolling a disk with a proper size larger than the given radius r but less than the infinitely large radius. Finally if the profile segment in evaluation could hold an empty disk with radius r by its two ends, namely the disk has no contact with other sample points, then the simplex composed by these two

known contact points is a facet of the alpha shape and the recursion procedure is completed. In summary the search for the contact points uses the disk with radius ranging from infinitely big down to r.

4.3 Recursive algorithm

Based on the proposed propositions and comments of the contact points, a practical recursive algorithm is constructed. Instead of performing the Delaunay triangulation, the algorithm searches for the facets encompassed by the contact points by recursion. The algorithm for profile data is first presented and then extended to areal data.

4.3.1 Profile algorithm

The pseudocode of the algorithm to compute the contact points for morphological closing profile filter is presented in Figure 4.8. The algorithm starts with the left end point a and the right end point b of the profile, which are guaranteed to be the initial contact point as they are points on the convex hull. The algorithm then starts to search the contact points between a and b by applying Comment 4.1 to 4.4 in sequence. Once a contact point is found, say c, it is treated as a partition point and the profile (a,b) is partitioned into two segments (a,c) and (c,b). The same process is repeated on the two partitioned segments (a,c) and (c,b). The algorithm keeps partitioning the segments into smaller ones recursively until the segment being evaluated satisfies the condition specified by Comment 4.4 and that segment is accepted as the boundary facet. The vertices of all final boundary facets are then defined as the contact points and the envelope ordinates are achieved by interpolating points on the arcs determined by the final boundary facets.

```
Algorithm ContactPoints(X, r)
{Given a profile X and the chosen disk radius r,}
{ computes the contact points Contacts.}

    a ← the left end point of X.
    b ← the right end point of X.
    Partition(a, b);

    Procedure Partition (a, b)
    if {p_i} above ab
        c ← the furthest point from ab in {p_i};
    else
        calculate the signed circumcircles radii R of {ab p_i } ;
        c ← the point with max(R);
        if ab <= 2r & max(R) < r
            Contacts. add(a, b);
            return;
        end if
    end

    Partition (a, c);
    Partition (c, b);
    end procedure
end algorithm
```

Figure 4.8 The recursive algorithm for the morphological closing profile filter

Although the presented algorithm is specific to the circular structuring element, it is even easier to apply the basic algorithm to the horizontal line segment structuring element. See Figure 4.9. In this case the contact point is examined by checking the highest point (say c in $\{p_1, p_2, c\}$) between two known contact points (say a, b). If that point is lower than two given contact points (say a, b is lower than c) and the horizontal distance between the two contact points is smaller than the length of the given line segment (say $|ab| < L$), the recursion procedure exits and the simplex composed by those two contact points is taken as the facet. The envelope ordinates are determined by the lower height of the two contact points.

Figure 4.10 illustrates an example closing envelope computed by the recursive algorithm. It employs the same experimental data and the disk radius as used in the previous chapters. The contact points are circled in the figure.

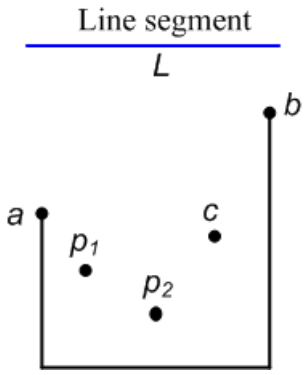

Figure 4.9 Examining the contact points by line segment structuring element

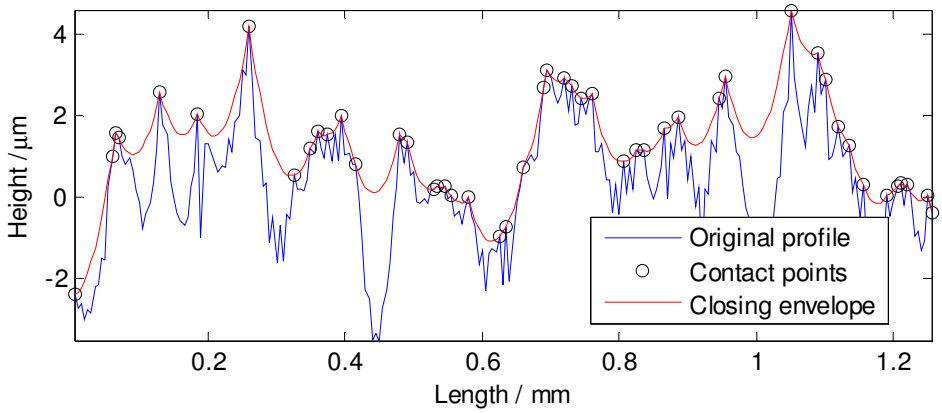

Figure 4.10 The closing envelope and contact points computed by the recursive algorithm

4.3.2 Areal algorithm

It is obvious that the propositions and comments also hold for areal data if the disk is replaced by a ball and the circumcircle is replaced by a circumsphere. In such a case, instead of starting with the initial points for the recursion procedure as the left and right profile ends in scenario of profile data, it is easier to start with the convex hull faces for areal data and thereafter perform the recursion procedure on each convex hull face. Figure 4.11 illustrates an example surface with 50 × 50 points on which the convex hull faces are presented as the triangular meshes. For each face of the convex hull, the algorithm searches the contact points by computing the signed circumsphere radius and performs the partition procedure in a similar manner to that of profile data. For instance, starting with a convex hull face σ_{abc}, a contact point d is found by seeking the largest circumsphere radius of $\{\sigma_{abcp_i}\}$, where $\{p_i\}$ are the sample points inside the circumsphere of σ_{abc}. Then σ_{abc} is removed and partitioned

into three new simplices σ_{abd} , σ_{bcd} and σ_{cad} . The partition process is repeated on each new generated simplex until the simplex in evaluation can hold an empty circumsphere.

The highlighted triangle in Figure 4.11 denotes one of convex hull faces. The resulting boundary facets are highlighted in Figure 4.12. The searching process completes when the partition of all convex hull faces are finished. Finally the vertices of the obtained boundary facets are the desired contact points, as shown in Figure 4.13. Similar to the profile data, the closing envelope coordinates are computed by interpolating points on the caps determined by the final boundary facets. Figure 4.14 illustrates the resulting closing envelope of the original surface.

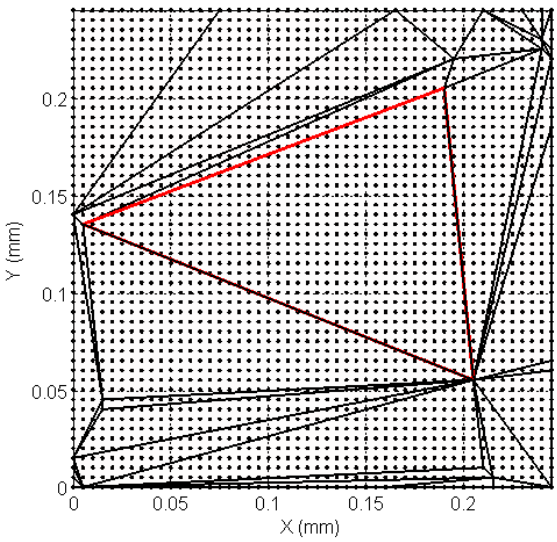

Figure 4.11 The convex hull faces of the surface areal data

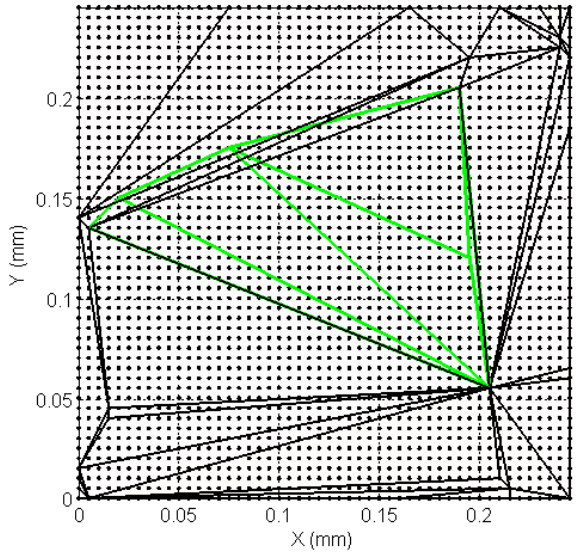

Figure 4.12 The facets generated by applying the partition procedure on one of the convex hull faces

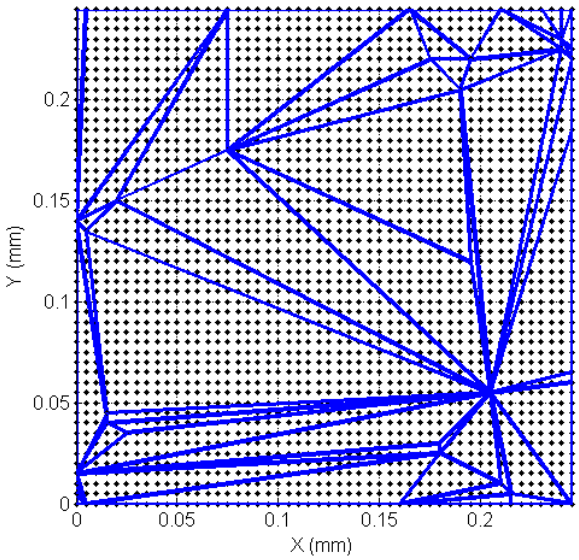

Figure 4.13 The final boundary facets resulting from the partition procedures

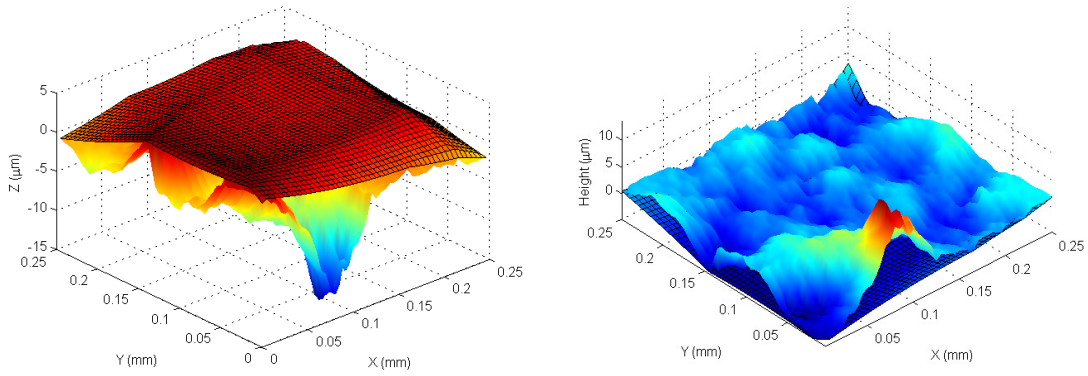

(a) (b)

Figure 4.14 The generated closing envelope. (a) Normal view. (b) Inverted view

4.4 Modified Graham scan algorithm

The recursive method and the alpha shape method are based on the relationship between morphological envelopes and the alpha hull. Nevertheless another relationship between morphological envelopes and a geometrical structure — the convex hull is targeted.

Morphological operations, as created, were first utilized to examine the geometrical structure of rock cross sections (Matheron & Serra 2002). It then led to a new quantitative approach in image analysis. This image processing method was introduced into surface texture analysis as a non-linear filtering technique (Srinivasan 1998). The measured data uniformly sampled on the surface are treated in a similar manner to image pixels. In fact the naive algorithm is a typical image processing method. It however inherits some limitations by dealing with the measured data as image pixels. Image has to be planar, unable to rotate in space, while the workpiece surface is a physical object existing in space, invariant under translation and rotation. It is thus more reasonable to view the sampled data as the point set in space rather than image pixels. As illustrated in Figure 2.10, the closing envelope is obtained by rolling a disk over profile from above and taking the lower boundary of the disks. If consider the set of sample points as the discrete representation of the physical profile, it is equivalent to roll the disk over these discrete points. This operation turns out to be a computational geometry problem instead of an image processing issue.

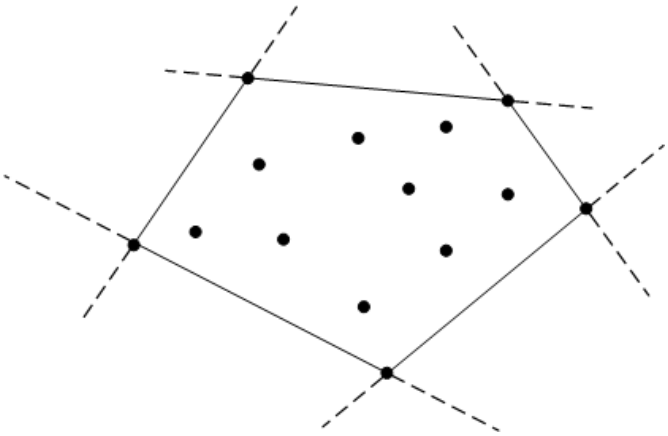

Figure 4.15 Pivoting the infinitely extending line around the point set yields the convex hull

In computational geometry, the convex hull is the most ubiquitous structure, playing a central role in many engineering computations. Intuitively the convex hull of a point set in 2D is obtained by pivoting an infinitely extending line around the point set, see Figure 4.15. The line-segment envelope bounding the point set is called the convex hull. In the mathematical morphology point of view, the point set is equivalent to the image being processed and the infinitely extending line serves as the structuring element. If replacing the infinitely extending line by the desired geometrical object, for example, a disk, the convex hull becomes the morphological envelopes. In this sense, the convex hull could be viewed as a special morphological envelope with the infinitely extending line or the disk with infinitely large radius being the structuring element. Based on that, it is possible to correlate the convex hull computation technique with the morphological envelope calculation.

Among various convex hull calculation methods, the Graham scan algorithm was a very efficient method for planar point set (Graham 1972). As illustrated in Figure 4.16, the algorithm sorts the points by angle counter-clockwise firstly. Then the algorithm proceeds to consider each of the sorted points in sequence. It maintains a stack structure to hold the points on the convex hull found so far. For each point, it is determined whether moving from the two previously considered points to this point is a "left turn" or a "right turn". If it is a "right turn", it means that the second-to-last point is not part of the convex hull and should be removed from the stack. For example, in the figure, p_3, p_4 and p_5 forms a “right turn”, thus p_4 is popped out from the stack. Then the renewed chain, p_2, p_3 and p_5, forms a “left turn”, and p_5 is

pushed into the stack. This process is continued as long as the set of the last three points is a "right turn". As soon as a "left turn" is encountered, the point is pushed into the stack and the algorithm moves on to the next point in the sorted array. In the end, the points contained in the stack are all the convex hull points.

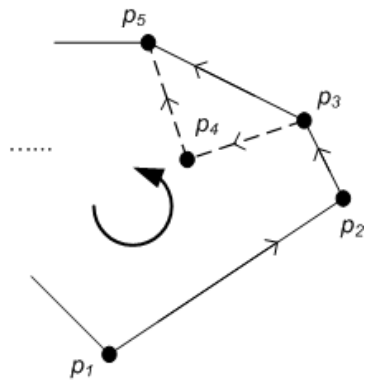

Figure 4.16 The Graham scan algorithm for convex hull

To compute morphological profile envelopes, we modify the Graham scan algorithm aiming to search the contact points. The modified algorithm does not sort the data as is required in the convex hull computation since the profile points are already naturally “sorted” in the sequence of sampling, but directly searches the contact points on the profile. Similar to the original convex hull method, the modified algorithm maintains a stack structure to contain the contact points.

The algorithm pseudocode is presented in Figure 4.17. At the beginning, the stack keeps the first two sample points as the initial elements. Then it processes the rest of points incrementally. Each time the coming point is evaluated with the top element p_t and the second top element p_{t-1} in the stack. The chain composed by the three points is checked whether the structuring element could contact the middle point p_{t-1}. If it is unable to touch p_{t-1}, the point in evaluation is pushed into the stack, otherwise the top element of the stack is popped out. The contact test is performed repeatedly until the test succeeds. Thus in this manner when all the points are processed, the points in the final stack are all the contact points.

```
Algorithm GrahamScan(X, B)
{Given a point set {p_i|i<n} and the structuring}
{ element B, computes the contact points.}

Stack stack = (p_1, p_2); t indexes top.
i = 3;
while i <= n do
    if  t < 2
        Push(stack, p_i);
        continue;
    end if;
    if CheckContact(p_{t-1}, p_t, p_i, B)
        Push(stack, p_i);
        i = i + 1;
    else
        Pop(stack);
    end if;
end while;
return stack;
```

Figure 4.17 Modified Graham scan algorithm for morphological filters

The envelope is calculated in a similar way to the previously presented algorithms. Figure 4.18 demonstrates the closing envelope of the experimental profile with disk radius 0.5 mm, computed by the modified Graham scan algorithm. The star marks in the figure are the contact points on the profile.

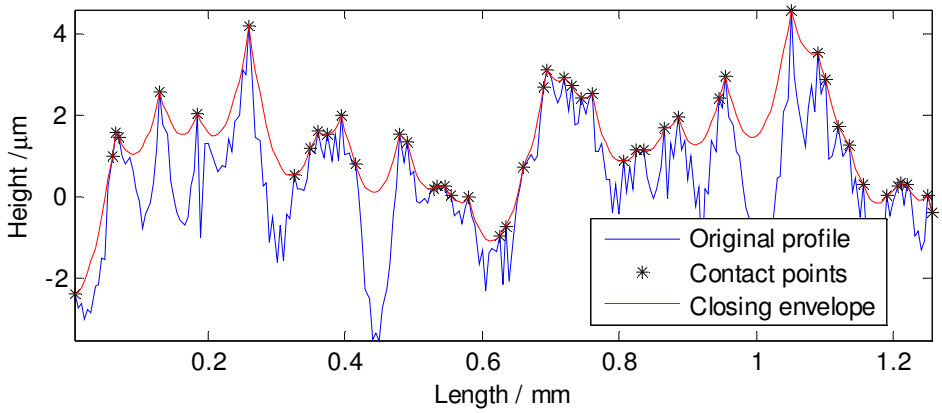

Figure 4.18 The closing envelope and contact points computed by the Graham scan algorithm

The presented Graham scan algorithm works well for profile data, however it would be hard to extend it to areal data. In that case, the scanning is performed by rolling a ball. There is no existing efficient Graham scan algorithm for 3D point set (Devadoss & O'Rourke 2011). However an algorithm called the ball pivoting

algorithm (Bernardini *et al.* 1999) was developed to reconstruct the surface from the discrete point cloud. It simulates rolling a ball over the areal point set. In this sense this method could be viewed as the extension of the modified Graham scan algorithm for profile data. This problem is this algorithm is poor in performance for large ball radius.

4.5 Summary

The alpha shape method solved the deficits of the traditional algorithms, however it has some limitations, for instance, the structuring element is restricted to be circular and the Delaunay triangulation is costly for large areal datasets. The recursive algorithm overcomes these limitations based on searching for the contact points on the surface. The definition of the contact point is given and a set of propositions and comments are proposed and mathematically proved based on alpha shape theory. With these propositions and comments, the recursive algorithm for morphological filters is developed for both profile data and areal data. The recursive algorithm does not require the Delaunay triangulation and is applicable for both circular and flat structuring elements, meanwhile it retains the merits of the alpha shape method.

By correlating the convex hull and morphological envelopes, the Graham scan algorithm for the convex hull computation is modified and adapted to compute the morphological operations. This algorithm outputs the same contact points as the recursive algorithm. The limitation of this method is that it only applies to the profile data.

5. ALGORITHM DISCUSSION AND COMPARISON

In the preceding chapters five different algorithms, two existing ones, the naive algorithm, the motif combination algorithm and three proposed ones, the alpha shape algorithm, the recursive algorithm and the modified Graham scan algorithm have been presented. These five algorithms achieve the same goal, whereas they are derived from distinct origins and have their respective advantages and disadvantages. Thus in order to expose their merits and shortcomings, we proceed to discuss these algorithms in following perspectives: algorithm verification, algorithm analysis, performance evaluation and area extension.

5.1 Algorithm verification

For the purpose of verifying the algorithms, they are applied to a milled surface profile. The profile contains 1000 points with sampling interval 10 μm. The profile is filtered by the morphological closing filter with disk radius 500 mm. The results from the five algorithms are graphed in Figure 5.1. It is clear from the figure that the five envelopes overlap except at the two ends of the profile. It indicates that the algorithms are in agreement with each other. The edge distortion is caused by the end effect of filtration on the open surface data. The end effect correction will be discussed in Chapter 6.

The same profile is thereafter filtered by the line-segment structuring element with length 1 mm. The alpha shape method is not applicable because this method is limited to circular structuring elements. As illustrated in Figure 5.2, except at the end region of the profile, four resulting envelopes from the naive algorithm, the recursive algorithm, the modified Graham scan algorithm and the recursive algorithm are matched except at the two ends.

To verify the algorithms on areal data, the naive algorithm, the alpha shape algorithm and the recursive algorithm are applied to an experimental surface with 100×100 points. See Figure 5.3(a). The surface is 1×1 mm^2 in area with sampling interval 0.01 mm. The surface was filtered by the morphological closing filter with

ball radius 0.15 mm. Figure 5.3(b) presents the closing envelope resulting from the naive algorithm. The resulting envelope computed by the alpha shape method and the recursive algorithm is illustrated in figure 5.3(c). Figure 5.3(d) presents the comparison of two envelopes. The comparison reveals that the two results are basically in agreement except at the boundary region of the surface, which is caused by the end effect of filtration on the open surface data.

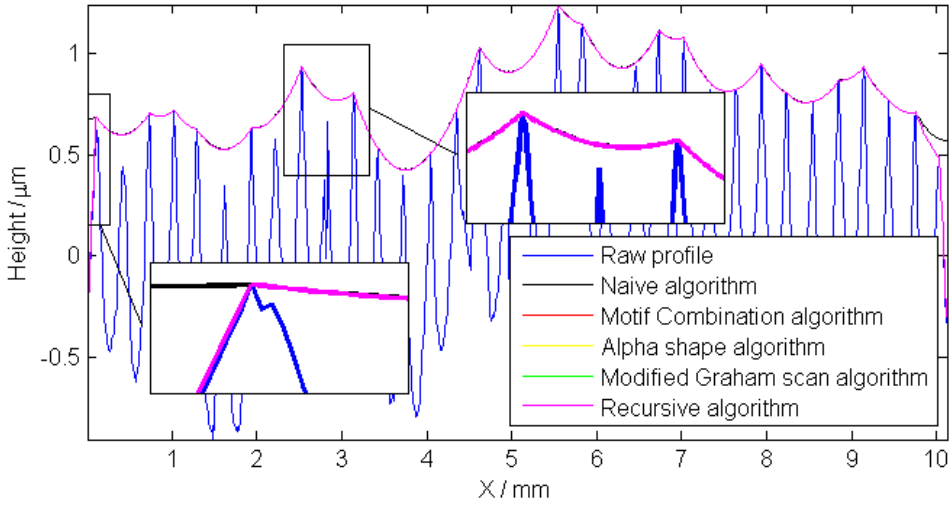

Figure 5.1 Morphological closing profile envelopes generated by the five algorithms with disk radius 150 mm

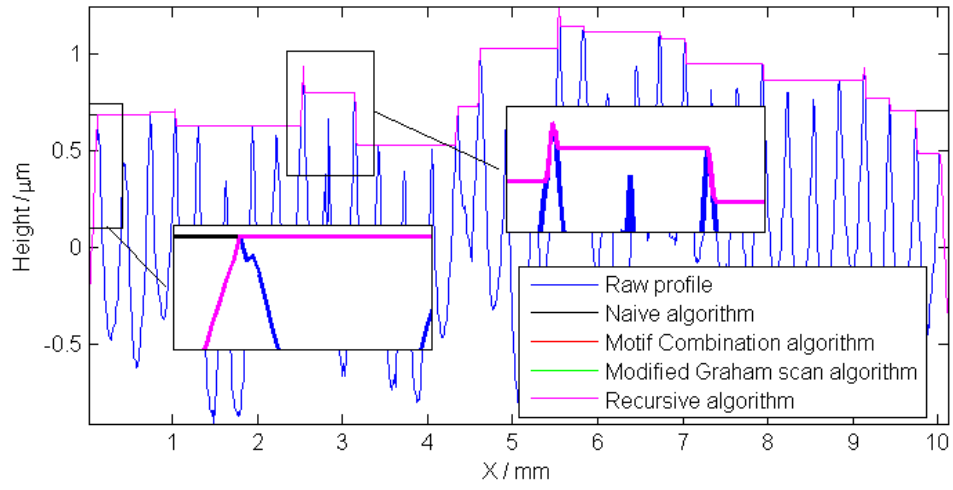

Figure 5.2 Morphological closing profile envelopes generated by the four algorithms with line segment 1 mm

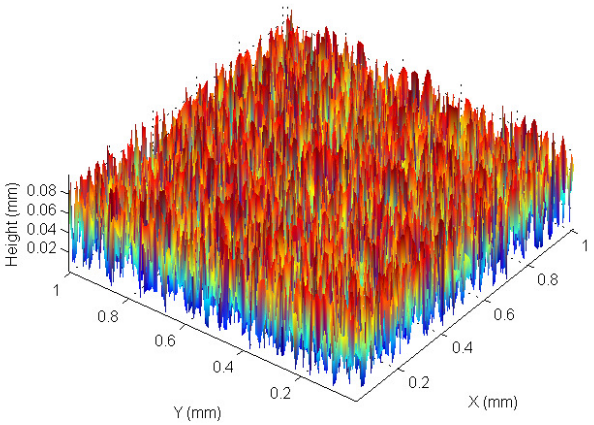
Height (mm)
0.08
0.06
0.04
0.02
1
0.8
0.6
0.4
0.2
Y (mm)
X (mm)

(a)

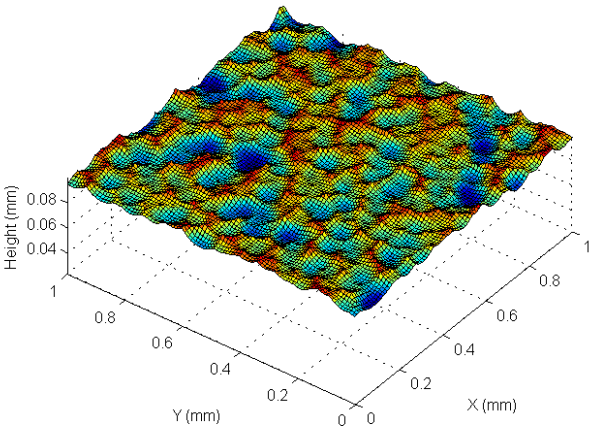
Height (mm)
0.08
0.06
0.04
1
0.8
0.6
0.4
0.2
0
Y (mm)
X (mm)

(b)

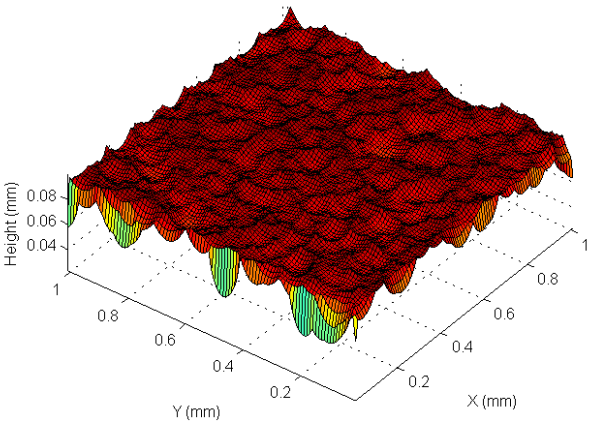
Height (mm)
0.08
0.06
0.04
1
0.8
0.6
0.4
0.2
Y (mm)
X (mm)

(c)

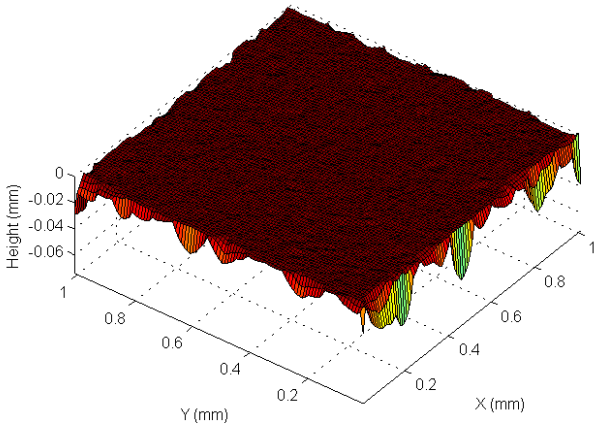

(d)

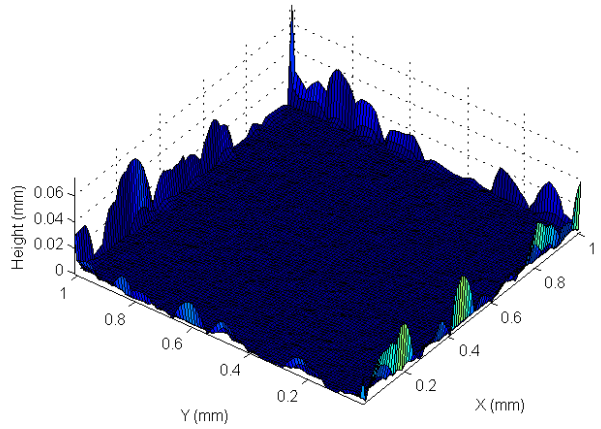

(e)

Figure 5.3 Morphological closing areal envelopes generated by the naive algorithm and the alpha shape algorithm (and the recursive algorithm) respectively. (a) Raw surface. (b) Closing envelope computed by the naive algorithm. (c) Closing envelope computed by the alpha shape algorithm and the recursive algorithm. (d) Deviation surface obtained by subtracting the closing envelope resulted from the naive algorithm from the one generated by the alpha shape algorithm. (e) Inverted deviation surface

5.2 Algorithm analysis

The naive algorithm, being a direct approach following the definition of morphological dilation and erosion, combines them to yield morphological closing and opening. This algorithm, which may be optimized by certain techniques (Sedaaghi 1997), is widely used in image processing. However it has some fatal limitations. For one thing, it is time-consuming for large datasets and large structuring elements. The maximum size of the structuring element is limited due to the huge computation requirement, while for many real applications they may desire the

structuring element size much larger than the profile length. For another, it is limited to planar data and uniform sampled data.

The motif combination algorithm emphasises the elimination of the insignificant motifs and obtains only the significant ones. It is an iterative process in that the motifs are merged repeatedly until no more combinations occur. The final events are the contact points on the profile. This algorithm is consistent with the functionality of morphological filters in that the features on the profile smaller than the structuring element in size are removed by the filter. By defining the motif combination test criterion, i.e. how two adjacent motifs are combined, various types of structuring elements are available, for instance, circular disks and horizontal line-segments. Although the structuring element is restricted to the convex object and is not allowed to tilt, it could satisfy most of the applications (Scott 1992).

The approach based on the alpha shape utilizes the relationship between the alpha hull and morphological operations that the boundary of the hull obtained by rolling the alpha ball over the point set is identical to the closing/opening envelope. Therefore the algorithm for computing the alpha shape could be used to calculate morphological closing and opening filters. This algorithm is based on the Delaunay triangulation. The triangulation data could be reused for multiple attempts of various disk radii. It could save a great deal of computing time since in real practice a multitude of trials may be made for an appropriate disk radius. Another merit is that it is suitable for non-uniform sampled data, bringing more generality over the naive algorithm. Although the link puts the restriction that the structuring element must be circular, the circular disk is most commonly used and is regarded as the default structuring element in ISO 16610.

In comparison to the naive algorithm as a typical image processing technique, which treats the measured data as image pixels, the modified Graham scan algorithm views the data as the point set in space. Regarding the measured data as the input set and the infinitely extending line as the structuring element, the convex hull could be viewed as a special morphological envelope. It links computational geometry techniques with the calculation of morphological envelopes. The Graham scan algorithm originally developed for the convex hull computation is modified and adapted to calculate morphological envelopes. The method is an incremental algorithm in that the profile data is processed in sequence and adding data will cause

the correction of the processed data. It simulates moving the structuring element over the profile and obtains the contact points. In this aspect it resembles the motif combination approach though they compute the contact points in different ways.

The alpha shape method depends on the Delaunay triangulation. The triangulation provides the information for generating the whole family of alpha shapes. It saves time for multiple trials of ball radii. However the Delaunay triangulation is costly for large datasets. For a given radius, the Delaunay triangulation is redundant for the computation of the desired alpha shape related with the given radius. The recursive algorithm solved this problem. It searches the contact points based on a series of comments. The algorithm partitions the profile into small segments and searches the contact point recursively until the two ends of the profile segment in evaluation could hold an empty disk with the given radius, similar for areal data.

The later four methods are geometrical algorithms, which output the contact points accurately. The naive algorithm, to catch the contact points, has to detect the points which do not change with the morphological closing or opening operations. Thus the results are limited to the accuracy of algorithm and are sensitive to round off errors in the calculation. This situation is further worsened by discretely sampling the disk.

Table 5.1 lists the thorough comparison of the algorithms, in which the computational performance and the real extension will be discussed as follows.

Table 5.1 The comparison of five algorithms

Algorithm	Analysis	Computation complexity	Areal extension
Naive algorithm	Direct method (image processing)	$O(n^2)$	Yes, costly
Motif combination algorithm	Iterative method	$O(n)$	No
Alpha shape algorithm	Delaunay triangulation	$O(n \log n)$	Yes, 3D Delaunay triangulation
Recursive algorithm	Recursive method	$O(n^2)$ worse, $O(n \log n)$ expected	Yes
Modified Graham scan algorithm	Incremental method	$O(n)$	Yes, costly

5.3 Performance evaluation

To evaluate the performance of the five algorithms, it is necessary to analyze the time complexity of the algorithms. For the naive algorithm, the worse case is when the size of the structuring element is equal to or larger than twice of the profile length. The calculation of each envelope ordinate involves the whole profile data, thus its time complexity is $O(n^2)$. The alpha shape method depends on the Delaunay triangulation with time complexity $O(n \log n)$ for both 2D and 3D data, therefore its time complexity is $O(n \log n)$. For the motif combination approach, the iterative process has the time complexity $O(n)$. The Graham scan algorithm does not need data sorting as required in the computation of the convex hull which may cost $O(n \log n)$ time, thus the computation of the contact points is also in $O(n)$ time. The Graham scan algorithm has the same time complexity as the motif combination algorithm; nonetheless it requires less memory because it is incremental and does not need to handle all the data simultaneously. The recursive algorithm, in the worse case that each set of divided segments of data is as skewed as possible, has the time complexity $O(n^2)$ although it rarely occurs in real practice. Its expected time complexity is $O(n \log n)$.

To assess the actual performance, experiments are carried out on the profile data with the point amount varying from 5000 points to 80,000 points. The profile data is sampled from a metal sheet surface in form of the propeller blade. It is measured with a Talysurf PGI (Taylor Hobson, UK) with sampling interval 1 μm. The morphological closing filter with disk radius 5 mm was performed on the profiles using the five algorithms. These algorithms were implemented by Visual C++ and ran on a computer with 3.16 GHz Intel Core Duo CPU and 3 GB RAM. The performance data are listed in Table 5.2.

Table 5.2 Algorithm running times over various amounts of profile data with the same disk radius

Data amount	5,000	10,000	40,000	80,000
Naive algorithm	0.0010s	1.0294s	4.8391s	9.9274s
Motif Combination algorithm	0.0076s	0.0157s	0.0609s	0.1238s
Alpha Shape algorithm	0.0124s	0.0508s	1.0112s	2.1531s
Modified Graham Scan algorithm	0.0079s	0.0158s	0.0636s	0.1253s
Recursive algorithm	0.0010s	0.0025s	0.0916s	0.1038s

The running time presented in Table 5.2 verifies the theoretical analysis of the time complexity of the algorithms. The naive algorithm is most time consuming, spending nearly 10 seconds for the 80,000 dataset. The alpha shape method is more efficient than the naive algorithm reducing the running time to about 2 seconds for the 80,000 dataset. The alpha shape method is dependent on the Delaunay triangulation which is costly in its data structure support, compared with the other algorithms. The motif combination algorithm and the modified Graham scan algorithm are much more efficient, only spending 0.1 second. The recursive algorithm also achieved good performance and even better than the motif combination algorithm and the Graham scan algorithm in some cases, although it has the worse theoretical computation complexity than the other two methods. This is because practical programming techniques used to implement algorithms have impacts on their performance. Algorithms with efficient data structures and memory operations usually have better performance.

Another experiment was carried out with an aim to assess the algorithm performances with the variation of structuring element size (disk radius in this experiment). The experiment was performed on the 80,000 dataset with the disk radius varying from 0.5 mm to 10 mm. The experimental data is presented in Table 5.3 and plotted in Figure 5.4. It is evident in the figure that the running time of the naive algorithm grows rapidly as the disk radius increases. The alpha shape algorithm and the recursive algorithm behave in an opposite manner: their running time decreases as the disk radius grows. It is reasonable considering the number of the alpha shape boundary facets decreases as the disk radius increases. For the recursive

algorithm, the recursion number reduces either with the increase of disk radius, which is evidenced by the fact that better performances can be observed with this algorithm when disk radius grows to 5 mm and 10 mm. As to the motif combination approach and the modified Graham scan approach, the disk radius variation has little impact on their performances.

Table 5.3 Algorithm running times with various disk radii and the same profile data

Disk radius	0.5mm	1mm	5mm	10mm
Naive algorithm	1.0167s	2.0086s	9.9274s	19.3092s
Motif Combination algorithm	0.1537s	0.1386s	0.1238s	0.1200s
Alpha Shape algorithm	2.4061s	2.2214s	2.1531s	2.0540s
Modified Graham Scan algorithm	0.1293s	0.1302s	0.1253s	0.1259s
Recursive algorithm	2.2728s	1.5197s	0.1038s	0.0190s

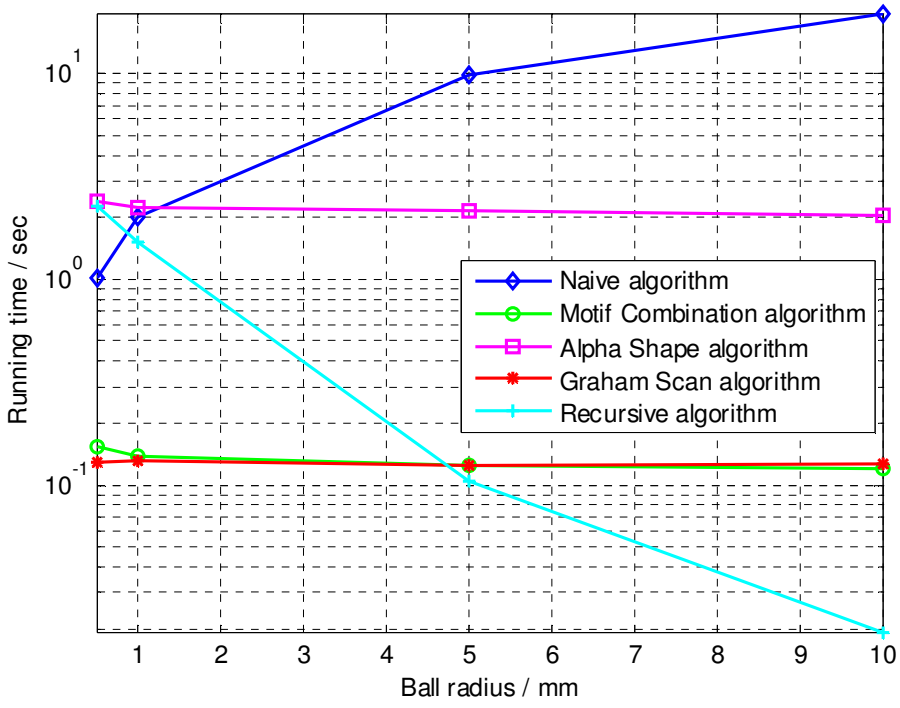

Figure 5.4 Algorithm running times on the same profile data using various disk radii

Experiments were also carried out for areal data aiming to evaluate the performance of the naive algorithm, the alpha shape method with and without the divide and conquer optimization and the recursive algorithm. The sample matrices for

areal data range from 100 × 100 to 1000 × 1000 points. They are filtered by morphological closing filter using a 10 mm ball respectively. The algorithm running time are illustrated in Table 5.4. It is evident that the proposed recursive algorithm achieved superior performance over the other two, especially for large areal data. The alpha shape method has better performance than the naive algorithm. However its running time rises rapidly with the increase of the areal data size due to the costly 3D Delaunay triangulation. The divide and conquer optimization significantly improved its performance. In this test, the minimum sub-divided surface is of 128×128 points in size. Experiments show that this size is a balanced selection in that the divide and conquer method achieves good performance with this configuration since the Delaunay triangulation on this size of dataset usually costs less than 1 second and it will not produce too much recursions. The naive algorithm is even worse with large areal datasets, rising sharply with the increasing data size. It spent more than 12 hours in dealing with the 1000×1000 dataset.

Table 5.4 Algorithm running time over various amounts of areal data with the same ball radius

Data amount	100×100	250×250	500×500	750×750	1000×1000
Naive algorithm	2.79 s	100.87 s	1822.6 s	10334.9 s	46208.8 s
Alpha shape algorithm	0.85 s	10.3 s	73.1 s	292.6 s	715.4 s
Alpha shape algorithm with the divide and conquer optimization	1.06 s	7.14 s	27.83 s	62.72 s	111.62 s
Recursive algorithm	0.16 s	1.42 s	19.7 s	57.6 s	250.4 s

Similarly, the experiment was carried to test the performance of the areal algorithms in response to the variation of the structuring element size (ball radius in this experiment). The experimental data listed in Table 5.5 reveals the same trend as to the situation of the profile data. The running time of the naive algorithm grows rapidly as the disk radius increases. The recursive algorithm decreases in its running time as the disk radius grows. The computation time of the alpha shape method runs steadily in that the Delaunay triangulation makes up the majority of the computation and the alpha shape facet extraction costs much less.

Table 5.5 Algorithm running time with various ball radii and the same areal data (512 x 512)

Ball radius	0.5 mm	1 mm	5 mm	50 mm
Naive algorithm	520.6 s	1786 s	1948 s	5155 s
Alpha shape algorithm	80.23 s	80.21 s	78.78 s	78.54 s
Alpha shape algorithm with the divide and conquer optimization	32.69 s	31.91 s	30.72 s	30.91 s
Recursive algorithm	249.53 s	80.69 s	13.05 s	2.74 s

5.4 Areal extension

All the five algorithms work for morphological profile filters. It could be easily recognized that the naive algorithm could apply to areal data by replacing the profile structuring element with its areal counterpart. For instance, the disk used in profile data becomes the ball in areal data. In this case, extreme points are achieved by evaluating the vector sum of the ball and the areal data in range overlapped by the ball.

The alpha shape method is also able to extend to the areal data if replacing the disk with the ball. Instead of a series of 2-simplices resulted by the 2D Delaunay triangulation, the 3D Delaunay triangulation yields a series of 3-simplices. Subsequently by checking the smallest circumsphere of these 3-simplices, the boundary facets of the alpha shape are obtained. Then the spatial envelope coordinates are achieved by interpolating points on the caps determined by the alpha shape boundary facets.

The motif combination algorithm has no obvious extension to the areal data because the motif combination test could be complex in the spatial case. Although there are areal extensions to profile motifs (Scott 1998; Scott 2004; Barre & Lopez 2000), the motif combination of areal motifs are quite different from morphological areal filter in functionality.

For the modified Graham scan algorithm, there is no existing extension for 3D data. An algorithm called the ball pivoting algorithm (Bernardini 1999) was developed to reconstruct the surface from the discrete point cloud. It simulates rolling a ball over the areal point set. In this sense this method could be viewed as the

extension of the modified Graham scan algorithm for profile data. As already presented, the recursive algorithm could handle areal data.

5.5 Summary

In this chapter, the comparison of the five algorithms is discussed in four aspects: algorithm verification, algorithm analysis, performance evaluation and areal extension. The experimental results show that the five algorithms are in agreement with each other except at the end regions. The naive algorithm is a direct implementation to morphological operations but it is time consuming for large datasets and large structuring elements. It has several limitations, such as the size of the structuring element is restricted and unable to handle freeform surfaces and unsuitable for non-uniform sampled surfaces. Opposed to these limitations, the alpha shape algorithm provides more feasibility and flexibility as well as easy extension to areal data. The divide and conquer optimization helps to improve its performance. The motif combination approach and the Graham scan approach are most efficient in performance with the linear time complexity. However they are hard to extend to areal data. Experiments show that the recursive algorithm is also an efficient method for profiles. A great merit of the recursive algorithm is that it is easy to extend to areal data which would be efficient for large areal datasets and large structuring elements.

6. END EFFECTS CORRECTION

End effects are common in the filtration of open surfaces. They are unintentional changes in the filtration response in the end portions of an open surface. ISO 16610-28 (2010) presents a couple of end effects correction methods for linear filtration techniques. In this chapter, methods are proposed to correct the end effects of morphological filters for open surfaces.

6.1 End effects for open surface filtering

End effects appear in the end portions of the surface measured by the nesting index, for instance, half length of the cut-off wavelength for the Gaussian filter, or half length of the structuring element used in morphological filters. As a consequence, the confidential area of the reference surface obtained by filtration techniques which is valid for surface characterization is confined to the middle portion with the end effect regions removed. The truncation caused by end effects produces negative impact on filtering because the assessment data is shortened. This means that no longer the entire measured data set is available for further evaluation, or that a longer measurement length is needed at all. This is particularly inconvenient in the case of long cut-off wavelengths or large sizes of structuring elements.

Figure 6.1 presents the end effect of Gaussian filtering on the experimental open profile with cut-off wavelength 0.08 mm. In contrast, the reference line generated by the first order Gaussian regression filter is also presented in the figure, which does not have the end effect. It is evident that the end effect exists on two end portions within half length of the cut-off wavelength (0.04 mm), which is marked by the bold vertical lines in the figure.

There are similarity and difference between the end effects of morphological filters and the Gaussian filter. The similarity is the end effect of morphological filters occurs within the range of half length of structuring element, while it differs from the Gaussian filter in that not all those regions of the morphological envelope are distorted, but only a portion of it. Figure 6.2 illustrates such an example. The same

experimental profile is applied by the morphological closing filter with disk radius 0.2 mm. Two closing envelopes are presented in the figure, one without end correction, and one with correction by applying the linear prediction method which will be discussed in Chapter 6.5. It could be noticed that the closing envelope at two ends are not totally distorted, but only a small portion of the end region.

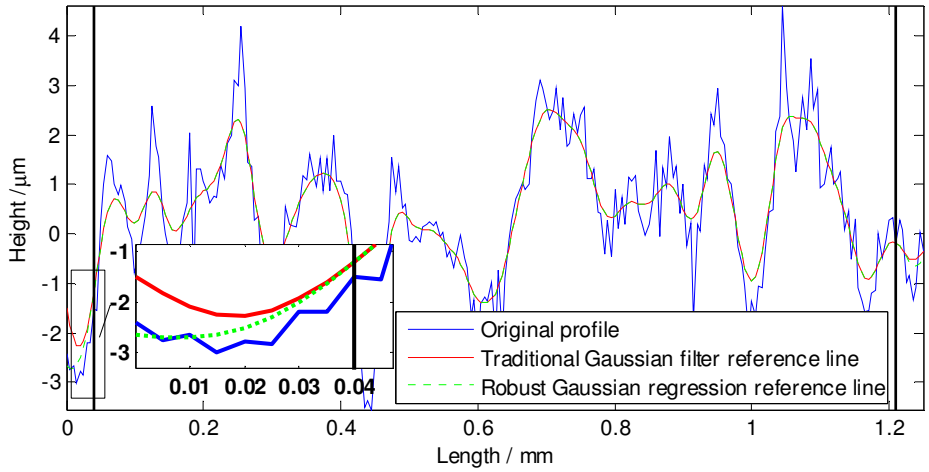

Figure 6.1 The end effect of the Gaussian filter on an open profile

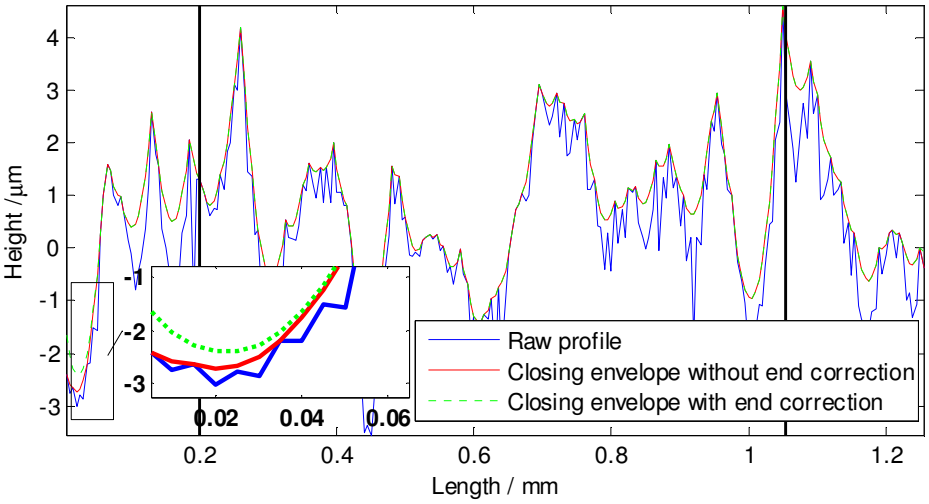

Figure 6.2 The end effect of the morphological closing filter on an open profile

6.2 Infinity padding

A common and simple solution for mean-line filters is to add sufficient zeros to two ends of the profile, referred as zero-padding (ISO 16610-28 2010). As to

morphological filters, the solution is similar to zero-padding: the profile is assumed to drop down to the negative/positive infinity outside of the profile for dilation/erosion respectively, known as infinity padding (ISO 16610-41 2010). It pads sufficient extreme ordinates for half size of the structuring element on both ends. Figure 6.3 illustrates the infinity padding method for the computation of the dilation operation using a disk. A surface profile $z(x)$ with measuring length l_t is padded with zeros over length l at the left side and right side of the profile,

$$\tilde{z}(x) = \begin{cases} \min(z), & -l \le x < 0 \\ z(x), & 0 \le x < l_t \\ \min(z), & l_t \le x \le l_t + l \end{cases} \quad (6.1),$$

where $l = \min(r, l_t)$ and r is the disk radius or half length of the horizontal line segment. The extreme value at the negative infinity is replaced by the minimum value of profile heights for practical computation. Vice versa, values equal to the maximum height are padded in the end portions of the surface for the computation of the erosion operation.

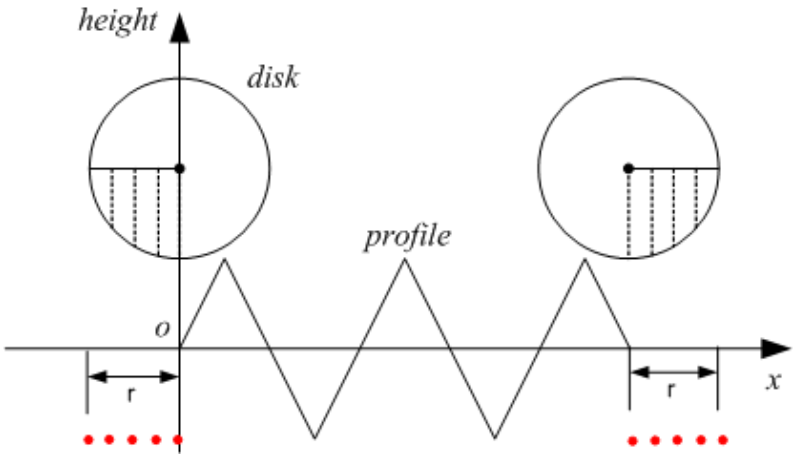

Figure 6.3 Infinity padding on two ends of the profile for the computation of the dilation operation

As presented in Chapter 2.4.1, the naive algorithm employs infinity padding such that the dilation or erosion ordinates in the profile ends could be calculated. A practical example of the closing envelope generated by the naive algorithm and infinity padding is illustrated in Figure 2.27.

As regarding to the other methods, i.e. the motif combination algorithm, the alpha shape algorithm, the recursive algorithm and the modified Graham scan algorithm, they do not pad extra points to extend the surface. They assume that the raw surface is confined to the measured region, namely no surface exists outside the measured portion. Nevertheless, for planar surfaces, this situation could also be viewed that the surface drops down to the negative infinity for the closing operation and rises up to the positive infinity for the opening operation, which is similar to the infinity padding even though they do not really pad extra points. It is obvious that the moving structuring element will contact the end points of the measured profile, thus the envelope will overlap with the measured profile at the two ends. This could be verified in the examples presented in the preceding chapters.

Figure 6.4 illustrates the experimental profile extended by infinity padding and its resultant closing envelope with disk radius 0.5 mm, obtained by the alpha shape method. It is shown in the figure that the resulting envelope is identical to the one presented in Figure 3.8 within the range of the raw profile, whereby the envelope is obtained without padding extra points.

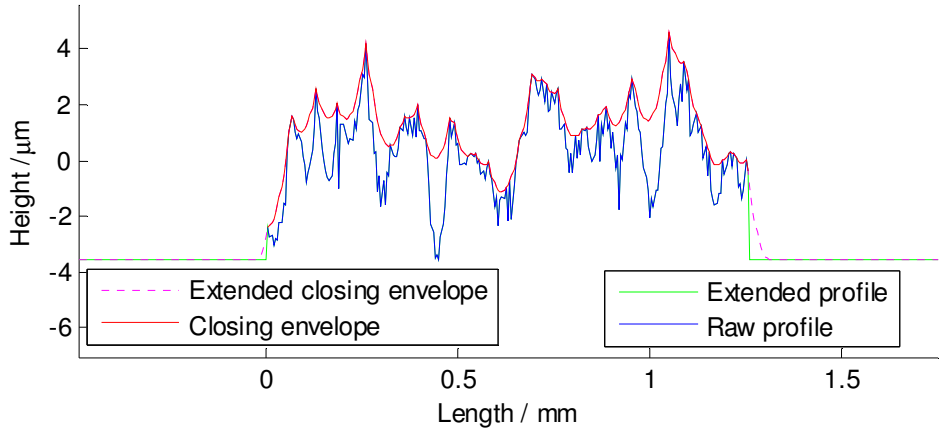

Figure 6.4 The profile extended by infinity padding and the closing envelope generated by the alpha shape algorithm

6.3 Symmetrical reflection

A measured profile is extended by symmetric extension on the left hand and right hand respectively. The reflection could be about the axis or the end points.

6.3.1 Line symmetrical reflection

A surface profile $z(x)$ with measuring length l_t is extended by horizontal reflection on the left hand and right respectively, and is defined by

$$\tilde{z}(x)=\begin{cases} z(-x), & -l \le x < 0 \\ z(x), & 0 \le x < l_t \\ z(2l_t - x), & l_t \le x \le l_t + l \end{cases} \quad (6.2),$$

where $l = \min(r, l_t)$ and r is the disk radius or half length of the line segment.

Figure 6.5 presents an example of line symmetrical reflection. The example profile is extended by reflection with the given disk radius 0.5 mm. The extended profile is then filtered by the morphological closing filter. The achieved morphological closing envelope is truncated by removing the portion on the extended length. The remaining portion within the range of measured length yields the final envelope. It could be recognized in the figure that the resulting envelope differs from the one generated by infinity padding (see Figure 6.4) in the end portions of the profile while it is the same in other regions.

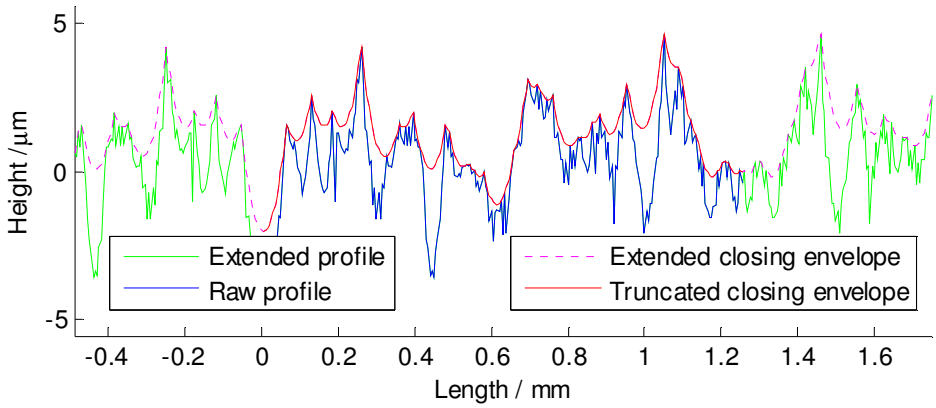

Figure 6.5 The line symmetrical reflection of the profile

Although reflecting the profile is an easy solution in an implementation point of view, it raises a computational issue. Reflection will aggravate computation performance, especially in the case of large datasets, because the input data of morphological filtration is significantly enlarged by the extension. This problem could be solved by reflecting the contact points on the profile instead of the raw profile data.

As stated in Chapter 3.5, the morphological envelope is determined by the contact points on the surface and other sample points have no influence upon it. Therefore reflecting the profile is identical to reflecting contact points in respect of end effects correction. Meanwhile reflecting contact points will not increase computation too much because the contact points are usually much less than the sample points.

Figure 6.6 demonstrates an example of reflecting contact points on a profile. At the beginning, all the contact points are located on the measured profile. Then the obtained contact points are reflected in a line symmetrical manner at the two ends within the region of disk radius. The newly created contact points are merged with the original contact points to generate an enlarged contact point set, which will be filtered again to yield the updated contact point set with those fake ones removed on joint portions. Finally the morphological envelope is computed using these updated contact points.

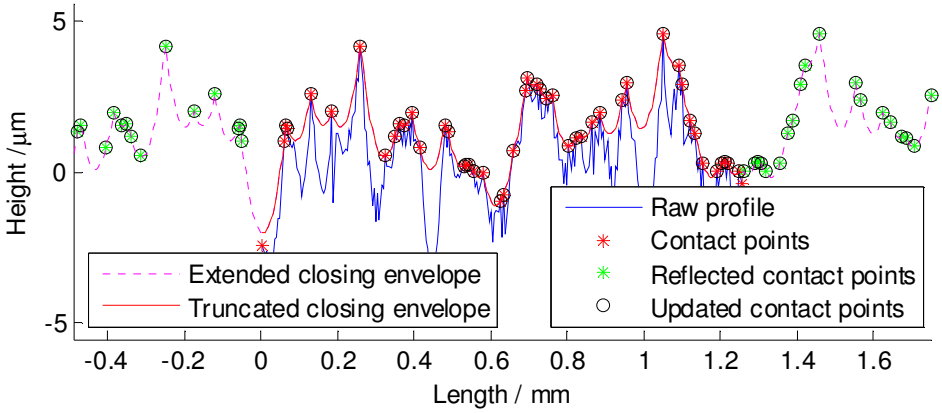

Figure 6.6 The line symmetrical reflection of the contact points on the profile

6.3.2 Point symmetrical reflection

A surface profile $z(x)$ with measuring length l_t is extended by horizontal reflection in conjunction with vertical reflection on the left hand and right hand respectively, and is defined by:

$$\tilde{z}(x)=\begin{cases} 2\times z(x=0)-z(-x), & -l\le x<0 \\ z(x), & 0\le x<l_t \\ 2\times z(x=l_t)-z(2l_t-x), & l_t\le x\le l_t+l \end{cases} \quad (6.3),$$

where $l = \min(r, l_t)$ and r is the disk radius or half length of the line segment.

Figure 6.7 presents an example of point symmetrical reflection. All the steps to produce morphological envelopes are same to the line symmetrical reflection, except the profile is reflected in a point symmetry manner. Similarly the point symmetrical reflection could also be optimized by only reflecting contact points in order to improve the algorithm performance. See Figure 6.8.

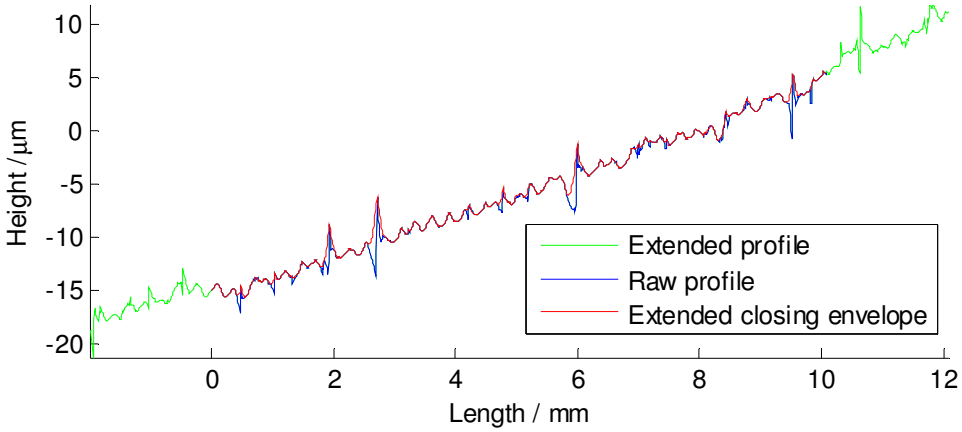

Figure 6.7 Point symmetrical reflection of the profile

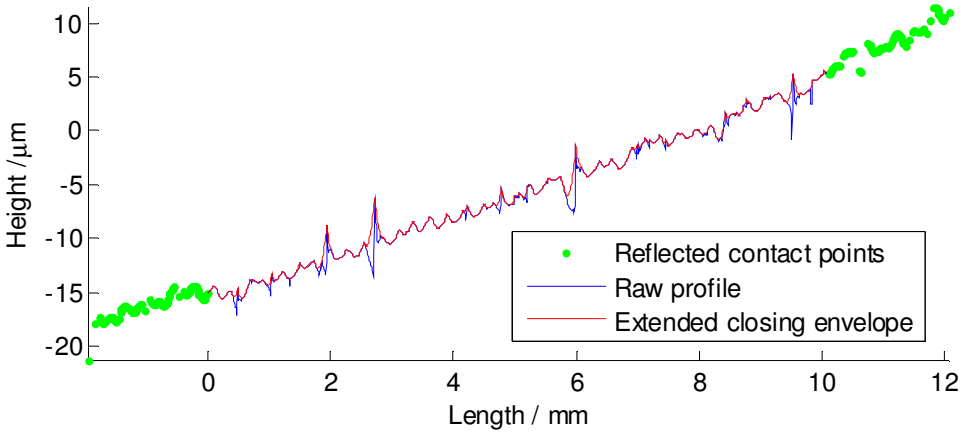

Figure 6.8 Point symmetrical reflection of the contact points on the profile

6.4 Polynomial extrapolation

A measured profile is extended by fitting a polynomial curve on the left hand and right hand using the least square method.

6.4.1 First order polynomial extrapolation

A polynomial in first order, $ax+b$, which equal to a least square line, is fitted to the profile $z(x)$ within the left and right end effect regions with length l:

$$\int_0^l \left(z(x)-a_l x-b_l\right)^2 dx \to \min_{a_l,b_l} \text{ and } \int_{l_t-l}^{l_t} \left(z(x)-a_r x-b_r\right)^2 dx \to \min_{a_r,b_r}. \qquad (6.4)$$

The profile is then extended to

$$\tilde{z}(x)=\begin{cases} a_l x+b_l, & -l \le x<0 \\ z(x), & 0 \le x<l_t \\ a_r x+b_r, & l_t \le x \le l_t+l \end{cases}, \qquad (6.5)$$

where $l=\min(r,l_t)$ and r is the disk radius or half length of the line segment.

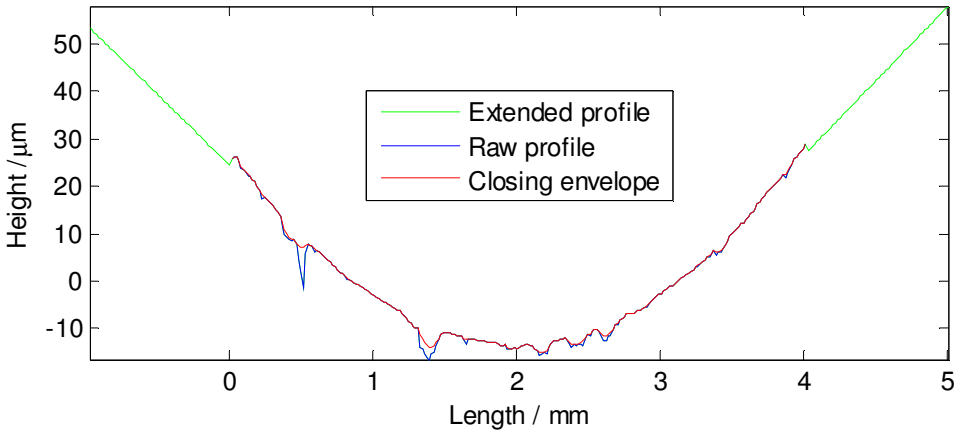

Figure 6.9 First order polynomial extrapolation to the profile

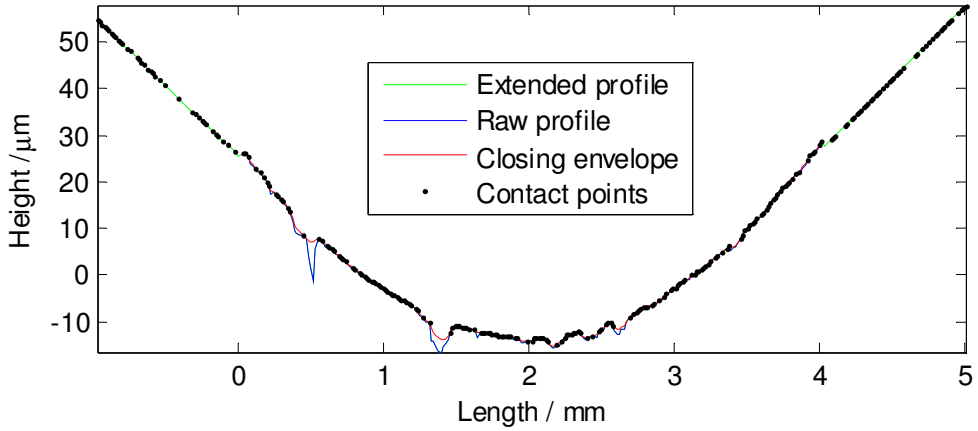

Figure 6.10 First order polynomial extrapolation based on the contact points on the profile

Figure 6.9 presents an example of the extension to a profile by linear extrapolation and its closing envelope with disk radius 1 mm. Figure 6.10 differs from Figure 6.9 in that the least square line is based on the contact points within the evaluation length l on the left and right end, aiming to reduce computation. The points of the extended profile are extrapolated on the least square line at sampling positions which reflects those of the corresponding contact points.

6.4.2 Second order polynomial extrapolation

A polynomial curve with second order, ax^2+bx+c, is fitted to the profile within the left and right end effect regions:

$$\int_0^{l}\left(z(x)-a_l x^2-b_l x-c_l\right)^2 dx \to \min_{a_l,b_l,c_l} \text{ and } \int_{l_t-l}^{l_t}\left(z(x)-a_r x^2-b_r x-c_r\right)^2 dx \to \min_{a_r,b_r,c_r} . \quad (6.6)$$

The profile is now extended to

$$\tilde{z}(x)=\begin{cases} a_l x^2+b_l x+c_l & -l \le x<0 \\ z(x) & 0 \le x<l_t \\ a_r x^2+b_r x+c_r & l_t \le x \le l_t+l \end{cases}, \quad (6.7)$$

where $l=\min(r,l_t)$ and r is the disk radius or half length of the line segment.

Figure 6.11 present an example of the extension to a profile by second order extrapolation and its closing envelope with disk radius 1 mm. In Figure 6.12, the least square curve is determined on the basis of the contact points within the evaluation

length l on the left and right end. The points of the extended profile are extrapolated on the least square curve at sampling positions by reflecting those of the corresponding contact points.

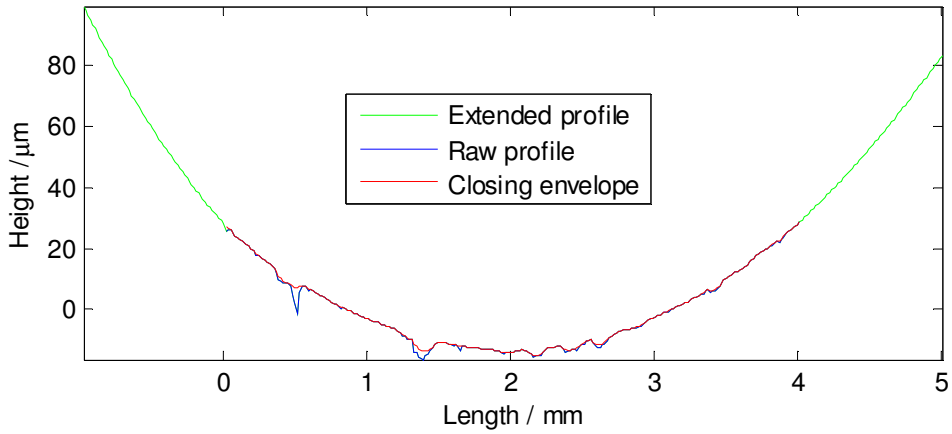

Figure 6.11 Second order polynomial extrapolation to the profile

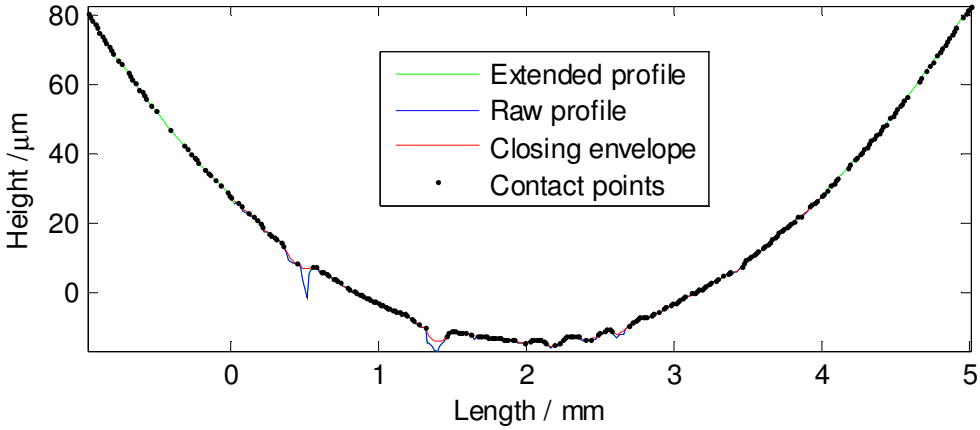

Figure 6.12 Second order polynomial extrapolation based on the contact points on the profile

6.5 Linear prediction

Linear prediction is a technique to predict the value of sample s_n using a linear combination of p most recent past samples, where p is called the prediction order (Makhoul 1975; Gopinath & Rangaraj 1993; Gary 2003; Vaidyanathan 2008).

The estimate of s_n has the form: $\overline{s}_n = -\sum_{k=1}^{p} a_k s_{n-k}$. The error (residual) between the actual value and the estimated value is

$$e_n = s_n - \overline{s}_n = s_n + \sum_{k=1}^{p} a_k s_{n-k} . \tag{6.8}$$

The parameters a_k are obtained by minimizing the mean or total squared error

$$E = \sum_n e_n^2 = \sum_n \left(s_n + \sum_{k=1}^{p} a_k s_{n-k} \right)^2 \to \min_{\{a_i\}} . \tag{6.9}$$

E is minimized by setting $\frac{\partial E}{\partial a_i} = 0$, $1 \le a_i \le p$:

$$\frac{\partial E}{\partial a_i} = 2 \sum_n \left\{ \left(s_n + \sum_{k=1}^{p} a_k s_{n-k} \right) \bullet s_{n-i} \right\} = 0 . \tag{6.10}$$

Thus it leads to

$$\sum_{k=1}^{p} a_k \sum_n s_{n-k} s_{n-i} = -\sum_n s_n s_{n-i} , \tag{6.11}$$

which is a set of p equations with p unknowns and can be solved for the predictor efficiencies $\{a_k, 1 \le i \le p\}$.

Assume that the error E is minimized over the infinite duration $-\infty < n < +\infty$, then Equations (6.9) reduce to:

$$\sum_{k=1}^{p} a_k R(i-k) = -R(i) , \tag{6.12}$$

where $R(i) = \sum_{n=-\infty}^{\infty} s_n s_{n+i}$ is the autocorrelation function of the signal s_n .

Thus the linear prediction technique could be employed to extend the measured profile using the data already sampled. Figure 6.13 presents the extension of the experimental profile using the linear prediction with prediction order 10 and the resulting closing envelope with disk radius 1 mm.

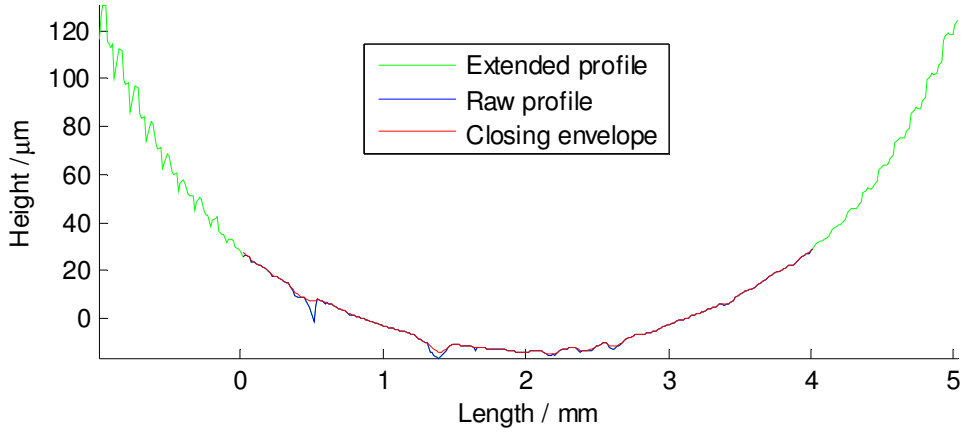

Figure 6.13 Tenth order linear prediction to the profile

6.6 Discussion

End effects are common in the filtration of open surfaces. They will cause distortions to the resulting surface generated by the filter and further influence the evaluation of surface textures. Both mean-line based filters (e.g. the Gaussian filter) and morphological filters have end effects. However they are different in respect to the generation of end effects. The Gaussian filter is a typical convolution operation of the measured surface and the Gaussian weighting function. The distortions are caused by the convolution operation of the data in the end regions of the surface within the length of half of the cut-wavelength. Thus the whole end regions of the open surface experience this distortion. Morphological filters have the similar problem, however they behaviour somewhat differently. Theoretically, the end effect regions of morphological filters are related to the size of structuring element, for example, the disk radius. Nevertheless it is easily noticed that the distortion does not occur to all the problematic end regions, but only a portion of them. The reason is end effects of morphological filters are determined by geometrical properties of the end regions and the structuring elements. Certain portions of end regions close to the central part of surface may not be affected. In this aspect, end effects of morphological filters are not as serious as that of the Gaussian filter.

Another notable difference between morphological filters and mean-line based filters in terms of end effects is the necessity of correction. As aforementioned, it is necessary to correct end effect of open surface filtration for surface texture separation, whereas morphological filters could serve in other purposes, for instance, contact

functional evaluation related with contact phenomenon. In some cases the end effect correction is not necessary as it is in the roughness evaluation. The reason is that the geometrical algorithms for morphological filters by themselves assume that there exists no extension beside the surface being evaluated, which is physically natural for functional analysis. A good example will be presented in Chapter 7.1, which set out to extract topographical features on engineering surfaces.

6.7 Summary

This chapter lists a couple of correction methods. In general, the central idea of these correction methods is to extend the measured surface to their neighbourhood, trying to reproduce their geometrical properties using the given measured data. Infinity padding used in the naive algorithm is a limited method, which takes the prerequisite that the surface is planar. The reflection methods with two options, either the point symmetry or the line symmetry, are suitable for surfaces with linear slope. The appropriate selection of two options depends on whether the method could better follow the trend of the surface. Polynomial extrapolation and linear prediction are more robust in surface extension as against to infinity padding and reflections. They can handle surfaces with more complex geometry. As illustrated in the above examples, the contact points of the surface may help to reduce the computation enlarged by the data extension.

Last but not least, it is obvious that these end effect correction methods for profile data could be easily extended to areal data. The areal extension of linear prediction can be found in the references (Digalakis 1993; Marple 2000).

7. CASE STUDIES

In this chapter, four case studies are presented to demonstrate the feasibility and applicability of the proposed morphological methods. At the beginning, the proposed areal methods are utilized to extract topographical features from engineering surfaces, including surfaces measured from a tooth implant, a femoral component of artificial knee joint and a bullet. Afterward they are employed to perform the filtration on a freeform surface and a non-uniform sampled surface. Following that, the morphological filters are employed in roundness filtration. Finally the algorithms searching for contact points are applied to the assessment of the underlying form of the textured surface of hip replacement taper junction.

7.1 Extraction of topographical features from engineering surfaces

7.1.1 Surface topography analysis

Surface topography is comprised of different surface components, i.e. roughness, waviness and form, and multi-scales of topographical features, such as random peaks/pits and ridges/valleys. Topographical features are functionally critical for component performance. For example, during the functional operation of interacting surfaces, peaks and ridges will act as sites of high contact stresses and abrasion. Consequently wear particles and debris will be generated by such kind of surface topographical features, whereas pits and valleys will affect lubrication and fluid retention properties (Jiang *et al.* 2011b). Thus the functional assessment of surface topography must not only appropriately separate roughness, waviness and form error, but also extract the topographical features from surfaces.

In surface texture analysis, the separation of roughness and waviness components is usually conducted by the filtration techniques. The mean-line based filters, for instance, the Gaussian filter, as well as the average statistical parameters are widely used techniques to detect the manufacturing process. However, the significant events on the surface, such as peaks and pits, are usually smoothed during the filtration

process. It is these topographical features that play more important roles in functional performance. In contrast, morphological filters are more relevant to geometrical features of surfaces and suitable for functional prediction of components in terms of tribology. As a result, morphological filters are valid candidates for the extraction of topographical features.

7.1.2 Methodology

The naive algorithm for morphological filters however has two limitations on its application on surface topography analysis. For one thing, the maximum size of the structuring element is limited due to the huge computation requirement, whereas for many real applications they may desire the structuring element size much larger than the size of the surface in evaluation. For another, the naive algorithm in its implementation has the end effect corrected by infinity padding.

The end effect correction by infinity padding will cause distortion to the extraction of topographical features. Refer to Figure 7.1 as an example. The profile in evaluation is a simulated data in form of the parabola curve superimposed by the intentionally made pits, see Figure 7.1(a). To extract the pit features, using the traditional method, the simulated profile is applied by the morphological closing filter with disk radius 5 mm to yield a closing envelope which is graphed in the figure as the dash line. The closing envelope is then subtracted from the original profile to obtain a residual profile. It is obvious in Figure 7.1(b) that this end effect corrected profile has distortions at the two end of the profile on which the pit features are not properly extracted. It will definitely influence the precise evaluation of topographic features, especially for surfaces having significant form components.

In comparison to the naive algorithm, the alpha shape method and the recursive method are more competent in using large structuring elements. Another merit of these algorithms is that the obtained morphological envelope follows the form of the surface all over including the boundary regions, thus there are no distortions to the extraction of topographical features. As presented in the example of Figure 7.1, the closing envelope obtained by the alpha shape method, which is graphed by the dotted line in the figure, follows the profile with no distortions at the profile end. As a result, the pit features on the profile are extracted without distortion.

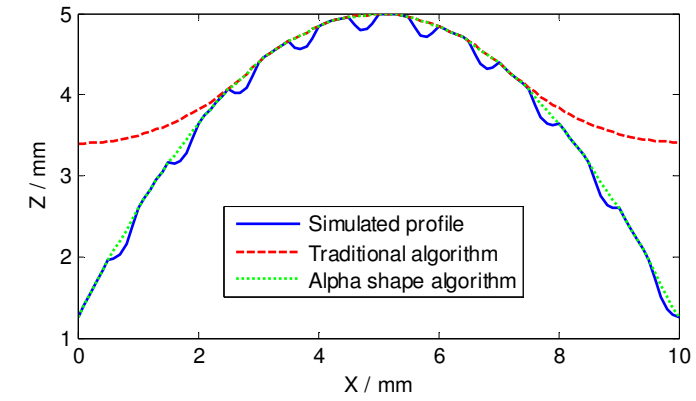

(a)

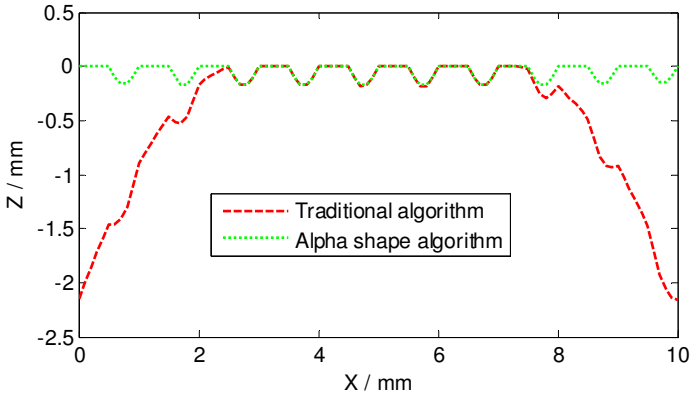

(b)

Figure 7.1 Morphological closing envelopes generated by the traditional method and the alpha shape method. (a) raw profile and closing envelopes; (b) Residual profiles obtained by subtracting the closing envelopes from the raw profile

7.1.3 Application

Aiming to verify the capability of the proposed morphological methods, a set of typical engineering surfaces from the bioengineering industry and the weapon industry are selected as the objectives for the extraction of topographical features.

Figure 7.2(a) presents a surface measured from a tooth implant, which is widely used to facilitate osseointegration of human/animal tissues (Wang et al. 2011). It was made from titanium materials and produced by fine grinding, sandblasting and acid etching. The specific surface texture has a critical role on the component's functionality in terms of cellular adhesion and proliferation. Using the proposed morphological areal methods, a morphological closing filter with ball radius 5 mm is first applied to the raw measured surface to generate a closing envelope, see Figure 7.2(b). The residual surface obtained by subtracting the closing envelope from the raw surface is illustrated in Figure 7.2(c). It is evident from the residual surface that the

manufacture marks have been successfully extracted and could be used for further functional evaluation.

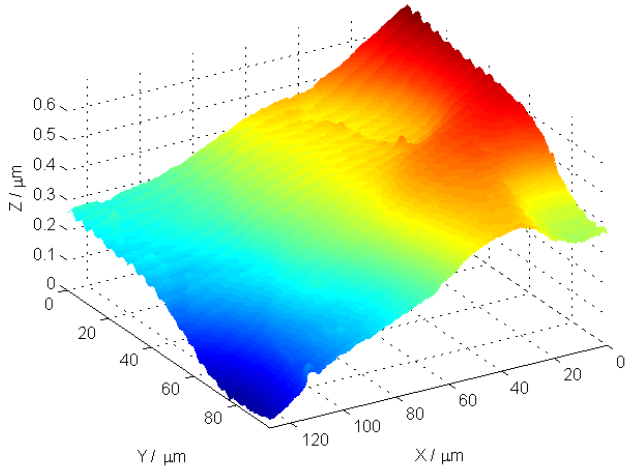

(a)

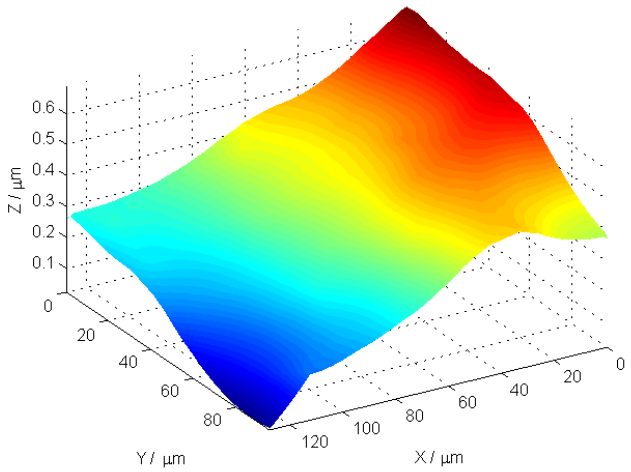

(b)

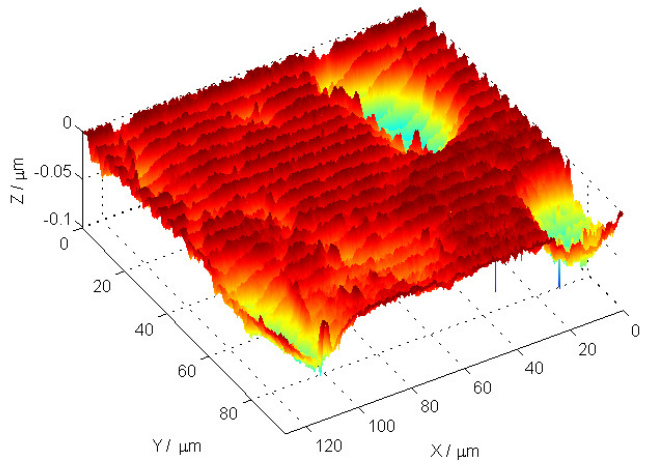

(c)

Figure 7.2 The titanium tooth implant surface. (a) Raw measured surface; (b) Closing envelope; (c) Residual surface

Figure 7.3(a) illustrates a surface measured from a worn artificial knee femoral component. The femoral component is critical for the knee joint system because it not only enables leg bending motions, but is also able to resist long term wear in service. The wear property of the knee femoral component surface is of paramount importance for the lifetime of the whole artificial knee joint system. It is shown in the figure that the surface topography consists of the roughness component and wear marks. It is reported that in comparison to roughness and waviness components, the wear rates of surfaces in the operational service are more affected by topographical features like pits, valleys, scratches (Jiang & Blunt 2004). From the functional evaluation point of view, these topographical features will impact directly on wear mechanics and physical properties of the component.

To reduce the effect of roughness, the alternating symmetrical filter with ball radius 1 mm is applied to generate a smoothed surface, as shown in Figure 7.3(b). Afterwards, a morphological closing filter with ball radius 50 mm is applied to generate a closing envelope. See Figure 7.3(c). By comparing the closing envelope and the smoothed surface, the residual surface is obtained, on which wear marks are clearly presented. See Figure 7.3(d).

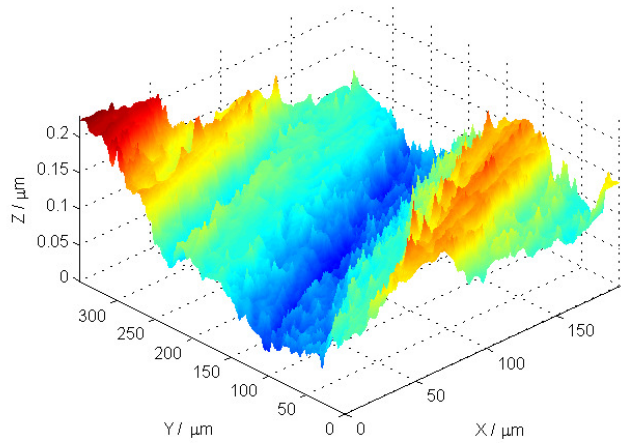
Z / µm
0.2
0.15
0.1
0.05
0
300
250
200
150
100
50
0
Y / µm
0
50
100
150
X / µm

(a)

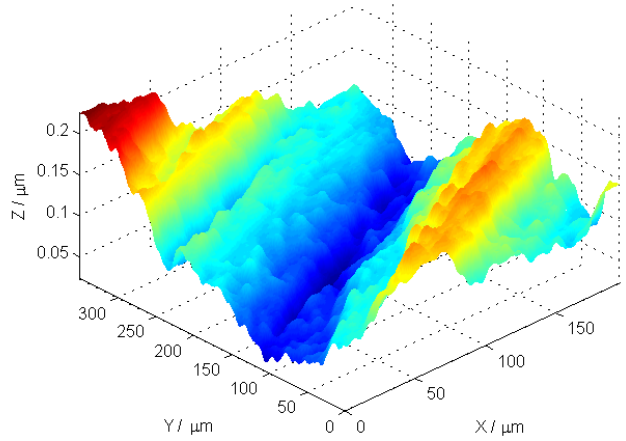
Z / µm
0.2
0.15
0.1
0.05
300
250
200
150
100
50
0
Y / µm
0
50
100
150
X / µm

(b)

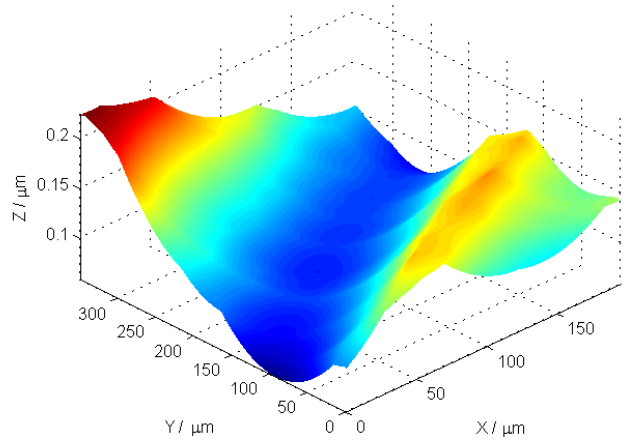
Z / µm
0.2
0.15
0.1
300
250
200
150
100
50
0
Y / µm
0
50
100
150
X / µm

(c)

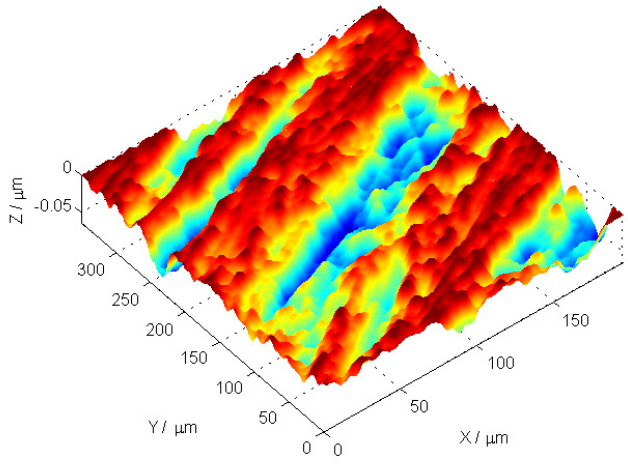

(d)

Figure 7.3 The worn surface of an artificial knee femoral component. (a) Raw measured surface; (b) Smoothed surface; (c) Closing envelope; (d) Residual surface

Figure 7.4(a) illustrates a used bullet surface on which some wear and deformation marks can be observed. When a bullet is fired and travelling through the barrel which is usually manufactured to have spiral grooves to stabilize the flight of the bullet and improve its accuracy, the bullet rubs against the inner surface of the barrel driven by the massive propellant, and the bullet surface is deformed and worn during this process. It follows that by examining the surface topography of bullet it is able to identify the flaws of bullets and gun barrels. A reference surface is obtained by applying the morphological alternating filter, first a closing with ball radius 50 mm followed by an opening with ball radius 1 mm. Then the topographical features are extracted in the residual surface and these deform and wear marks can be analysed for the purpose of characterisation. It should be noticed that the radial mark presented on the surface is not the wear mark but the clamping section of the bullet and its case.

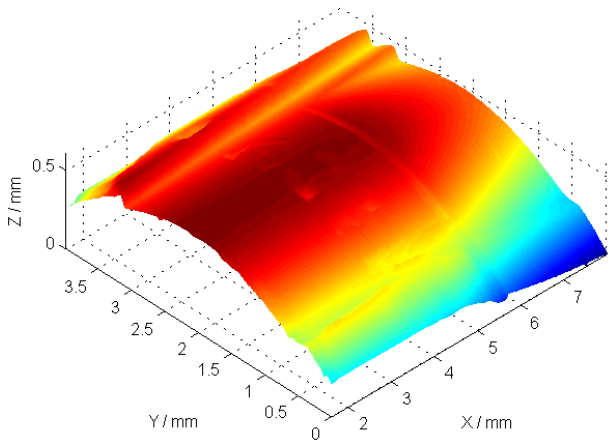

(a)

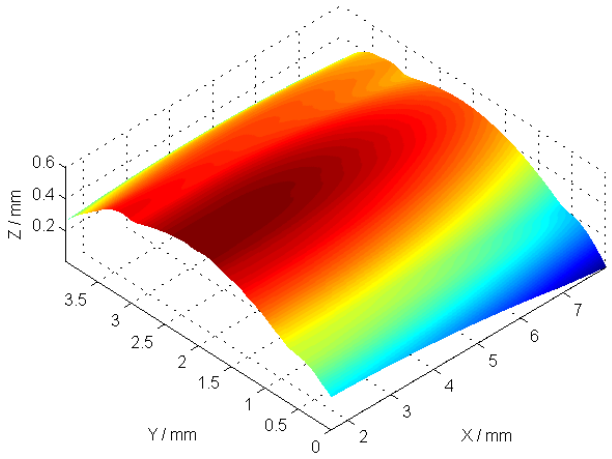

(b)

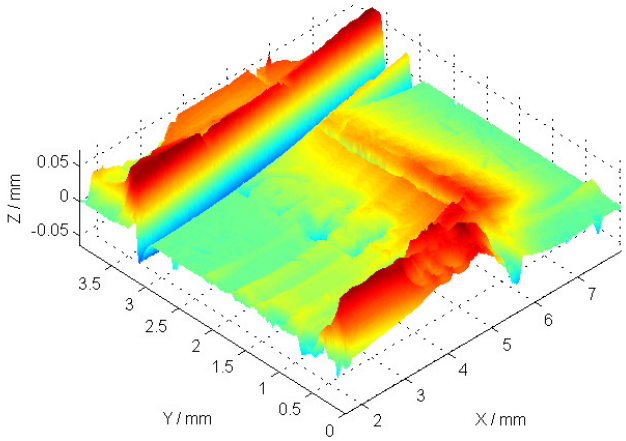

(c)

Figure 7.4 The used bullet surface. (a) Raw measured surface; (b) Reference surface; (c) Surface with extracted topographical features

7.2 Filtration of freeform and non-uniform sampled surfaces

Three experimental surfaces are employed to illustrate the capabilities of the proposed areal methods for morphological filters on freeform surfaces and nonuniform sampled surfaces respectively. In Figure 7.5(a), a saddle surface is presented, which has a number of tiny bumps and also some “twisted” underlying waves on the surface topography. Morphological symmetrical filters (closing followed by opening) are applied to this surface with ball radius 0.5 mm and 2 mm respectively. Figure 7.5(b) and Figure 7.5(c) illustrate the generated surfaces. It is evident that bump features are suppressed by the filter in Figure 7.5(b) and wave features are also smoothed in Figure 7.5(c). By comparing the three surfaces, these special topographical features of the surface can be analysed.

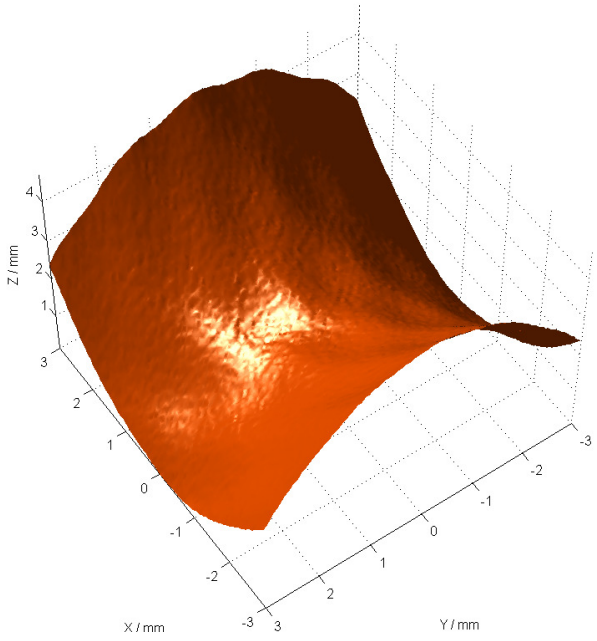

(a)

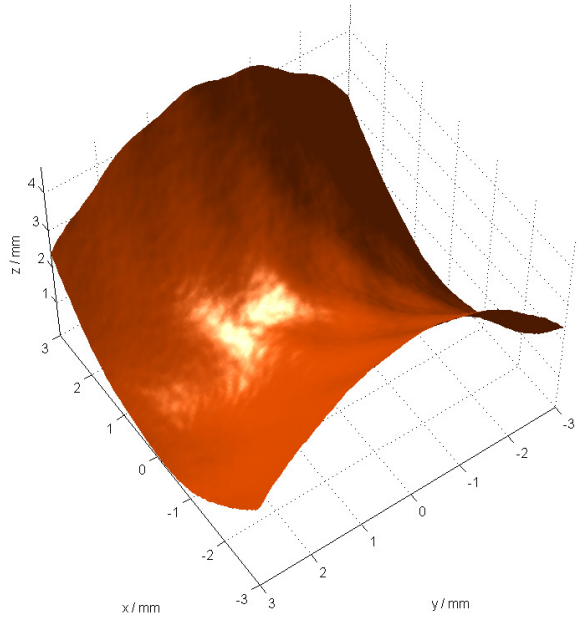

(b)

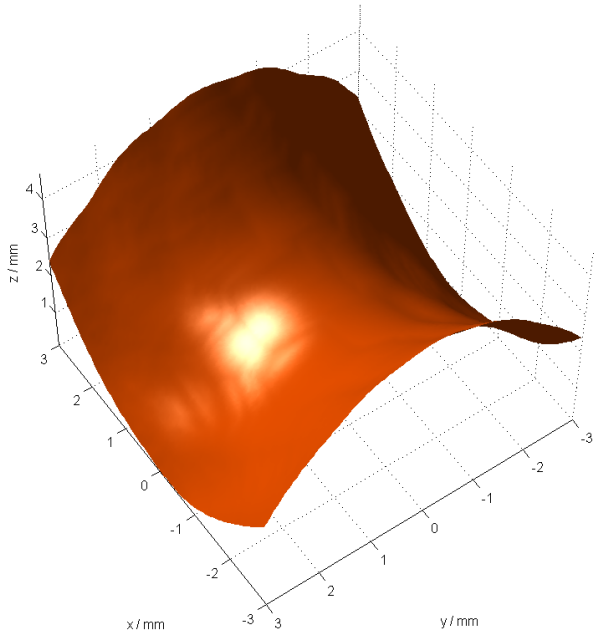

(c)

Figure 7.5 The surface in saddle shape. (a) The raw surface; (b) The surface generated by a ball with radius 0.5 mm; (c) The surface generated by a ball with radius 2 mm

In the second experiment, Figure 7.6(a) is a surface measured from an optical F-theta lens, which is widely used in laser printers and scanners. F-theta lenses are designed to have a smooth and continuous freeform figure to achieve specific optical

functions and usually have ultra-precision geometry with sub-micrometre shape error and nanometre roughness. Using a morphological closing filter with ball radius 2.5 mm, a covering envelope surface is generated. See Figure 7.6(b). The surface presented in Figure 7.6(c) is the residual surface obtained by subtracting the envelope surface from the original surface. The defects of the materials and the manufacturing marks possibly produced by the diamond fly-cutting are easy to detect on the residual surface.

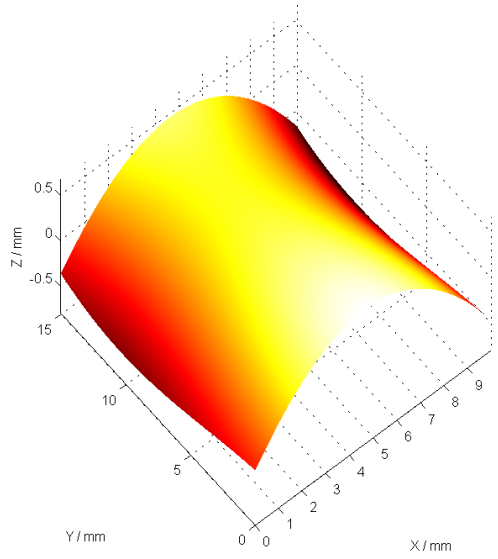

(a)

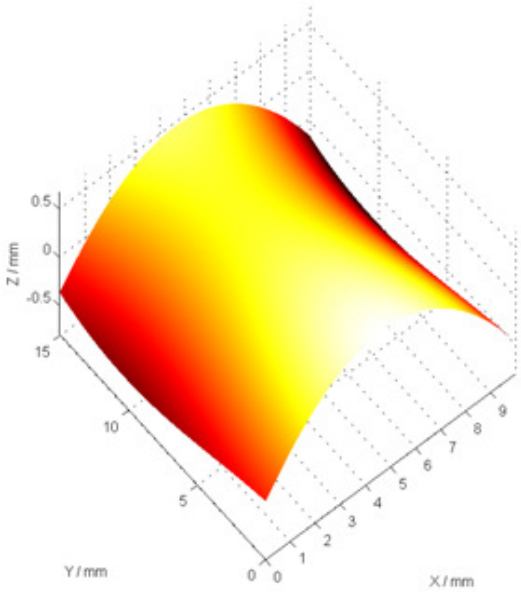

(b)

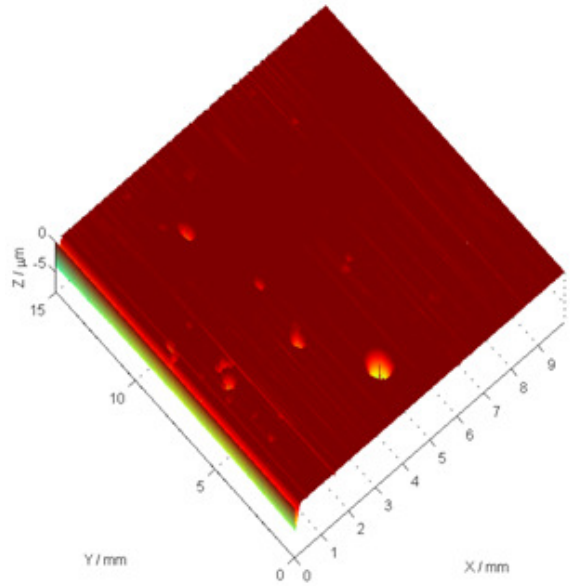

(c)

Figure 7.6 The F-theta surface. (a) Raw surface; (b) Closing envelope; (c) Residual surface

Another experiment was performed on a milled surface. The surface area is 5.11 x 5.11 μm^2 with 2962 sampling points. As marked by the dots in Figure 7.7(a), these sampling points are non-uniform sampled on the surface. The morphological closing filter with a 15 µm ball, using either the alpha shape algorithm or the recursive algorithm, was performed on these non-uniform sampled points. The resulting envelope points are illustrated in Figure 7.7(b), shown as the dots above the original surface. The ability of filtration on non-uniform samples can be useful in coordinate measurement for freeform surfaces whereby CMMs may sample the surface adaptively according to local curvatures of the surface.

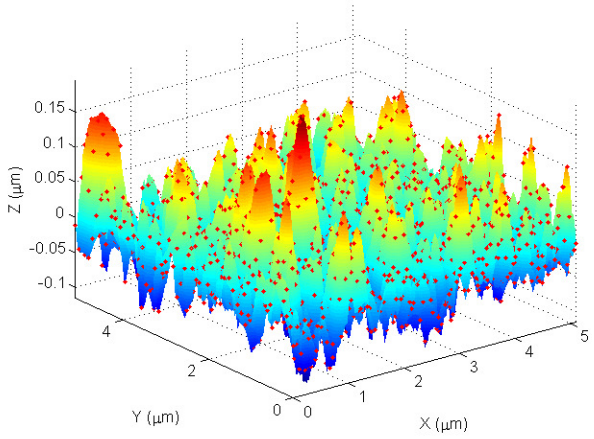

(a)

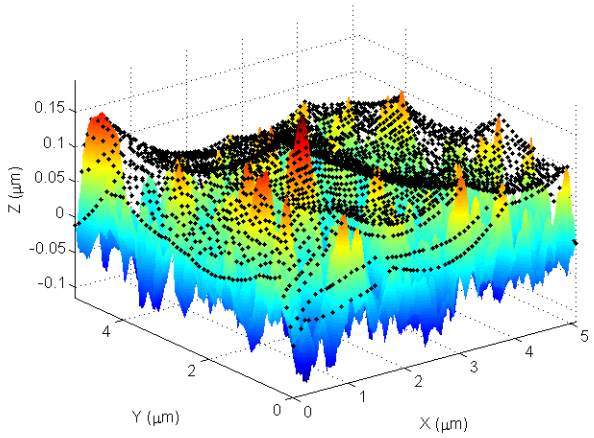

(b)

Figure 7.7 Morphological closing filter on the non-uniform sampled surface: (a) The original surface with the non-uniform sampled points; (b) The original surface with the closing envelope points

7.3 Roundness filtration

Having presented the application of morphological filters to open surfaces, it is interesting to examine if they could be applied to closed surfaces. Unlike open profiles measured on planar surfaces, roundness profiles, such as those obtained using a rotating-spindle stationary probe roundness instrument, are closed profiles in shape. The roundness data should also be partitioned into different wavelength regimes to better understand process parameters and functional performance (Muralikrishnan & Raja 2009).

Conventionally, the data measured by roundness instruments are radius suppressed, which means the data only reflects the radial deviation while is insensitive

to the radius itself. In such a situation, the Gaussian filter and the spline filter have been successfully employed to decompose roundness data (Krystek 1996b; Zeng *et al.* 2011b). However there is no literature showing that morphological filters can be applied for roundness filtration, even though theoretically it is possible. They should work on the unsuppressed roundness profiles, which means the component's radius and radius deviations are compounded together. Both the state of art roundness instruments and the Coordinate Measurement Machine (CMM) can provide such kind of data.

Using a disk with suitable size and rolling it over the roundness profile, the resulting boundary profile formed by the rolling disk is the morphological envelope. The naive algorithm was developed on the pre-requisite that surfaces are assumed to be open and planar and it cannot be extended to closed surfaces. Nevertheless the proposed alpha shape method can solve this limitation and is suitable for roundness filtration in that it does not need to take care of the joint portion of the start and end of the roundness data, as is requested by the motif combination method and the modified Graham scan method.

The procedures of using the alpha shape method to compute morphological envelopes for roundness data is listed as following:

1. Perform the Delaunay triangulation of the roundness data as Figure 7.8 illustrates.

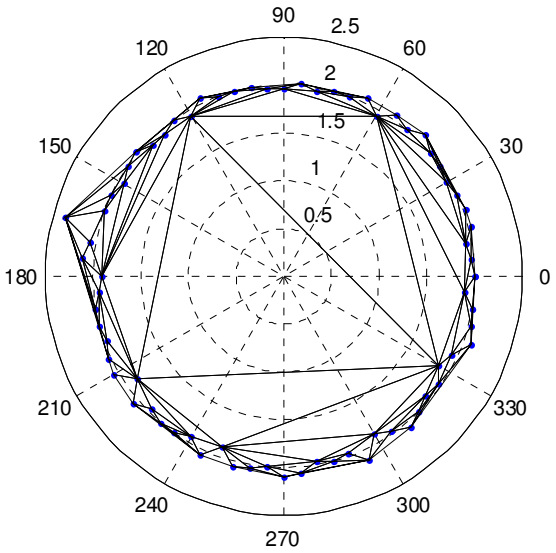

Figure 7.8 The Delaunay triangulation of roundness data

2. Extract the alpha shape boundary facets in terming of the given radius. See Figure 7.9.

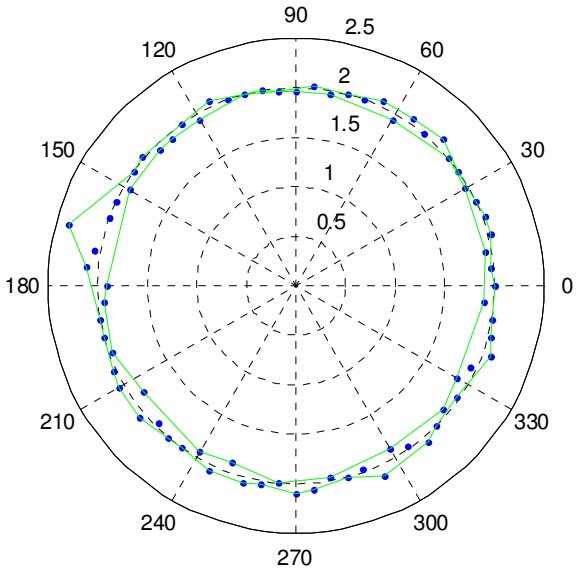

Figure 7.9 The extraction of alpha shape boundary facets of the roundness data

3. The closing envelope is determined by the external facets while the opening envelope depends on the internal facets. The ordinates of the envelope are obtained by interpolating points on the arcs determined by these facets. Figure 7.10 presents the closing envelope resulted from the external facets.

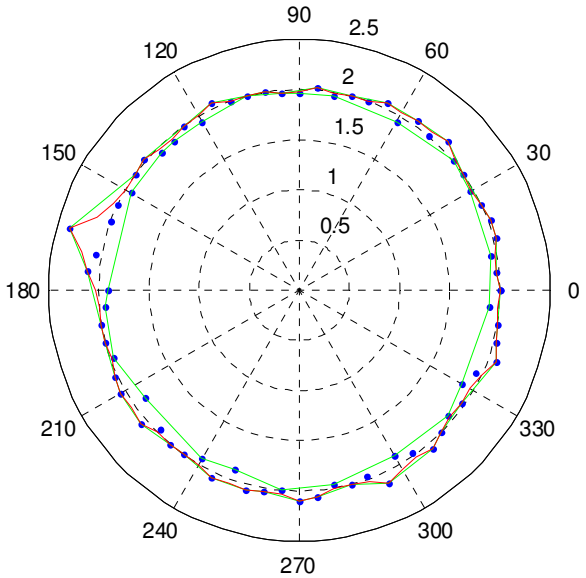

Figure 7.10 The closing envelope of the roundness data

Figure 7.11 presents an example of applying the morphological alternating symmetrical filter (closing followed by opening) on a roundness profile measured from a cylinder part by a CMM. The cylinder is about 10 mm in radius and the roundness data is filtered with a disk of radius 1 mm. It should be noticed that for convenience of visualization both the roundness profile and the morphological envelope are radius suppressed (reduced by 9 mm).

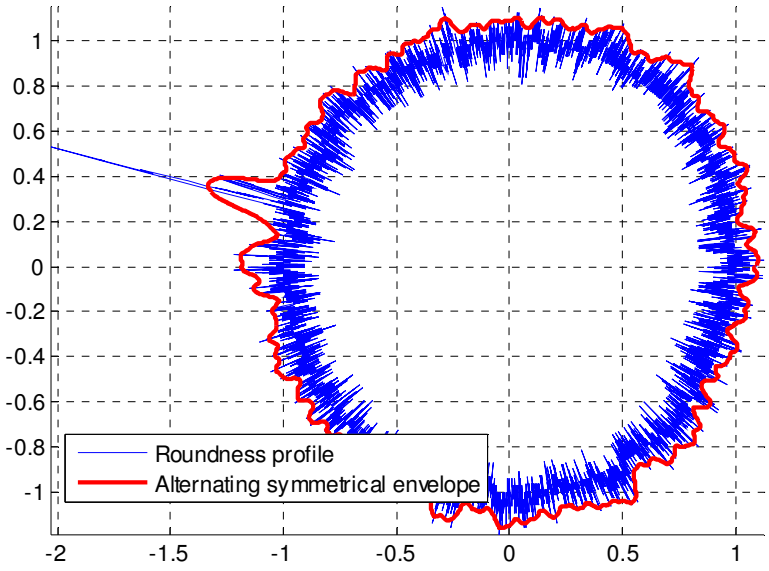

Figure 7.11 The morphological envelope obtained by the alternating symmetrical filter with disk radius 1 mm (Part radius suppressed)

7.4 Evaluation of hip replacement taper junctions

In hip replacement the introduction of modular large head metal-on-metal (LHMoM) hips promised low wear rates and reduce chances of dislocation couple with an increased range of motion compared to the conventional metal-on-metal hips. The clinical experience of the use of LHMoM hip replacements shows that they exhibit a significantly higher revision rate compared to other types of implant, at 5 years the revision rate is 7.8% compared to 6.3% for hip resurfacings and 2% for conventional cemented implants (Medical Device Alert 2010). The difference in revision rate between resurfacings and LHMoM hips has been attributed to the neck/taper junction (Bolland *et al.* 2011), thus the specification and measurement of this area of the component is key to the understanding of the operation of the implant and the failure mechanisms at this interface.

The interlocking male taper surface that mates with the femoral head female counterpart has a structured micro-threaded surface, see Figure 7.12. The specification of such surfaces is not well understood but has been shown to be important as possible corrosion and wear at this interface have been identified as a possible source of debris that could cause tissue reaction and progress to implant failure. Analysis of this structured conical surface requires the extraction and examination of the conical form and contact. In this example vertical measurements are performed axially relative to the aligned component axis such that the outputted value of profile straightness can then be used as a measure of conical form.

Figure 7.12 Total hip replacement femoral stem with highlighted micro-threaded taper surface

The combined effect of form and roughness has long been recognised in the measurement of the form of machined rough surfaces (Radhakrishnan 1970). The effect of the surface structure on the resulting form value can be disproportionate, thus the size of the probe relative to texture spacing has to be large (Whitehouse 1994; Reason 1966). Thus current industry practice in the measurement of hip stem tapers is to attempt to perform this task through use of mechanical filtering, by using a large diameter ruby stylus on a CMM. However, this is largely performed on a trial and error basis and makes no account of how much useful data is being discounted or erroneous data included through the bridging of surface contact points. Furthermore the use of such a large stylus method is suboptimal as the required component accuracy is on the limit of that of the CMM (< 1μm). This coupled with the difficulties in locating data points when using a prohibitively large measurement stylus means that this method is far from ideal.

Aiming to the deficits of the mechanical filtering by traversing the stylus on CMM, the morphological method is developed to improve measurement accuracy and to extract the contact points. To achieve this, a number of new hip replacement

femoral stems were measured, a series of linear measurements are performed on each component, axially along the neck taper. The measurements were performed using a Talyrond 365 roundness machine (Taylor Hobson, UK) with a 5 µm diamond stylus. Figure 7.13 presents such an example profile with sampling length 8 mm and sampling interval 0.25 µm. For convenience of visualization, the profile was first translated and rotated by the angle of the least square line of the profile. See Figure 7.14. Afterwards, the morphological closing filter is applied to the rotated data with disk radius 5 mm. The contact points are extracted from the texture imposed by the presence of the micro-threaded surface profile. Finally the form error of the straightness of the profile was calculated by applying the minimum zone method (Venkaiah & Shunmugam 2007) to the contact point set. The obtained straightness is 1.43 µm in the example.

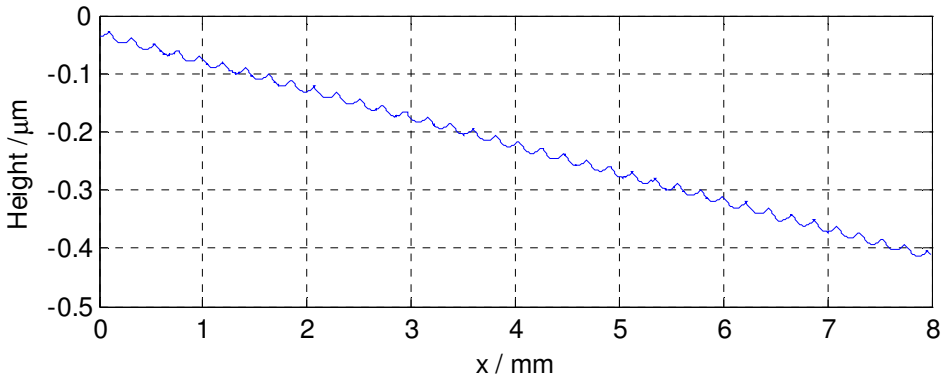

Figure 7.13 Surface profile measured along the neck taper

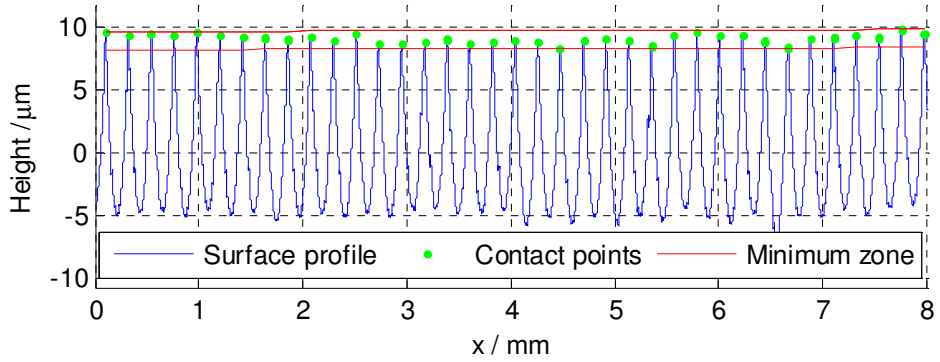

Figure 7.14 The extracted contact points and the minimum zone

The morphological filtering method searching the contact points allows for the optimization of mechanical traversing process by the determination of what equivalent stylus size would be required to perform this task. The use of a roundness

machine and morphological filter allows for data to be captured at a higher density and accuracy (Gauge resolution ~30 nm) with a greater level of control in the extraction of the true envelope profile.

7.5 Summary

This chapter presented four case studies. The proposed areal morphological methods are applied to the extraction of topographical features from engineer surfaces. They overcome the shortcomings of traditional algorithms, such as the restriction of the size of structuring elements and end distortions to the extraction of topographical features. A series of surfaces from the bioengineering industry and the weapon industry were analyzed. The experimental results show that topographical features are successfully extracted, enabling further functional analysis to the components. Afterwards the morphological filtration is applied to two freeform surfaces and a non-uniform sampled surface. These capabilities will be useful in coordinate measurement of freeform surfaces, where adaptive sampling might be required. Following that, the morphological filter is applied in roundness filtration. Finally the morphological method searching contact points is employed to evaluate the underlying form of the textured surface of hip replacement taper junction. In industry the evaluation is done by traversing the surface with a large diameter ruby stylus on a CMM, which is neither stable nor precise. The use of surface texture instrument and the proposed morphological method guarantees the precision of measurement and accuracy of evaluation and allows for more accurate specification of component form which has been shown to be of prime importance to component performance.

8. CONCLUSIONS AND FUTURE WORK

8.1 Conclusions

In response to the emergence of advanced surfaces produced by modern manufacturing technologies, efficient and competent supporting algorithms for morphological filters are required. The aim of this thesis is to investigate and develop efficient discrete algorithms for morphological filtration on modern surfaces including freeform surfaces, nonuniform sampled surfaces and closed surfaces, and explore their applications in the field of surface metrology and dimensional metrology.

The research work accomplished in this thesis is listed below.

1. The literature review is conducted mainly in the field of morphological filters for geometrical metrology. Compared to the mean-line filtering techniques, such as the Gaussian filter, morphological filters are more relevant to geometrical properties of surfaces and suitable for the prediction of contact related functions. Although morphological filters are useful and generally accepted, the conventional implementation has a number of fatal drawbacks. The naive algorithm is time-consuming, especially for large datasets and large structuring elements and it does not support non-uniform sampled surfaces and freeform surfaces. The motif combination algorithm, although an efficient method for profile data, is hard to be extended to areal data.

2. A novel approach based on the alpha shape is proposed with the merits that enables arbitrary large ball radii and applies to freeform surfaces, non-uniform sampled surfaces and closed surfaces. The proposed approach utilizes the theoretical link between the alpha hull and the morphological closing and opening operations. A practical algorithm has been developed that corrects possible singularities caused by data spikes and reduces the amount of computation for open surfaces/profiles. The proposed alpha shape method is dependent on the Delaunay triangulation, bringing in an additional merit that the triangulation data is reusable for the computation of multiple radius attempts, saving a great deal of computation time. The performance bottleneck due to the costly 3D Delaunay triangulation on large areal datasets is solved by the divide-and-conquer method.

3. Aiming to overcome the limitations of the alpha shape method that the structuring element is restricted to be circular and the computation relies on the Delaunay triangulation, a novel method is proposed by searching contact points on the surface. The formal definition of the contact point is presented and a set of associated propositions and comments are proposed and mathematically proved based on alpha shape theory. With these propositions and comments, a recursive algorithm for morphological filters has been developed for both profile data and areal data. The proposed algorithm does not require the Delaunay triangulation and is applicable for both circular and flat structuring elements. Meanwhile it retains the merits of the alpha shape method.

4. The naive algorithm is a typical image processing method. We introduced computational geometry techniques into the computation of morphological filters by correlating the convex hull and morphological envelopes. Viewing the convex hull as a special morphological envelope, the Graham scan algorithm, originally developed for the convex hull, is modified to compute morphological profile envelopes, which achieves an excellent performance.

5. The three proposed methods, the alpha shape algorithm, the recursive algorithm and the modified Graham scan algorithm, along with the two traditional methods, the naive algorithm and the motif combination algorithm have been compared and analyzed in four aspects: algorithm verification, algorithm analysis, performance evaluation and areal extension. By looking into these aspects, the merits and shortcomings of these algorithms are evaluated and compared.

6. Morphological filters have end effects on the end regions of open surfaces in a similar manner to the mean-line based filters. However they differ in their essences. In comparison to end effects of the Gaussian filter which is caused by the convolution operation, end effects of morphological filters are related to the geometrical property of the boundary regions of the surface. Four methods are proposed to correct end effects of morphological filters, namely infinity padding, symmetrical reflection (point or line style), polynomial extrapolation and linear prediction. Contact points could be employed in the computation to improve the performance. These methods are further analyzed and discussed to derive their advantages and disadvantages.

7. Case studies are presented to demonstrate the capabilities of the proposed algorithms. The proposed areal algorithms for morphological filters (the alpha shape algorithm and the recursive algorithm) are utilized to extract the topographical features from engineering surfaces, including surfaces measured from a tooth implant, a femoral component of artificial knee joint and a bullet. These methods are also applied to the filtration of freeform and non-uniform sampled surfaces. These abilities could be useful in coordinate measurement for freeform surfaces where surfaces might be adaptively sampled. The alpha shape algorithm can be modified in order to apply morphological filters to the roundness filtration, whereas the naive algorithm is not qualified for this task. The contact points are employed to evaluate the underlying form of the textured surface of hip replacement taper junction. The use of surface texture instrument and the proposed morphological method guarantees the precision of measurement and accuracy of evaluation and allows for more accurate specification of component form.

To sum up, the three proposed algorithms provide morphological filters with the capabilities in dealing with modern surfaces, which match the current trend of the development of production technologies. The alpha shape algorithm is more robust for surfaces with complex shapes. The divide and conquer method solved the performance bottleneck of the alpha shape algorithm when dealing with surfaces larger than 1024×1024 points in size. In comparison, the recursive method is novel and achieved better performance. The modified Graham-scan algorithm with high efficiency is very suited for filtering profiles and capturing contact points with excellent performance. The end effects of morphological filters are determined by geometrical properties of boundary regions of open surfaces and structuring elements. Except for open surface filtration, morphological methods have more extensive applications in geometrical metrology, including topographical feature extraction, roundness filtration and contact function evaluation.

8.2 Future work

In this thesis, three novel discrete algorithms, i.e. the alpha shape algorithm, the recursive algorithm and the modified Graham scan algorithm, have been proposed and developed. In comparison to the traditional methods, they are more competent in

processing modern complex surfaces with better performance. Case studies have demonstrated the feasibility and superiority of these proposed methods. There is, however, a key research issue for future work.

The recursive algorithm computes the morphological envelope by searching contact points. It achieves better performance than the alpha shape method, especially when ball radii are large. However it needs to be further optimized in two aspects:

(1) Improve its performance. Currently it employs recursion for the partition process. Recursion is implemented as a method to call itself to solve sub-tasks. As the recursion level goes deep, the manipulation and maintenance of stack increase drastically and it may invoke the risk of stack overflow. In practical programming, recursion is usually replaced by iteration.

(2) Improve its robustness against possible arbitrary geometrical features on surfaces. State-of-the-art manufacturing technologies (e.g. the 3D printing) and advanced measurement instruments (e.g. tomography) have enabled the production and inspection of high-added-value components with real 3D complex geometrical structures. The application of morphological methods on this kind of surfaces is challenging. The recursive algorithm therefore should to be enhanced in dealing with this kind of surfaces.

REFERENCES

Asano, A., 1999 Texture analysis using morphological pattern spectrum and optimization of structuring elements, *Proceedings of the 10th International Conference on Image Analysis and Processing*, 209-214.

Barber, C. B., Dobkin, D. P., and Huhdanpaa, H. T. 1996 The Quickhull algorithm for convex hulls, *ACM Transactions on Mathematical Software*, 4(22): 469-483.

Barre, F. and Lopez J. 2000 Watershed lines and catchment basins: a new 3D-motif method, *International Journal of Machine Tools and Manufacture*, 40: 1171-1184.

Bernardini, F., Mittleman, J., Rushmeier, H., Silva, C. and Taubin, G. 1999 The ball-pivoting algorithm for surface reconstruction, *IEEE Transactions on Visualization and Computer Graphics*, 5: 349-359.

Bolland, B., Culliford, D., Langton, D., Millington, J., Arden, N., and Latham, J. 2011 High failure rates with a large-diameter hybrid metal-on-metal total hip replacement: clinical, radiological and retrieval analysis, *Journal of Bone and Joint Surgery-British*, 93(5): 608-615.

Brinkmann, S., Bodschwinna, H. and Lemke, H. W. 2001 Accessing roughness in three-dimensions using Gaussian regression filtering, *International Journal of Machine Tools and Manufacture*, 41: 2153-2161.

Brinksmeier, E. and Preuss W. 2012 Micro-Machining, *Philosophical Transactions of the Royal Society A*, 370: 3973-3922.

Bruzzone A.A.G., Costa H.L., Lonardo P.M. and Lucca D.A., 2008 Advances in engineered surfaces for functional performance, *CIRP Annals – Manufacturing Technology*, 57: 750-769.

Cormen, T.H., Leiserson C. E. and Rivest R. L. 1989 *Introduction to Algorithms*, The MIT Press.

Dagnall, H. 1998 *Exploring Surface Texture*, Taylor Hobson.

David, J. K. and Fransiska, S. F. 1993 Envelope reconstruction of probe microscope images, *Surface Science*, 294: 409-419.

De Chiffre, L., Kunzmann, H., Peggs G. N., and Lucca D. A. 2003 Surfaces in precision engineering, microengineering and nanotechnology, *CIRP Annals – Manufacturing Technology*, 52: 561–577.

Decenciere, E. and Jeulin, D. 2001 Morphological decomposition of the surface topography of an internal combustion engine cylinder to characterize wear, *Wear*, 249 482-488.

Devadoss, S. L. and O'Rourke, J. 2011 *Discrete and Computational Geometry*, Princeton University Press.

Dietzsch, M., Gerlach, M. and Groger, S. 2008 Back to the envelope system with morphological operations for the evaluation of surfaces, *Wear* 264: 411-415.

Dietzsch, M., Groger, S., Gerlach M. and Krystek M. 2007 Extraction of the mechanical surface in measurement of nano structures *CIRP Annals - Manufacturing Technology*, 56: 537-539.

Digalakis, V. V. 1993 Three-dimensional linear prediction and its application to digital angiography, *Multidimensional Systems and Signal Processing*, 4: 307-329.

Digital surf, MountainsMap software, http://www.digitalsurf.fr/.

Dougherty, E. R. 1992 *An Introduction to Morphological Image Processing*, Bellingham: SPIE Optical Engineering Press.

Dubuc, B., Zucker S. W., Tricot, C., Quiniou, J. F. and Wehbi D. 1989 Evaluating the fractal dimension of surfaces, *Proceedings of the Royal Society A*, 425: 113-127.

Edelsbrunner, H. and Mucke, E. P. 1994 Three-dimensional alpha shapes, *ACM Transactions on Graphics*, 13(1) 43-72.

Fahl, D. 1982 Motif combination – a new approach to surface profile analysis, *Wear* 83 : 165-179.

Fischer, K. 2000 Introduction to alpha shapes, *http://www.inf.ethz.ch/personal/fischerk/pubs/as.pdf*.

Garg, M. 2003 Linear prediction algorithms, *www.mohrahit.in/find/predict.pdf*.

Gopinath, R. K. and Rangaraj, M. R. 1993 An algorithm for direct computation of 2D linear prediction coefficients, *IEEE Transactions on Signal Processing*, 41: 996-1000.

Goto, T., Miyakura, J., Umeda, K., Kadowaki, S. and Yanagi K. 2005 A robust spline filter on the basis of L2-norm, *Precision Engineering*, 29: 157-161.

Graham, R. 1972 An efficient algorithm for determining the convex hull of a finite planar set, *Information Processing Letters*, 1: 132-133.

Haesing, J. 1964 Bestimmung der Glaettungstiefe rauher Flaechen, *PTB-Mittelungen*. 4:339-340.

Haralick, R. M., Zhuang, X., Lin, C. and Lee, J. 1988 The digital morphological sampling theorem. *Circuits and Systems*, 3: 2789-2793.

Heijmans, H. J. A. M. 1995 Mathematical morphology: a modern approach in image processing based on algebra and geometry, *SIAM Review* 37(1): 1-36.

ISO 11562 1996 *Surface texture: Profile method – Metrological characteristics of phase correct filters*, Switzerland.

ISO 14406 2003 *Geometrical Product Specifications (GPS) - Extraction*, Switzerland.

ISO 16610-1 2010 *Geometrical product specifications (GPS) - Filtration - Part 1: Overview and basic concepts*, Switzerland.

ISO 16610-20 2010 *Geometrical product specifications (GPS) - Filtration - Part 20: Linear profile filters: Basic concepts*, Switzerland.

ISO 16610-21 2010 *Geometrical product specifications (GPS) - Filtration - Part 21: Linear profile filters: Gaussian filters*, Switzerland.

ISO 16610-22 2010 *Geometrical product specifications (GPS) - Filtration - Part 22: Linear profile filters: Spline filters*, Switzerland.

ISO 16610-28 2010 *Geometrical Product Specification (GPS)-Filtration-Profile Filters Part 28: profile filters: End effects*, Switzerland.

ISO 16610-29 2010 *Geometrical product specifications (GPS) - Filtration - Part 29: Linear profile filters: Spline wavelets*, Switzerland.

ISO 16610-30 2010 *Geometrical product specifications (GPS) - Filtration - Part 30: Robust profile filters: Basic concepts*, Switzerland.

ISO 16610-31 2010 *Geometrical product specifications (GPS) - Filtration - Part 31: Robust profile filters: Gaussian regression filters*, Switzerland.

ISO 16610-32 2010 *Geometrical product specifications (GPS) - Filtration - Part 32: Robust profile filters: Spline filters*, Switzerland.

ISO 16610-40: 2010 *Geometrical Product Specification (GPS)-Filtration, Part 40: Morphological profile filters Basic concepts*, Switzerland.

ISO 16610-41: 2010 *Geometrical Product Specification (GPS)-Filtration, Part 41: Morphological profile filters Disk and horizontal line-segment filters*, Switzerland.

ISO 16610-49: 2010 *Geometrical Product Specification (GPS)-Filtration, Part 49: Scale space techniques*, Switzerland.

ISO 25178-2 2007 *Geometrical product specification (GPS) - Surface texture: Areal - Part 2: Terms, definitions and surface texture parameters*, Switzerland.

ISO 3274 1996 *Surface texture: Profile method – Nominal characteristics of contact (stylus) instruments*, Switzerland.

ISO/TC 213 1996 *Resolution 180 (Paris 28/1996)—Advisory group 9*, Resolutions adopted at the inaugural meeting of ISO/TC 213 on 14 June 1996 AFNOR, Paris, France, Document ISO/TC 213 N16.

Jiang, X. 2009 The evolution of surfaces and their measurement, *The 9th International Symposium on Measurement Technology and Intelligent Instruments*, 54-60.

Jiang, X. 2010 Robust solution for the evaluation of stratified functional surface, *CIRP Annals–Manufacturing Technology*, 59: 573-576.

Jiang, X., and Blunt, L. 2004 Third generation wavelet for the extraction of morphological features from micro and nano scalar surfaces, *Wear* 257: 1235-1240.

Jiang, X., Blunt, L. and Stout, K. J. 2000 Development of a lifting wavelet representation for surface characterization, *Proceedings of the Royal Society A*, 456(2001): 1-31.

Jiang, X., Blunt, L. and Stout, K. 2001 Application of the lifting wavelet to rough surfaces, *Precision Engineering*, 25 (2): 83-89.

Jiang, X., Scott, P. J., Whitehouse, D. J. and Blunt, L. 2007a Paradigm shifts in surface metrology, Part I. Historical philosophy, *Proceedings of the Royal Society A*, 463(2085): 2071-2099.

Jiang, X., Scott, P. J., Whitehouse, D. J. and Blunt, L. 2007b Paradigm shifts in surface metrology, Part II. The current shift, *Proceedings of the Royal Society A*, 463(2085): 2071-2099.

Jiang, X., Copper, P. and Scott, P. J. 2011a Freeform surface filtering using the diffusion equation, *Proceedings of the Royal Society A*, 467(2127) 841-859

Jiang, X., Zeng, W. and Scott, P. J. 2011b *Wavelet Analysis for the Extraction of Morphological Features for Orthopaedic Bearing Surfaces*, London: Bioengineering, InTech - Open Access Publisher.

Jiang, X. and Whitehouse, D. J. 2012 Technology shift in surface metrology, *CIRP Annals – Manufacturing Technology*, 61(2): 815-836.

Krystek, M. 1996a Form filtering by splines, *Measurement*, 18: 9-15.

Krystek, M. 1996b Discrete L-spline filtering in roundness measurements, *Measurement* 18: 129-138.

Krystek, M. 1997 Transfer Function of Discrete Spline Filters, *Advanced Mathematical Tools in Metrology III*, 203-210.

Krystek, M. 2004 Morphological filter in surface texture analysis, *XIth International colloquium on surfaces*, 43-55.

Krystek, M. 2005 Spline filters for surface texture analysis, *Key Engineering Materials*, 295: 441-446.

Krystek, M., Scott, P. J. and Srinivasan, V. 2000 Discrete linear filters for metrology, *Proceedings of the 16th IMEKO World Congress*, http://home.mit.bme.hu/~kollar/IMEKO-procfiles-for-web/congresses/WC-16th-Wien-2000/Papers/Topic%2014/Krystek.PDF.

Kumar, J. and Shunmugam, M. S. 2005 A new approach for filtering of surface profiles using morphological operations, *International Journal of Machine Tools and Manufacture*, 46: 260-270.

Kumar, J. and Shunmugam, M. S. 2006 Morphological operations on engineering surfaces using a 3D-structuring element of an appropriate size, *Measurement Science Technology*, 17: 2655-2664.

Liang, S. R. and Lin, A. C. 2002 Probe-radius compensation for 3D data points in reverse engineering, *Computers in Industry*, 48: 241–251.

Lou, S., Jiang, X., Scott, P. J. 2011 Morphological Filters Based on Motif Combination for Surface Functional Evaluation, *Proceedings of the 17th International Conference on Automation & Computing*, 133-137.

Makhoul, J. 1975 Linear prediction: A tutorial review, *Proceeding of the IEEE*, 63: 561-580.

Malburg, C. M. 2002 Fitting, Filtering and Analysis: Feature extraction in dimensional metrology applications, *International Dimensional Workshop*, www.digitalmetrology.com.

Malburg, C. M. 2003 Surface profile analysis for conformable interfaces, *Transactions of ASME*, 125: 624-627.

Marple, S. L. 2000 Two-dimensional lattice linear prediction parameter estimation method and fast algorithm, *Signal Processing Letters*, 7: 164-168.

Matheron, G. 1989 *Random Sets and Integral Geometry*, New York: John Wiley & Sons.

Matheron, G. and Serra, J. 2002 The birth of mathematical morphology, *Proceedings of. 6th International Symposium on Mathematical Morphology*, 1-16.

Mayer, J. R. R., Mir Y A, Trochu, F. Vafaeesefat, A. and Balazinski, M. 1997 Touch probe radius compensation for coordinate measurement using kriging interpolation, *Proceedings of the Institution of Mechanical Engineers, Part B*, 211: 11-18.

Medical Device Alert: All metal-on-metal (MoM) hip replacements (MDA/2010/033) 2010 http://www.mhra.gov.uk/home/groups/dts-bs/documents/medicaldevicealert/con079162.pdf.

Minkowski, H. 1903 Volumen and oberflache, *Mathematical Annals*, 57: 447-495.

Muralikrishnan, B. and Raja, J. 2005 Functional filtering and performance correlation of plateau honed surface profiles, *Journal of Manufacturing Science and Engineering*, 127: 193-197.

Muralikrishnan, B. and Raja, J. 2009 *Computational surface and roundness metrology*, London: Springer-Verlag.

Nyquist, H. 1928 Certain topics in telegraph transmission theory, *Transactions of the American Institute of Electrical Engineers*, 47: 617-644.

Olsen, K. V. 1963 The standardization of surface roughness, Proceeding of the International Conference of Production Engineering and Research, 655-658.

O'Rourke, J. 1994 *Computational Geometry in C*, New York: Cambridge University Press.

Peters, J., Bryan, J. B., Eslter, W. T., Evans, C., Kunzmann, H., Lucca, D. A., *et al* 2001 Contribution of CIRP to the development of metrology and surface quality evaluation during the last fifty years, *CIRP Annals - Manufacturing Technology*, 50 (2): 471-488.

Peters, J., Vanherck, P. and Sastrodinoto, M. 1979 Assessment of surface typology analysis techniques, *CIRP Annals - Manufacturing Technology*, 2:1-25.

Radhakrishnan, V. 1970 Effect of stylus radius on the roughness values measured with tracing stylus instruments, *Wear* 16(5):325-335.

Radhakrishnan, V. 1972 Selection of an enveloping circle radius for E-system roughness measurements, *International Journal of Machine Tools and Manufacture*, 12: 151-159.

Radhakrishnan, V. and Von Weingraber, H. 1969 Die Analyse Digitalisierter Oberflaechenprofil nach dem E-System, *Fachberichte fu¨r Oberflaechentechnik*. 7(11/12): 215-223.

Radhakrishnan, V. and Weckenmann, A. 1998 A close look at the rough terrain of the surface finish assessment, *Proceedings of the Institution of Mechanical Engineers, Part B*, 212: 411-420.

Raja, J., Muralikrishnan, B. and Fu, S. 2002 Recent advances in separation of roughness, waviness and form, *Precision Engineering*, 26: 222–235.

Reason, R. E., 1966 *Report on the Measurement of Roundness*, Rank Organisation.

Reason, R. E. Hopkins, M. R. and Garrod, R. I. 1944 *Report on the Measurement of Surface Finish by Stylus Method*, Leicester, UK: Rank Taylor Hobson.

Roger S., Dietzsch M, Gerlach M., Jeβ S. 2005 “Real mechanical profile” – the new approach for nano-measurements, *Journal of physics: conference Series*, 13: 13-19.

Sayles, R. S. 2001 How two- and three-dimensional surface metrology data are being used to improve the tribological performance and life of some common machine elements, *Tribology International*, 34: 299-355.

Schmoeckel, D. and Staeves, J. 1997 Function oriented 3D filtering for tribological assessment of sheet metal surfaces in deep drawing, *7th International Conference on Metrology and Properties of Engineering Surfaces*, 438-444.

Scott, P. J. 1992 The mathematics of motif combination and their use for functional simulation, *International Journal of Machine Tools and Manufacture*, 32: 69-73.

Scott, P. J. 1998 Foundations of topological characterization of surface texture, *International Journal of Machine Tools and Manufacture*, 38: 559-566.

Scott, P. J. 2000 Scale-space techniques, *Proceedings of the X International Colloquium on Surfaces*, 153-161.

Scott, P. J. 2004 Pattern analysis and metrology: the extraction of stable features from observable measurements, *Proceedings of the Royal Society A*, 460(2050): 2845–2864.

Sedaaghi, M. H. 1997 Direct implementation of open-closing in morphological filtering, *Electronic Letters*, 33: 198-199.

Seewig, J. 2006 Linear and robust Gaussian regression filters. *Journal of Physics: Conference series*, 13:254-257.

Serra, J. 1982 *Image Analysis and Mathematical Morphology*, Academic Press New York.

Shih, F. Y. 2009 *Image processing and mathematical morphology: fundamentals and applications*, CRC Press.

Shunmugam, M. S. and Radhakrishnan, V. 1974 Two-and three dimensional analyses of surfaces according to the E-system, *Proceedings of the Institution of Mechanical Engineers, Part B*, 188:691-699.

Soille, P. 1999 *Morphological Image Analysis Principles and Applications*, Berlin: Springer-Verlag.

Srinivasan, V. 1998 Discrete morphological filters for metrology, *Proceedings of the 6th ISMQC Symposium on Metrology for Quality Control in Production*, 623-628.

Srinivasan, V., Scott, P. J. and Krystek, M. 2000 ISO Standards for Geometrical Filters, *Proceedings of the 16th IMEKO World Congress*, <http://home.mit.bme.hu/~kollar/IMEKO-procfiles-for-web/congresses/WC-16th-Wien-2000/Papers/Topic%2014/Srinivasan.PDF>

Tholath, J. and Radhakrishnan, V. 1999 Three-dimensional filtering of engineering surfaces using envelope system, *Precision Engineering*, 23: 221–228.

Thomas, T. R. 1999 *Rough Surfaces*, London, UK: Imperial College Press.

Trumpold, H. 2001 Process related assessment and supervision of surface textures, *International Journal of Machine Tools and Manufacture*, 41: 1980-1993.

Unswoth, A. 1995 Recent developments in the tribology of artificial joints, *Tribology International*, 28: 485-495.

Vaidyanathan, P. P. 2008 *The Theory of Linear Prediction*, Morgan & Claypool publisher.

Venkaiah, N. and Shunmugam, M. S. 2007 Evaluation of form data using computational geometric techniques - Part I Circularity error, *International Journal of Machine Tools and Manufacture* 47: 1229-1236.

Villarrubia, J. S. 1996 Scanned probe microscope tip characterization without calibrated tip characterizers. *Journal of Vacuum Science and Technology B: Microelectronics and Nanometer Structures* 14(2): 1518–1521.

Von Weingraber, H. 1956 U¨ ber die Eignung des Hu¨llprofils als Bezugslinie f¨ur die Messung der Rauheit, *CIRP Annals - Manufacturing Technology*, 5: 116-128.

Wang, J., Jiang, X., Gurdak, E., Scott, J. P., Leach, R., Tomplins, P. and Blunt, L. 2011 Numerical characterisation of biomedical titanium surface texture using novel feature parameters, *Wear*, 271 (7-8): 1059-1065.

Westberg, J. 1997 Opportunities and problems when standardising and implementing Surface Structure parameters in Industry, *International Journal of Machine Tools and Manufacture*, 38: 413-416.

Whitehouse, D. J. 1967/68 An improved type of wave filter for use in surface-finish measurement, *Proceedings of the Institution of Mechanical Engineers, Part B*, 192: 306-318.

Whitehouse, D. J. 1978 Surfaces - a link between manufacture and function, *Proceedings of the Institution of Mechanical Engineers, Part B*, 192(19): 179-188.

Whitehouse, D. J. 1994 *Handbook of Surface Metrology*, Bristol and Philadelphia: Institute of Physics.

Whitehouse, D. J. 2001 Function maps and the role surfaces, *International Journal of Machine Tools and Manufacture.* 41:1847-1861.

Whitehouse, D. J. 2002 *Surfaces and their Measurement*, London, UK: Hermes Penton Ltd.

Whitehouse, D. J. 2012 Surface geometry, miniaturization and metrology, *Philosophical Transactions of the Royal Society A*, 370: 4042-4065.

Whitehouse, D. J. and Reason, R. E. 1963 *The equation of the mean line of surface texture found by an electric wave filter*, Leicester, UK: Rank Taylor Hobson.

Worring, M. and Smelders, W. M. 1994 Shape of arbitrary finite point set in R2, *Journal of Mathematical Image and Vision*, 4: 151-170.

Wozniak, A., Mayer, J. R. R. and Balazinski M. 2009 Stylus tip envelop method corrected measured point determination in high definition coordinate metrology, *International Journal of Advanced Manufacturing Technology*, 42: 505-514.

Xiao, S., Jiang, X., Blunt, L. and Scott, P. J. 2001 Comparison study of the biorthogonal spline wavelet filtering for areal rough surfaces, *International Journal of Machine Tools and Manufacture*, 41(13-14): 2103-2111.

Yin, Z., Zhang, Y. and Jiang, S 2003 Methodology of NURBS surface fitting based on off-line software compensation of errors of a CMM, *Precision Engineering*, 27: 299-303.

Zeng, W., Jiang, X. and Scott, P. J. 2010 Fast algorithm of the robust Gaussian regression filter for areal surface analysis, *Measurement Science and Technology*, 21(5): 055108.

Zeng, W., Jiang, X. and Scott, P. J. 2011a A generalized linear and nonlinear Spline filter, *Wear*, 3: 544-547.

Zeng, W., Jiang, X. and Scott, P. J. 2011b Roundness filtration by using a robust regression filter, *Measurement Science and Technology*, 22(3): 035108.